PhD degree in Systems Medicine (curriculum in Molecular Oncology)

European School of Molecular Medicine (SEMM),

University of Milan and University of Naples "Federico II"

Settore disciplinare: BIO/10

NuMA:LGN hetero-hexamers promote the assembly of cortical protein network to control planar cell divisions

Laura Pirovano

European Institute of Oncology (IEO), Milan

Matricola n. R11475

Supervisor: **Dr. Marina Mapelli**

European Institute of Oncology (IEO), Milan

Anno accademico 2018-2019

TABLE OF CONTENTS

GLOSSARY

ABL1	Ableson Leukemia Kinase-1
ACD	Asymmetric Cell Division
BD	Binding Domain
BSA	Bovine Serum Albumine
Caco-2	Human Colorectal Adenocarcinoma Cells
CC	Coiled-Coild
Cdk1	Cyclin-Dependent Kinase 1
Co-IP	Co-Immunoprecipitation
Dlg	Disc Large
DMSO	Dimethyl Sulfoxide
Dvl	Dishevelled
ECM	Extracellula Matrix
FRAP	Fluorescence Recovery After Photobleaching
FRET	Fluorescence Resonance Energy Transfer
Fz	Frizzled receptor
GEF	Guanine Nucleotide Exchange Factors
GTP/GDP	Guanosine Triphospate/Diphospate
Gαi	The Alpha Subunit of Adenyl-Cyclase-Inhibitory Heterotrimeric G Protein
HEK293T	Human Embryonic Kidney 293 Cells
HeLa	Human Cervical Cancer Cells
LGN	Leu-Gly-Asn Repeat-Enriched Protein
LIC	Light Intermediate Chain
MT	Microtubule
NB	Neuroblast
NLS	Nuclear Localization Signal
NuMA	Nuclear Mitotic Apparaturs
Par	Partioning-Defective
Pins	Partner of Inscuteable
Plk1	Polo-Kinase-1
Ran	Ran Related Nuclear Protein
RCC1	Regulator of Chromosome Condensation
Ric8A	Resistance To Inhibitors Of Cholinesterase 8
S2	Drosophila Shneider-2 Embryonic Cells
SEC	Size Exclusion Chromatography
shRNA	Short-Hairpin RNA
SLK	Ste20-Like Kinase
SOP	Sensory Organ Precursor
TIPs	Microtubules Plus-End Tracking Proteins
TPR	Tetratrico-Peptide Repeats
TPX2	Xenopous Kinesin-Like Protein 2

FIGURE INDEX

ABSTRACT

Mitotic spindle orientation is a prerequisite for the correct completion of mitosis, and is essential for tissue morphogenesis and maintenance. Divisions occurring within the plane of epithelia, or planar divisions, shape the architecture of epithelial sheets, whereas vertical divisions along the apicobasal axis are associated with asymmetric fate specification and stratification. Several studies described the evolutionary conserved trimeric Gαi:LGN:NuMA complex as the core constituent of the spindle orientation machinery. In mitosis Gαi:LGN:NuMA complexes localize at the cortex and orient the spindle by generating pulling forces on astral microtubules emanating from the spindle poles, via interaction of NuMA with the minus-end directed motor proteins dynein/dynactin. Biochemical and structural studies identified the minimal binding domains of the NuMA:LGN interaction, showing that a 30-residues stretch in the C-terminal part of NuMA binds to the inner groove formed by the eight TPR repeats at the N-terminus of LGN. However, how such interaction is organized at the cell cortex and triggers microtubules-motor activation still remains largely unclear.

My PhD project focused on the characterization of the NuMA:LGN interaction and on the analysis of the role of the microtubule-binding domain of NuMA. Studies conducted during this thesis revealed that NuMA and LGN assemble in hetero-hexameric structures organized in a donut-shape architecture. In such arrangement, the LGN helices preceding and following the TPR repeats, and a NuMA motif preceding the shortest LGN-binding motif, are essential for the interaction. Consistently, an LGN oligomerization-deficient mutant cannot rescue misorientation defects caused in HeLa cells and Caco-2 three-dimensional cysts by endogenous LGN ablation. Importantly, in cells expressing the oligomerization-deficient mutant, force generators are correctly localized at the cell cortex. We provided evidence that LGN and NuMA assemble high-order oligomers in cells, and that the 3:3 stoichiometry of the NuMA:LGN complex combined with the dimeric state of NuMA coiled-coils promote

the formation of a large proteins network. We also showed that ectopic targeting of an oligomerization-deficient NuMA mutant at the cortex is not sufficient to orient the spindle, indicating that the molecular organization of NuMA in complex with LGN is required to orient the spindle in metaphase. Furthermore, we provided evidence that the NuMA:LGN oligomers are compatible with the direct association of NuMA to microtubules, and that the microtubules-binding domain of NuMA is required to correctly localize NuMA at the poles and at the cortex, and to orient the spindle. Collectively, our findings suggest a model whereby cortical LGN:NuMA hetero-hexamers favor the accumulation of dynein motors at cortical sites. We speculate that direct binding of NuMA to astral microtubule plus-tips assists the processive movement of dynein along the depolymerizing astral microtubules to promote spindle placement.

1. INTRODUCTION

During my PhD, I focused on the mechanisms of oriented cell divisions and on the role of NuMA and LGN, two master regulators of mitosis, in mammalian cells in metaphase. For this reason, the introduction below will contextualize spindle orientation in the known literature in mammalian cells and in invertebrate systems.

1.1 Cell division

The ordered sequence of coordinated processes that produces two new daughter cells is called cell cycle. In eukaryotes this process can be divided in two main stages: interphase, in which cells grow, replicate DNA and accumulate nutrients, and mitosis (M phase), when duplicated chromosomes are distributed in the daughter cells that physically separate through cytokinesis. The mitotic phase can be further divided into five phases: prophase, prometaphase, metaphase, anaphase and telophase (Figure 1). During prophase, chromatin condensates into chromosomes, and mitotic spindle starts assembly. Prometaphase starts with the break of the nuclear envelope, and ends when all the sister chromatids are attached to the microtubules of the spindle. In metaphase chromosomes align at the cell equator, forming the metaphase plate, and then divide during anaphase. Mitosis completes in telophase, when chromosomes and nuclear component are repackaged into daughter cells nuclei (O Morgan, 2007).

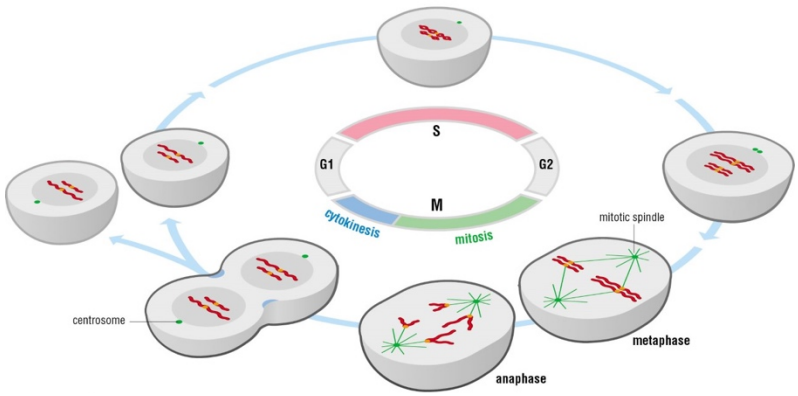

Figure 1 – Eukaryotic cell cycle

Cell cycle stages are defined on the basis of chromosomal events. DNA replication takes place during the S phase, followed by chromosomes segregation during mitosis (M phase) and cell division during cytokinesis. G1 is the gap phase between the M phase and the S phase. G2 is the second gap occurring before M phase. *Adapted from David O. Morgan, The Cell Cycle: Principles of Control, 2007.*

1.1.1 The mitotic spindle

The correct partitioning of chromosomes in the two daughter cells depends on the mitotic spindle, a microtubules-based machine. The mitotic spindle is a highly dynamic structure based on a bipolar array of microtubules, each constituted by α– and β-tubulin dimers that associate head to tail and form a polar structure in which at one end, called plus end, β-tubulin is exposed, while at the other end, called minus end, α-tubulin emerges (Desai and Mitchison, 1997). As a consequence of this polarization microtubules show a different polymerization rate. The dynamic behavior in which microtubules undergo events of polymerization and depolymerization coupled to GTP hydrolysis is called dynamic instability. GDP-tubulin binds less tightly to microtubules compared to GTP-tubulin, resulting in a rapid dissociation and in a switch from the growing to the shrinking phase. Three classes of microtubules (MTs) form the mitotic spindle: astral MTs, interpolar MTs, and kinetochore MTs. Astral MTs extend from the spindle poles and link the cell cortex to the mitotic spindle (Izumi *et al.*, 2006; Kotak, Busso and Gönczy, 2013). Interpolar MTs tie the poles to each other in the midzone of the spindle, while kinetochore MTs connect the kinetochores on the chromatids to the spindle poles (Izumi *et al.*, 2006; Siller, Cabernard and Doe, 2006).

1.1.2 Mitotic spindle assembly

During G2/M transitions, pericentriolar matrix (PCM) surrounding the centrioles increases in size and starts nucleating and anchor MTs, in a process called centrosome maturation

(Meraldi and Nigg, 2002). This process requires the activity of several motor proteins and mitotic kinases, including polo-like kinase 1 (Plk1), cyclin-dependent kinase 1 (Cdk1) and Aurora-A (Wang, Jiang and Zhang, 2014). In the first stages of spindle assembly, spindle poles formation and centrosome separation require the activation of two motor proteins, Eg5 and dynein (Figure 2). Eg5 is a slow motor protein whose architecture consists of an N-terminal head domain containing the motor, a C-terminal domain and a central coiled-coil. Its activity is regulated by cell-cycle-dependent phosphorylation by Cdk1 and Aurora-A, and is required for poles separation (Blangy *et al.*, 1995; Uzbekov *et al.*, 1999). Eg5 forms homotetramers, linking the MTs emanating from each centrosome, this way sliding antiparallel MTs on one another.

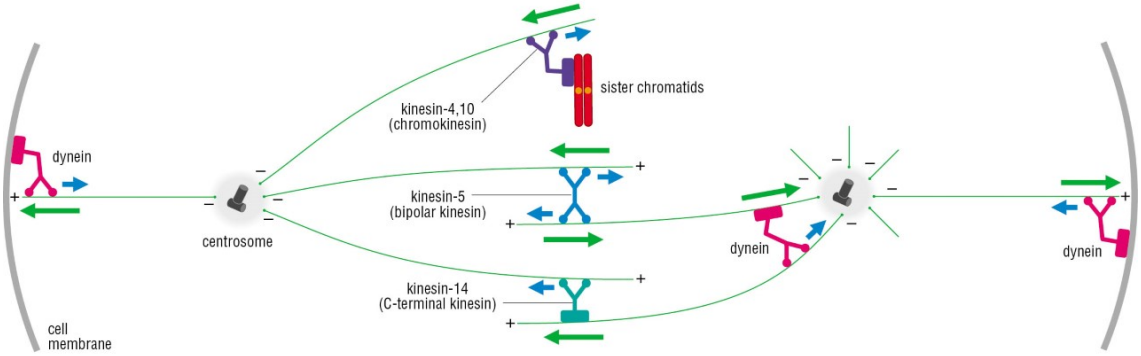

Figure 2 – Motor proteins in spindle assembly

Several types of motor proteins contribute to spindle assembly. The plus-ends directed motor protein kinesin-5 (Eg5) crosslinks antiparallel MTs and pushes centrosomes apart. Kinesin-14 acts redundantly to kinesin-5 to separate spindle poles. The minus-ends directed dynein focus MTs minus-ends at the spindle poles. Kinesin-4 and kinesin-10 link interpolar MTs to chromosomes arms, pulling chromosomes toward the poles. *Adapted from David O. Morgan, The Cell Cycle: Principles of Control, 2007.*

Inhibition of Eg5 activity prevents poles separation, resulting in a monopolar spindle (Uzbekov *et al.*, 1999). Centrosome separation requires the activity of an additional microtubules-motor, cytoplasmic dynein, a minus-end directed motor protein. Dynein is a multi-subunit ATPase complex, composed by heavy chain motor proteins, intermediate chains, light chains and additional interactors. It has been shown to interact with $p150^{Glued}$

dynactin-subunit, an adaptor protein helping targeting dynein to specific cellular compartments, including the cell cortex, astral MTs, and the nuclear envelope (Kardon and Vale, 2009). At the onset of mitosis, after nuclear envelope breakdown, the pool of dynein localized into the nucleus is involved in centrosomes separation (Gadde and Heald, 2004). Besides its role in mitotic spindle formation, cortical dynein plays an important role in spindle positioning through the generation of pulling forces on astral MTs, while a pool of dynein localizing at the spindle poles, together with dynactin and the master regulation of mitosis NuMA, works to focus MTs minus-ends at the centrosomes (Merdes *et al.*, 1996, 2000; Kotak, Busso and Gönczy, 2012). The dynein/NuMA interaction will be better described in paragraph 1.5.2. Additional mechanisms act redundantly to Eg5 and dynein to promote bipolar spindle assembly, including chromokinesin, kinesin-12, 10 and 14, which display a plus-end-directed motility. An important role in spindle assembly is played also by chromosome-associated proteins, which promote localized microtubules stabilization and cross-linking.

The small GTP-associated protein Ran (Ras-related nuclear protein) was first identified as regulator of nuclear transport in association with importins and exportins, and then described to be a promoter of MTs assembly by favoring the release of spindle assembly factors from importins (Figure 3). The Ran-GTP cycle is regulated by the guanine nucleotide exchange factor RCC1, which promotes the dissociation of GDP and hence the GTP-bound state of Ran, and by the GTPase activating protein (GAP) RanGAP, which in turn enhances the hydrolysis of GTP to GDP. The RanGTP pathway works both in mitosis and in interphase. In interphase, RCC1 is bound to chromatin, while RanGAP localize in the cytoplasm, generating a RanGTP/RanGDP gradient between nucleus and cytoplasm that allows proteins transport across the membrane. During mitosis, chromosomes-associated RCC1 generates a Ran-GTP gradient. This gradient allows the release of proteins containing a nuclear-localization signal, which are bound to β-importin, in proximity of condensed chromosomes (Clarke and Zhang, 2008).

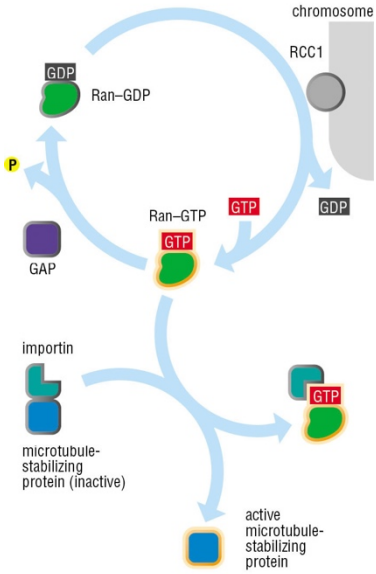

Figure 3 – The Ran-GTP cycle

In mitosis, chromosomes associated guanine-nucleotide exchange factor (GEF) RCC1 results in the local production of active GTP-bound form of Ran. Ran-GTP triggers the release of microtubules-associated proteins bound to importin-β near the chromosomes. The activity of the GTPase-activating protein GAP promotes the hydrolysis of GTP to GDP in the cytoplasm, establishing a RanGTP gradient from the chromosomes. *Adapted from David O. Morgan, The Cell Cycle: Principles of Control, 2007.*

1.2 Spindle orientation

During development, correct spindle orientation is required for tissue architecture establishment and for morphogenesis. Oriented divisions imply an active process in which the mitotic spindle aligns along a specific axis determined by cellular polarity, that is generally inherited by the tissue in which the cell is embedded. Divisions within the plane of epithelia shape epithelial tissue architecture, while divisions along the apico-basal axis are associated to tissue stratification or asymmetric fate specification of the two daughter cells. Consistently, disruption of the mechanisms governing mitotic spindle orientation are often associated with tissue disorganization and tumor-like proliferation (Knoblich, 2010). The positioning of the mitotic spindle is determined by force generators located at specific regions of the cell cortex, that interact with the astral microtubules emanating from the spindle poles. In mammalian cells in metaphase, the mitotic spindle is placed at the cell equator, in order to correctly segregate sister chromatids during anaphase. Its positioning plays a key role in determining the axis of cell division, and the cleavage furrow positioning, this way regulating daughter cell placement within a proliferating tissue. Mitotic spindle orientation in animal cells can be influenced by several factors, including internal and external cues, and geometric cues.

1.2.1 Players of the spindle orientation

Several studies have identified an evolutionary conserved trimeric complex composed by the Gαi subunit of the heterotrimeric G-protein, the switch protein LGN, and the nuclear protein NuMA as a fundamental assembly of cortical force generators (Morin and Bellaïche, 2011). Gαi:LGN:NuMA complexes localize to cortical regions above the spindle poles, acting as a molecular bridges between the cell cortex and the astral microtubules, and promoting dynein/dynactin cortical recruitment (Figure 4). The Gαi:LGN:NuMA complex has been initially identified in *C. elegans* zygotes and *Drosophila* neuroblasts, and later found conserved in mammals (Figure 5). During mitosis, the GDP-loaded inhibitory subunit of the heterotrimeric G-protein Gαi associates with the plasma membrane through its N-terminal myristoyl group, and recruits LGN at the cell cortex by direct interaction. Interestingly, only the GDP-bound form of Gαi can bind to LGN, suggesting that a non-canonical G-protein signaling pathway governs the assemble of Gαi:LGN:NuMA complexes at the membrane.

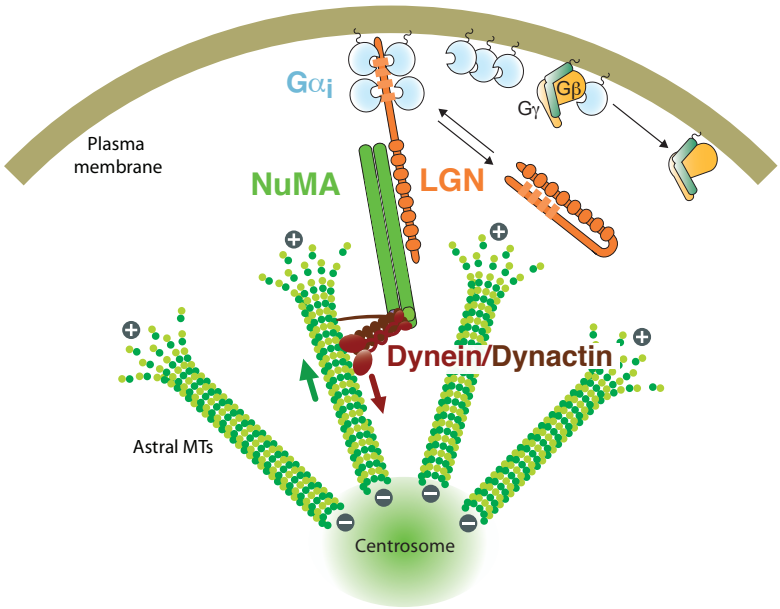

Figure 4 – The spindle orientation machinery

During mitosis, cortically localized Gαi:LGN:NuMA complexes anchor astral microtubules to the cell cortex. The scaffold protein LGN (orange) is recruited at the cortex by binding of its C-terminal

GoLoco domain to four membrane-localized Gαi-GDP proteins (cyan) associated to the plasma membrane via their myristoyl group. LGN acts as a conformational switch that goes from a closed conformation (orange, right) to an open conformation (left) upon binding to Gαi-GDP and to NuMA (green). NuMA in turn can interact with the minus-ends directed dynein/dynactin motor proteins (red).

In the canonical G-protein signaling pathways, the binding of a ligand to a G-protein coupled receptor (GPCR) triggers a conformational change of the receptor that acts as a guanine exchange factor (GEF) for the Gα subunit of the heterotrimeric G-proteins, and induces GDP-GTP exchange. This results in the dissociation of Gα subunit from the Gβγ heterodimer, allowing Gα-GTP and Gβγ binding to downstream effectors. Conversely, in the non-canonical pathway, intracellular GEFs such as Ric-8 (Resistance to inhibitors of Cholinesterase 8) catalyze the release of GDP from Gαi, limiting the concentration of Gαi-GDP molecules available for the interaction with LGN and NuMA (Hepler and Gilman, 1992). Ric-8 has been implicated in asymmetric cell division in *Drosophila* neuroblasts and *C. elegans* zygotes, as well as in symmetrically dividing mammalian cells (Bellaiche and Gotta, 2005; David *et al.*, 2005; Woodard *et al.*, 2010). The mammalian orthologue of Ric8, Ric-8A, has been shown to catalyze the guanine nucleotide exchange on Gαi bound to LGN and NuMA and release activated Gαi-GTP *in vitro* (Tall and Gilman, 2005).

Vertebrate	*Drosophila*	*C. elegans*
Gai	Gai/Gao	GOA-1/GPA-16
LGN	Pins	GPR-1/2
NuMA	Mud	LIN-5
mInsc	Insc	-
Par3	Bazooka	PAR-3
Par6	DmPar6	PAR-6
aPKC	D-aPKC	PCK-3
Afadin	Canoe	AFD-1

Figure 5 – Evolutionary conserved spindle orientation proteins
Orthologs of proteins involved in spindle orientation and cell polarity in vertebrates, *Drosophila* and *C. elegans*.

Moreover, impairment of Gα and Ric-8A expression or function in HeLa and MDCK cells causes spindle randomization and affects cortical recruitment of LGN, NuMA and dynein (Tall and Gilman, 2005; Woodard *et al.*, 2010; Peyre *et al.*, 2011a). Since Gα-GDP localizes uniformly at the cell cortex with Gβγ, what restricts Gαi-GDP:NuMA:LGN localization is unclear (Peyre *et al.*, 2011a).

LGN is recruited at the cortex by binding to Gαi via its four GoLoco motives. It acts as a molecular scaffold, and simultaneously binds NuMA via its eight N-terminal tetratrico-peptide (TPRs) repeats (Figure 6A-B), each consisting of a couple of antiparallel helices connected by a short turn. Most of the αA and αB helices of the TPR repeats of LGN are composed by 18 residues, 2-residues longer than the canonical TPR repeats, creating a right-handed superhelical twist (Culurgioni *et al.*, 2011; Zhu *et al.*, 2011). Another peculiar feature of LGN-TPR is represented by the presence of a set of asparagines (Leu-Gly-Asn, LGN) positioned between the third and the fourth turn of each αA helix, which provide a docking ridge for LGN ligands (Culurgioni *et al.*, 2011; Yuzawa *et al.*, 2011; Zhu *et al.*, 2011). A sequence of 100 residues joins the TPR domain with the C-terminal GoLoco motifs.

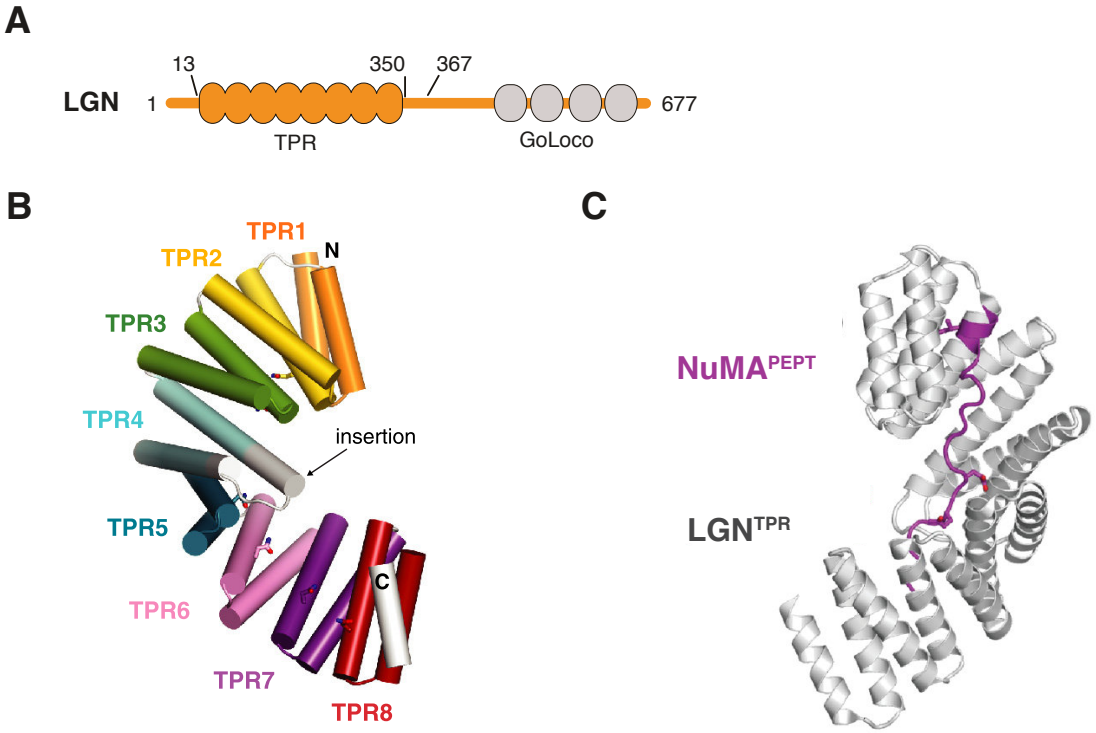

Figure 6 – LGN architecture and domain structure

(**A**) Domain structure of full-length LGN, with the eight N-terminal TPR repeats and the C-terminal GoLoco region joined by a linker region of 100 residues. (**B**) Cartoon representation of LGN^{TPR} architecture. Each TPR repeat consists of two antiparallel helices represented as cylinders. (**C**) Cartoon representation of LGN^{TPR} (grey) in complex with $NuMA^{PEPT}$ (purple). *Adapted from Culurgioni S et al.,, Proc. Natl. Acad. Sci. USA, 2011.*

FRET studies showed that LGN behaves as a conformational switch, adopting a closed conformation during interphase, and opening during mitosis (Du and Macara, 2004) (Figure 4). The inactive state is maintained through head-to-tail interactions between its TPR domain and the C-terminal portion, and displays low affinity for Gαi. After nuclear envelope breakdown, NuMA is released from the nucleus and recruited at the cortex by binding to the TPRs of LGN (Du, Stukenberg and Macara, 2001; Du and Macara, 2004; Zhu *et al.*, 2011). A small C-terminal peptide of NuMA has been shown to bind LGN with a 1:1 stoichiometry, in which residues 1899-1926 of NuMA binds the N-terminus of LGN encompassing residues 15-350 (Zhu *et al.*, 2011) (Figure 6C). In this interface, the interaction between NuMA and LGN is mainly mediated by electrostatic interactions and hydrogen bonds. Consistently, fluorescence polarization-based measurements of binding affinities showed that mutations affecting residues that mediate polar interactions strongly reduce NuMA/LGN interaction (Zhu *et al.*, 2011). The pool of NuMA at the cortex associates with dynein/dynactin, promoting the onset of MT-pulling forces (Kotak, Busso and Gönczy, 2012).

1.2.2 Mitotic spindle centering

In vertebrate cells, the mitotic spindle assembles in prometaphase with a random orientation, and then orients during metaphase thanks to dynein/dynactin-dependent pulling forces on the astral microtubules in order to achieve the correct division (Kotak, Busso and Gönczy, 2012; Kiyomitsu, 2015). Kiyomitsu and Cheeseman demonstrated that signals derived from

the spindle poles and the chromosomes can control cortical enrichment of spindle motors in HeLa cells (Kiyomitsu and Cheeseman, 2012). They showed that, in mitotic HeLa cells, LGN is initially uniformly recruited at the cell cortex, while in metaphase its localization becomes more confined at regions above the spindle poles, together with NuMA and dynein/dynactin (Kiyomitsu and Cheeseman, 2012). Specifically, during metaphase, a chromosomes-derived Ran-GTP gradient (see paragraph 1.1.2) would exclude LGN and NuMA from the regions above the metaphase plate, through molecular mechanisms that to date are not fully clear. The same Ran-GTP gradient is maintained active during anaphase, when the unequal distribution of myosin II at the cortex in response to spindle mispositioning can drive asymmetric localization of spindle motors via the scaffold protein Anillin (Ou *et al.*, 2010; Connell *et al.*, 2011). Intriguingly, this Ran-GTP pathway seems to work cooperatively with a Plk1-mediated centering pathway (Kiyomitsu and Cheeseman, 2012). Time-lapse experiments revealed that during metaphase, when the mitotic spindle comes in proximity to the cell cortex, dynein/dynactin display an asymmetric cortical enrichment, with a crescent of proteins accumulating at the opposite side of the pole approaching the cortex, while no asymmetric distribution of NuMA and LGN were visible. To explain this observation, Kiyomitsu and colleagues proposed a model in which Plk1 at the spindle poles phosphorylates NuMA and dynein/dynactin causing the dissociation of dynein/dynactin from Gαi:LGN:NuMA complexes at the cell cortex (Kiyomitsu and Cheeseman, 2012). Ectopic targeting of Plk1 at the cortex abolishes dynein recruitment, confirming that localized Plk1 causes motor proteins to dissociate from NuMA and LGN when poles are in close proximity to the cortex (Figure 7). According to these findings, a recent work from Sana and colleagues reports that Plk1 directly interacts and phosphorylates NuMA, negatively regulating its localization at the cell cortex (Sana *et al.*, 2018).

For cells that divide generating daughters with different size (see paragraph 1.3.2), such as *Drosophila* neuroblast and *C. elegans* oocytes and neuroblast, which have a relatively big size, the chromosomes-derived Ran gradient may not reach the cell cortex due to the distance

between chromosomes and membrane. In fact, studies in *C. elegans* neuroblast revealed that in these systems an asymmetric distribution of cortical myosin is generated in anaphase, and drives unequal cell division (Ou *et al.*, 2010; Connell *et al.*, 2011). In *Drosophila* neuroblast cortical myosin asymmetry is generated independently of chromosomes, but depends on polarity proteins (Izumi *et al.*, 2006; Siller, Cabernard and Doe, 2006; Cabernard, Prehoda and Doe, 2010), which allow the generation of asymmetric forces in order to displace the spindle (for details, see paragraph 1.3.2).

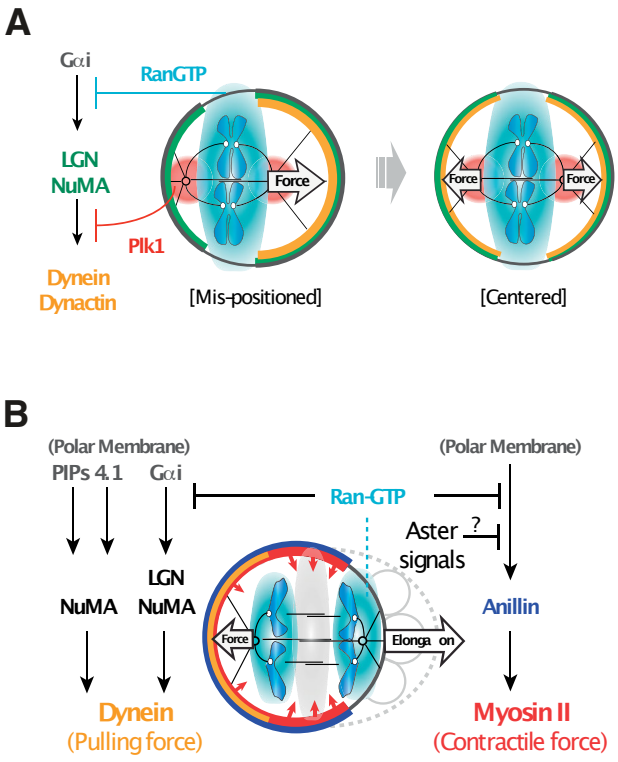

Figure 7 – Spindle-centering systems in metaphase and anaphase

Schematic representation of the Ran-GTP gradient (blue) and Plk1 kinase activity (red) that regulate spindle orientation protein cortical localization in metaphase and anaphase in HeLa cells. (**A**) In metaphase, chromosomes-derived Ran-GTP gradient excludes NuMA:LGN complexes from cortical regions close to DNA, this way confining LGN, NuMA (green) and dynein/dynactin (yellow) at cortical regions above the spindle poles. In addition, Plk1 signals from the spindle poles negatively regulates the localization of dynein/dynactin complexes at the cortex, promoting spindle centering. (**B**) In anaphase, Ran-GTP gradient reduces Anillin and Myosin at cortical regions near chromosomes, and promotes their accumulation to equatorial cell-cortex regions, promoting membrane elongation. *Adapted from Kiyomitsu T., Trends in cell biology, 2015.*

Moreover, in flies neuroblasts the mitotic spindle is directly assembled asymmetrically and with apico-basal orientation, generating an odd distance from the apical centrosome and the metaphase plate compared to the basal centrosome, leading to a different size of the large apical and the smaller basal daughter cells (Cai *et al.*, 2003; Siller and Doe, 2009). In *C. elegans* embryos, spindle displacement towards the posterior cell cortex is achieved through the asymmetric distribution of force generators on LIN-5:GPR1/2:GOA-1/GPA-1 complexes (the nematode counterpart of mammalian Gαi:LGN:NuMA, see Figure 5) (Nguyen-Ngoc, Afshar and Gönczy, 2007).

1.3 Oriented cell divisions

During development and adult life, oriented divisions create cellular diversity and shape epithelial architecture, regulating tissue formation and homeostasis. Consistently, in recent years, the orientation of the mitotic spindle emerged as a crucial event in maintaining tissue architecture, and in controlling cell fate choices of stem cells. During embryogenesis and regeneration, stem cells divide through oriented divisions, in which the mitotic spindle aligns along a specific axis determined by cellular polarity. Epithelial polarity is settled by antagonizing forces between apical Par3/Par6/aPKC and baso-lateral Scribble/Dlg/Lgl proteins. The orientation of the spindle in respect to the apico-basal polarity axis determines the result of the division, which can be symmetric or asymmetric (Morin and Bellaïche, 2011). In symmetric cell divisions, the mitotic spindle is positioned perpendicularly to the apico-basal polarity axis, and generates two equal-sized daughters, which inherit identical cellular content (Figure 8). Conversely, in asymmetric stem cell divisions, the spindle is aligned with the polarity axis, ensuring unequal partioning of fate determinants and asymmetric inheritance of niche contacts (Siller and Doe, 2009). In stem cells, symmetric divisions are associated to stem cell pool amplification, while in asymmetric divisions the

dividing cell generates one daughter that will remain stem, and a second daughter that will differentiate. The correct balance with symmetric proliferative versus asymmetric cell divisions ensures the equality of proliferation and differentiation.

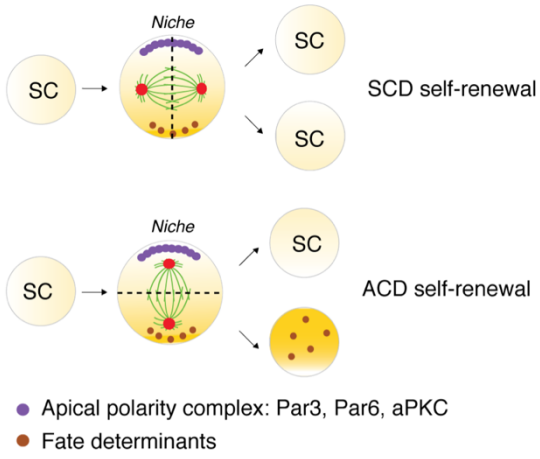

Figure 8 – Model of intrinsic symmetric and asymmetric cell divisions

Top: Schematic representation of a symmetric cell division (SCD). In SCD stem cells divide by orienting the mitotic spindle perpendicular to the apico-basal polarity axis (dashed black line), generating two identical daughter cells. Bottom: In asymmetric cell division (ACD) the mitotic spindle is oriented parallel to the apico-basal polarity axis, and leads to the generation of one daughter cell inheriting the fate determinants (brown dots) and which is committed to differentiation (gold), while the second daughter retain the stemness (pale yellow).

1.3.1 Mitotic spindle orientation in symmetric cell division

In symmetric cell divisions, the mitotic spindle is positioned within the plane of the epithelium, and needs to be positioned in the center of the cell to generate daughters of identical size that remain in the epithelial plane (Ragkousi and Gibson, 2014). Symmetric divisions have been extensively studied in tissues, isolated cells and three-dimensional model systems such as Caco-2 and MDCK cysts. HeLa cells represent a model system widely used to study basic mechanisms of mitotic spindle orientation in single cells. These unpolarized cells undergo symmetric divisions, and when plated on a fibronectin substrate divide by orienting the mitotic spindle parallel to the substratum, in a β1-integrin-depening manner (Toyoshima and Nishida, 2007). Symmetric polarized divisions, or planar divisions,

instead have been studied in MDCK and Caco-2 three-dimensional cysts, which provide a simple model to study oriented divisions in monolayered epithelia. Caco-2 and MDCK single cells plated in matrigel grow as highly-polarized cysts in which the apical surface faces a single central lumen (Ivanov *et al.*, 2008; Jaffe *et al.*, 2008; Hao *et al.*, 2010; Zheng *et al.*, 2010; Wei *et al.*, 2012). In these systems, mitosis occurs in the plane of the cyst surface, and the spindle is oriented perpendicular to the apico-basal polarity axis. More sophisticated systems are required to study symmetric stem cell divisions. Studies in murine neuroepithelial progenitors and developing epidermis revealed that early in development, stem cells divide symmetrically with the spindle parallel to the ventricle or the basement membrane to expand the stem cell pool (Huttner and Kosodo, 2005; Poulson and Lechler, 2010a). In these divisions both NuMA and LGN are localized al the lateral cortex, while they are excluded from the apico-basal region (Morin, Jaouen and Durbec, 2007; Gillies and Cabernard, 2011; Peyre *et al.*, 2011).

In all characterized polarized and unpolarized systems, Gαi, LGN and NuMA have been described to play a pivotal role in promoting correct spindle orientation. Consistently, depletion of Gαi, LGN and NuMA are associated to randomized orientation (Woodard *et al.*, 2010; Zheng *et al.*, 2010; Peyre *et al.*, 2011). During metaphase, membrane-bound Gαi recruits LGN at the cell cortex, which in turn targets dynein/dynactin motor proteins through NuMA. Silencing Gαi or LGN in HeLa cells confirmed that the cortical enrichment of LGN is required for NuMA and dynein/dynactin recruitment at the cortex. In addition, knocking-down NuMA precludes dynactin cortical targeting (Woodard *et al.*, 2010; Kotak, Busso and Gönczy, 2012) suggesting that NuMA can act as the dynein-activating adaptor at the cell cortex in mitosis. Intriguingly, overexpression of both LGN and Gαi causes excessive spindle movements and misoriented divisions, indicating that the amount of Gαi:LGN:NuMA complexes at the cortex must be properly regulated to orient the spindle (Du and Macara, 2004; Zheng *et al.*, 2010; Kotak, Busso and Gönczy, 2012). In chicken

neuroepithelial cells, the Gαi:LGN:NuMA complexes have been shown to localize in a lateral belt in the equatorial regions of the cortex (Peyre *et al.*, 2011). Similarly, in MDCK cysts LGN localizes at lateral cortical regions above the spindle poles, and its depletion is associated to spindle misorientation and multiple-lumen cyst formation (Zheng *et al.*, 2010). Which mechanisms organize and maintain the lateral organization of LGN is not fully understood. As already discussed in paragraph 1.2.2, live-imaging experiments performed in HeLa cells indicated that a Ran-GTP gradient excludes NuMA and LGN from the regions above the metaphase plate, confining them at cortical regions over the spindle poles (Kiyomitsu and Cheeseman, 2012). Studies in MDCK cysts revealed that the apical polarity protein aPKC (Atypical Protein Kinase C) phosphorylates Serine 401 in the LGN linker region, this way increasing the affinity of LGN for a 14-3-3 protein (Hao *et al.*, 2010). 14-3-3 competes with Gαi-GDP for LGN binding, leading to its release from the apical site and its localization to the lateral regions, where it can recruit NuMA (Hao *et al.*, 2010) to orient planar divisions. Furthermore, the association of phosphorylated LGN with the baso-lateral membrane associated protein Dlg1 (Disc Large 1) has been implicated in the regulation of cortical LGN localization in several systems, including *Drosophila* epithelium and chicken neuroepithelium (Bergstralh, Lovegrove and St Johnston, 2013; Saadaoui *et al.*, 2014).

1.3.2 Spindle orientation in asymmetric cell division

In epithelial tissues, asymmetric stem cell division can be described as a process in which the mitotic spindle aligns with the polarity axis, ensuring unequal partioning of cellular components, often referred to as fate determinants, and asymmetric inheritance of niche contacts between daughters (Morin and Bellaïche, 2011; Fuchs and Chen, 2012). In a simple model, asymmetric cell division is often described as a three steps process in which: 1) an apico-basal polarity axis is established or inherited by the tissue; 2) fate determinants localize asymmetrically at the cortex, and 3) the mitotic spindle aligns parallel to the apico-basal

polarity axis (Morin and Bellaïche, 2011). The mechanisms of asymmetric cell divisions have been extensively studied in invertebrates, from *Drosophila* neuroblast to *C. elegans* zygote, and then further explored in vertebrate neuroepithelial cells and basal skin progenitors (Betschinger and Knoblich, 2004; Gönczy and Rose, 2005; Siller and Doe, 2009; Peyre and Morin, 2012; Kulukian and Fuchs, 2013). In all these systems, cues from the cell cortex are transmitted to the mitotic spindle through the cortical force generators dynein/dynactin assembled on Gαi:LGN:NuMA complexes, in an evolutionary conserved mechanisms. While the mechanisms of force generation are highly conserved, the localization of polarity proteins and microtubules-associated proteins varies in different systems. Studies conducted over two decades ago in *Drosophila* neuroblasts paved to way for the identification of spindle orientation proteins, revealing that the dividing cells delaminate from the neuroepithelium and give rise to one self-renewing neuroblast that remains attached to the epithelium, and one small ganglion mother cell (GMC) that subsequently divides to generate neurons of the adult fly brain (Ito and Hota, 1992; Knoblich, 2010) (Figure 9A). Neuroblasts represent an example of intrinsic asymmetric cell division, in which the cell autonomously polarizes the cortex, even in isolated cells in culture. After cell division, the fate determinants Numb, BRAT and Prospero are confined in the differentiating cell (Kraut *et al.*, 1996). This localization is driven by two adaptors, PON (Partner of Numb) which recruits Numb, and Miranda, which binds to BRAT and Prospero (Knoblich, Jan and Jan, 1995). Asymmetric localization of fate determinants requires also another set of proteins accumulating at the apical cortex, that are the Par proteins Bazooka:Par6:aPKC. Par proteins localize at the apical cell cortex before mitosis, together with the adaptor protein Inscuteable, which recruits Pins (Partner of Inscuteable), the *Drosophila* counterpart of LGN (Kraut *et al.*, 1996; Schober, Schaefer and Knoblich, 1999; Wodarz *et al.*, 1999). In this system, loss of Mud (NuMA counterpart in flies), Pins or Inscuteable compromises spindle positioning and leads defects in the asymmetric division (Kraut *et al.*, 1996; Izumi *et al.*, 2006; Siller, Cabernard and Doe, 2006). *Drosophila* Mud

mutants fail to orient the spindle with the polarity axis, and overproliferate by symmetric divisions, confirming that proper distribution of fate determinants and microtubules motors is a prerequisite for the asymmetric outcome of the division (Bowman *et al.*, 2006; Siller, Cabernard and Doe, 2006; Cabernard and Doe, 2009). Similarly, depletion of LIN-5 (NuMA) and GPR1-2 (LGN) in *C. elegans* zygote (Figure 9B) results in failure of the asymmetric division, and in the generation of two identical daughter cells (Gotta *et al.*, 2003; Srinivasan *et al.*, 2003; Park and Rose, 2008). As neuroblasts, *Drosophila* germ-line stem cells (GSCs) self-renew by asymmetric divisions, orienting the mitotic spindle perpendicular to the niche (Knoblich, 2008). In GSCs however, the asymmetry is not intrinsic as in the neuroblast, but relies on contacts to the *niche* constituted by somatic cells that maintain the Jak-STAT signaling active in neighboring stem cells (Yamashita, Jones and Fuller, 2003).

In known vertebrate stem cells such as skin progenitors and neural stem cells, cell division orientation can be switched during development, moving from symmetric proliferative divisions to asymmetric differentiative divisions (Lechler and Fuchs, 2005; Williams *et al.*, 2011). One of the best characterized system to study asymmetric divisions in vertebrates is the mammalian skin, a stratified epithelium in which in early stages of development symmetric divisions allow an amplification of the stem cell pool increasing the surface area of the epithelium, followed by a second phase characterized by asymmetric divisions, which generate cellular diversity (Lechler and Fuchs, 2005; Poulson and Lechler, 2010b; Williams *et al.*, 2011; Fuchs, 2016) (Figure 9C). During embryonic development, murine epidermal progenitors reside in a single basal layer attached to the basement membrane via integrins contacting each other through adherent junctions (Clayton *et al.*, 2007; Fuchs, 2016). Williams and Fuchs demonstrated that at early stages of skin developments, murine basal progenitors divide planarly by aligning the mitotic spindle parallel to the basement membrane, to expand the epithelium. At later stages, division switch from planar to vertical, and cells divide with the mitotic spindle perpendicular to the epithelial plane, to allow skin stratification (Williams *et al.*, 2011).

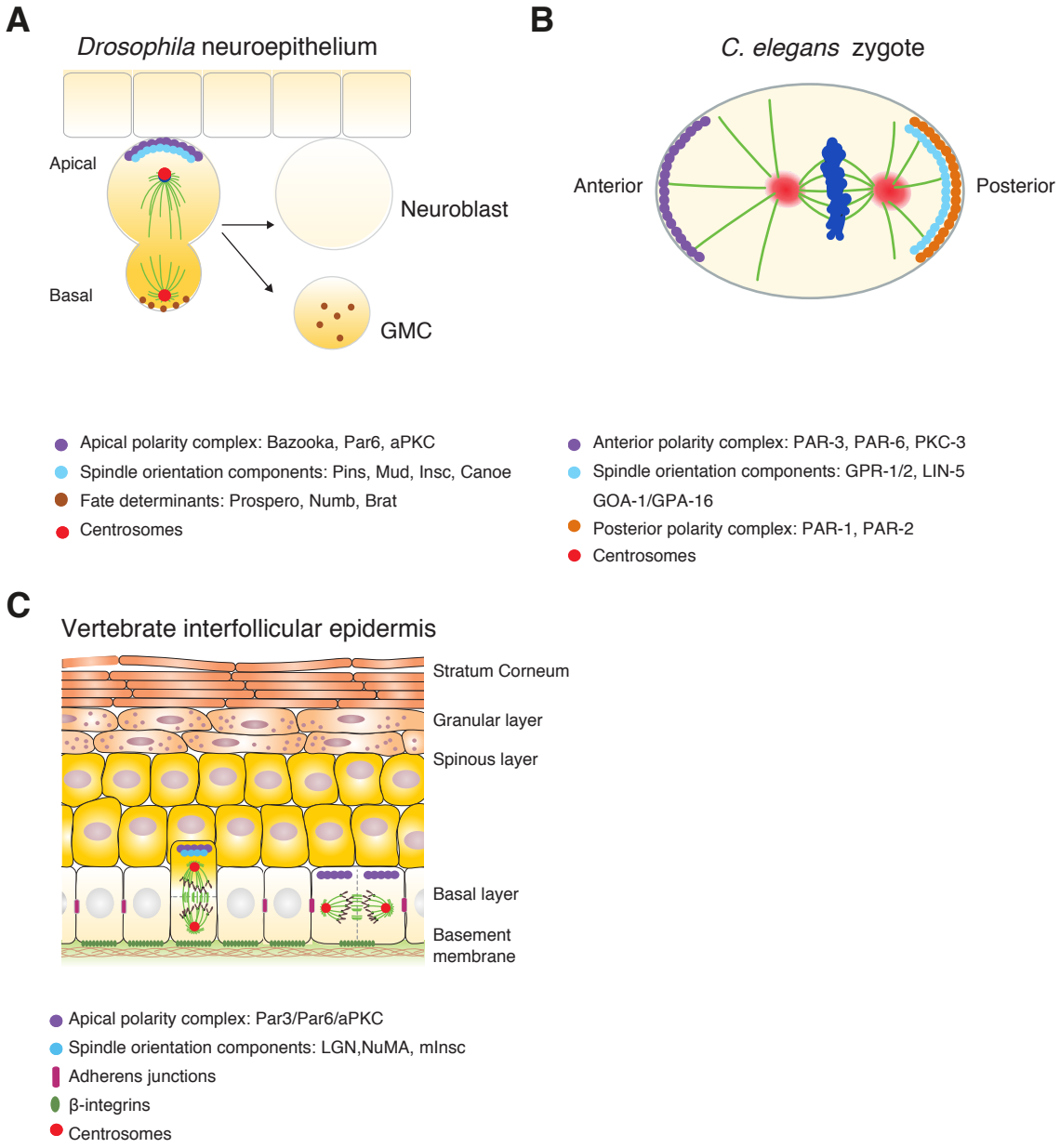

Figure 9 – Spindle orientation in asymmetric cell divisions

(**A**) Asymmetric cell division in *Drosophila* neuroepithelium, in which the diving cell delaminates from the epithelium and originates two different daughter cells: the small ganglion mother cell (GMC), which inherits the fate determinants and differentiate into a neuron, and the large neuroblast, which inherits the apical polarity complex (purple) and spindle orientation components (cyan), maintaining the stemness. (**B**) ACD in *C. elegans* zygote. Zygote polarizes along an anterior-posterio axis, through the segregation of PAR-3/PAR-6/PKC-3 at the anterior cortex and PAR-1/PAR-2 at the posterior. Spindle orientation is coupled to atero-posterior polarity via asymmetric localization of LIN-5/GPR1-2 at the posterior cortex. (**C**) Switch from symmetric proliferative to asymmetric differentiative divisions in murine skin. In the first stages of development stem cells are attached to the basement membrane (*niche*) via integrins (green) and adherens junctions (magenta), and divide through planar divisions. At later developmental stages, division switch from planar to vertical. In vertical ACDs, the mitotic spindle is oriented perpendicular to the plane of the epithelium, and

generate a basal progenitor which remain attached to the niche and a suprabasal initiating a Notch-dependent differentiation program.

These asymmetric divisions generate a basal stem cell and a suprabasal cell that will differentiate in a Notch-dependent manner. Molecularly, the players underlying this switch in the orientation of cell divisions are the same, and include mammalian Inscuteable (mInsc), aPKCλ, Gα LGN, NuMA and dynein/dynactin, which localize apically in dividing skin progenitors (Lechler and Fuchs, 2005; Niessen *et al.*, 2013). Ablation of LGN, NuMA or dynactin on the developing skin by in-utero electroporation of shRNA at E9.5 mice affects perpendicular division of stem cells and precludes skin stratification process (Williams *et al.*, 2011). Consistently, ablation of aPKCλ results in altered skin differentiation and loss of hair follicle stem cells (Niessen *et al.*, 2013).

A similar situation is found in vertebrate neuroepithelium, were neuroepithelial cells divide by planar divisions before switching to asymmetric division mode (Götz and Huttner, 2005). However, in this system, mechanisms of oriented divisions are less clear, probably due to the complexity of morphological organization of the tissue. Live-imaging experiments showed that ablation of LGN in mouse neural progenitors randomizes the division plane (Konno *et al.*, 2007). Similarly, in chicken neuroepithelium loss of LGN randomizes spindle orientation leading to the loss of neuroepithelial cells from the ventricular zone (Morin, Jaouen and Durbec, 2007).

1.4 Gαi:LGN:NuMA-independent pathways

1.4.1 Planar cell polarity pathway

Within tissues, cells are exposed to a combination of intrinsic signals and external stimuli that can influence the orientation of cell division. Recently, the Wnt signaling pathway has been identified as regulator of mitotic spindle orientation in invertebrates and in mammals (Segalen and Bellaïche, 2009; Ségalen *et al.*, 2010). Two different pathways have been described, the canonical and the non-canonical or planar cell polarity (PCP) pathway. The main effector of the Wnt-pathway is the cytoplasmic scaffolding protein Dishevelled (Dvl), which is activated upon binding of Wnt-ligands to the receptor Frizzled (Fz). In vertebrates, three isoforms of Dvl exists, Dvl1, Dvl2 and Dvl3, all sharing a common domain structure consisting of a DIX domain followed by a PDZ and a DEP domain (Figure 10A). In the Wnt-canonical pathway, the binding of Dvl to Fz recruits the destruction complex at the membrane, preventing the degradation of the transcription factor β-catenin and its translocation into the nucleus. In the PCP pathway instead, the interaction of Dvl to Fz activates a signaling cascade leading to actin-cytoskeleton rearrangements (MacDonald, Tamai and He, 2009). The role of PCP signaling in spindle orientation has been well characterized in *Drosophila* sensory organ precursor (SOP) and in zebrafish embryo by Ségalen and Bellaiche (Ségalen *et al.*, 2010). In *Drosophila* SOP cells, Dsh and Mud (*Drosophila* Dvl and NuMA counterparts) are localized at the posterior cortex, while Pins (the fly LGN) is enriched at the anterior side. In this system, spindle axis position is controlled in both apico-basal orientation by the Pins complex, while the antero-posterior orientation is regulated through the Fz/Dsh signaling pathway. The relevance of the Wnt pathway in orienting the spindle in *Drosophila* has been investigated by exploiting the so-called “induced cell polarity” assay in S2 cell-doublets. In this system, the junction protein Echinoid is used to localize a protein or a domain to the cell-cell contacts between cell pairs. Then, the orientation of the mitotic spindle compared to the cell-cell junction domain is

measured (Johnston *et al.*, 2009). Segalén and colleagues demonstrated that ectopic targeting of the DEP domain of Dsh at the cortex of S2 cells is sufficient to orient the spindle, and that Dsh acts upstream Mud/dynein to promote spindle orientation. In addition, they demonstrated that the PCP pathway modulates spindle orientation in a context of tissue morphogenesis, showing that both NuMA and Dvl are necessary to orient the spindle along animal-vegetal axis during zebrafish gastrulation (Ségalen *et al.*, 2010). The requirement of a Mud/Dsh interaction was further confirmed by data presented by Johnston and colleagues, which demonstrated that two Dsh-related pathways cooperate to orient the spindle in flies S2 cells. One involves Pins and Mud, while a second pathway involves the F-actin binding protein Canoe, that binds to the C-terminus of Dsh and regulates cortical F-actin through the downstream regulators Rho, RhoGEF2 and Diaphanous (Johnston *et al.*, 2013). Of the three Dvl isoforms identified in vertebrates, two have been implicated in spindle orientation in mammalian cells in culture. In particular, Dvl2 has been shown to localize at the spindle poles and at kinetochores of HeLa S3 cells, where it regulates mitotic spindle orientation and microtubules attachment to kinetochores (Kikuchi *et al.*, 2010). Dvl2 role in orienting the spindle depends on Plk1 phosphorylation on Thr206, as the expression of a phospho-mutant Dvl2 does not rescue spindle orientation (Kikuchi *et al.*, 2010). Consistently, ablation of Dvl2 in HeLa S3 cells leads to randomized spindle orientation and chromosomes misalignment (Kikuchi *et al.*, 2010). Also the Dvl3 isoform has been involved in orienting the spindle in HeLa cells. In this case, its functions depend on the interaction with NuMA, and are enhanced by the activity of the deubiquitinase CYLD, that increases the NuMA:Dvl3 interaction through the removal of ubiquitin chains from Dvl3, promoting cortical recruitment of NuMA and motor proteins (Yang *et al.*, 2014). Consistently, biochemical data showed that ubiquitination of the DIX domain of Dvl2 suppresses its polymerization, which is essential for signalosome assembly and Wnt pathway activation (Bienz, 2014; Madrzak *et al.*, 2015). How the Dvl3/NuMA pathway integrates with the requirement of LGN for cortical recruitment of NuMA during metaphase would need further investigation.

Last, localized Wnt signals have been recently shown to drive asymmetric cell divisions in embryonic stem cells in culture. In this system, elegant studies with Wnt-3a coated-beads induce asymmetric localization of Wnt-pathway components such as β-catenin and APC near the bead, and instruct mitotic spindle orientation perpendicularly to the Wnt-bead (Habib *et al.*, 2013).

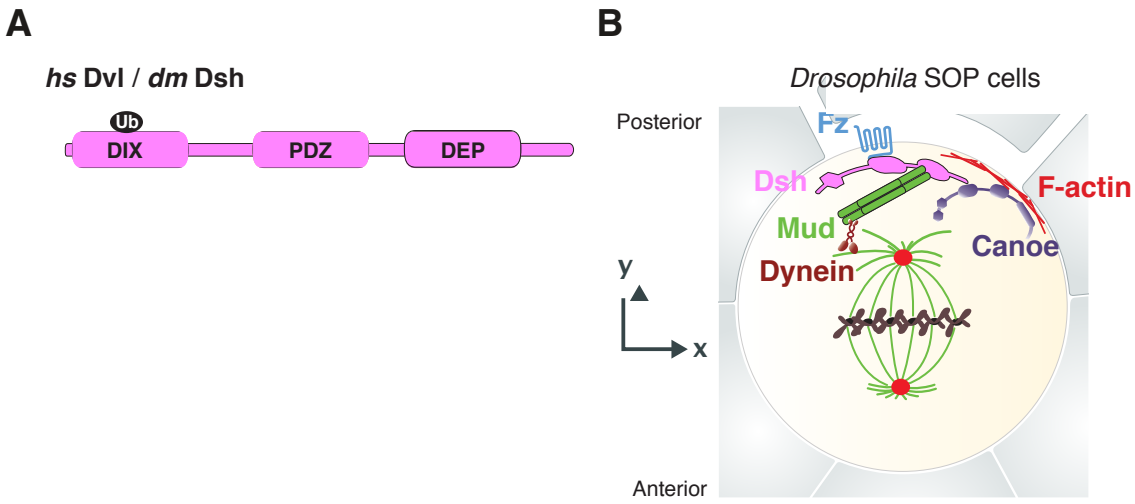

Figure 10 – *Drosophila* Dishevelled/Mud pathway in SOP divisions

(**A**) Conserved domain structure of human (Hs Dvl) and *Drosophila* (Dm Dsh) Dishevelled. Dishevelled proteins consist of a N-terminal DIX domain lying a ubiquitination site (black) followed by a PDZ and a DEP domain. (**B**) Model of planar division in *Drosophila* SOP. Upon ligand binding and Fz (cyan) receptor activation, Dsh (pink) is recruited at the posterior side of the cell. Here, Dsh recruits Mud (green) via its DEP domain and Canoe (purple), promoting spindle orientation.

1.4.2 Role of cell geometry and external forces

1.4.2.1 Cell geometry and acto-myosin cortex in spindle orientation

In epithelial tissues, cell shape and cortical tension have been also implicated in determining the mitotic spindle placement. At the end of 19th century, Oscar Hertwig observed that in sea urchin embryos the mitotic spindle was place at the center of the mass and perpendicularly to the long axis, formulating the "Hertwig rule" (Hertwig, 1884). However, deformation of the embryos shape resulted in modification of the spindle position, which aligned

accordingly to the elongated axis, suggesting that cells and the mitotic spindle can sense shape changes in response to external forces. In the last decades, this rule has been confirmed also in mammalian cells, although in a more complicated scenario. Artificially deformed rat cells dot not round up in mitosis, and divide along their longest axis during anaphase (O'Connell and Wang, 2000). However, despite the Hertwig rule can be applied to most shapes, specific shape with imperfect rounding does not conform to these predictions, raising to question of how force generators activities are integrated with cell shape (Minc, Burgess and Chang, 2011). Recent *in vitro* and *in vivo* experiments demonstrated that cell shape can directly influence the spindle orientation independently of cortical force generators, and that the knockdown of force generators does not completely randomize the spindle, with cells keeping dividing with a strong bias towards the main axis of elongation (Williams *et al.*, 2014; Lázaro-Diéguez, Ispolatov and Müsch, 2015).

In addition to intrinsic cortical cues, a new role for the mitotic actin cytoskeleton in spindle orientation is starting to emerge. At mitotic entry, the actin cytoskeleton undergoes dramatic rearrangement in a process known as mitotic cell rounding, in which cells organize a stiff acto-myosin cortex, and partially detach from the substrate to assume a more spherical shape (Lancaster and Baum, 2014). In epithelial tissues, mitotic round up is accompanied by reorganization of adherens junctions (Lancaster and Baum, 2014). Mitotic round-up is essential to establish a cell geometry that provides space for mitotic spindle formation and stiffness to counterbalance forces exerted by cortical motor proteins on the astral microtubules (Pietro, Echard and Morin, 2016). The cell cortex consists of a cross-linked network of actin, myosin and associated proteins such as members of the ezrin/radixin/moesin (ERM) family. ERM proteins are a family of actin membrane cross-linkers, required for correct mitotic spindle orientation in both flies and mammalian cells in culture. In HeLa cells, ERM proteins are activated at mitotic entry by phosphorylation from the Ste20-Like kinase (SLK) (Machicoane *et al.*, 2014). Notably, depletion of ERM proteins or impairment of their activation affects LGN and NuMA cortical recruitment, while no

effect was observed on Gαi localization, somehow implying that cortical integrity is a prerequisite for spindle motor recruitment and activity. In addition, overactivation of ERM perturbs NuMA localization at the cortex (Machicoane *et al.*, 2014). Molecularly, the ERM protein moesin has been reported to directly interact with microtubules, and to anchor astral MTs to the cell cortex (Solinet *et al.*, 2013). Consistently, depletion of moesin or impairment of its activation leads to cortical instability in both metaphase and anaphase cells and alters mitotic spindle length. Besides ERM proteins, other actin-associated proteins have been identified as mediators of the crosstalk between the acto-myosin cytoskeleton and the MTs. Among these, the actin-binding protein MISP has been reported to regulate spindle orientation in HeLa cells in a Plk1-dependent manner, possibly affecting astral MTs organization. In addition, MISP interact with $p150^{Glued}$,and regulate its cortical distribution (Zhu *et al.*, 2013). We recently showed that the actin-binding protein Afadin is involved in spindle orientation (Carminati *et al.*, 2016). The role of Afadin was initially described in *Drosophila* neuroblast, where Canoe (the Afadin counterpart in flies) is required for spindle alignment and Mud cortical recruitment. Consistently, we recently show that in HeLa cells Afadin knockdown affects cortical recruitment of LGN, NuMA and dynactin, and misorients the spindle in both HeLa and Caco-2 cyst. Afadin competes with NuMA for LGN interaction, although its affinity is lower. To explain spindle orientation functions of Afadin in spite of its competition with NuMA, we speculate that at mitotic entry Afadin instructs the localization of MTs-motors by simultaneous binding to cortical F-actin and LGN, and in presence of the high-affinity ligand NuMA, LGN dissociates from Afadin and recruits NuMA at the cell cortex (Carminati *et al.*, 2016).

ERM proteins and F-actin filaments are also part of tubular structures protruding from cell membrane called “retraction fibers”, which maintain rounded cells partially attached to the substrate during mitosis (Fink *et al.*, 2011). Recently, Kwon and colleagues reported that in mitotic cells actin is organized in subcortical clouds (Kwon *et al.*, 2015). These structures, defined as “actin clouds”, form in an Arp3-dependent manner and contribute to spindle

orientation through the actin motor Myosin-10. Interestingly, depletion of Myosin-10 reduce MTs interaction with the cell cortex and increase astral MTs dynamics, suggesting that Myosin-10 localized by actin acts as a bridge between actin and astral microtubules, this way regulating spindle orientation through the modulation of MTs dynamics.

1.4.2.2 Role of junctions in spindle orientation

Besides polarity cues and physical constrains within tissue, other external signals such as cell-extracellular matrix (ECM) and cell-cell junctions contribute to spindle orientation. Cell adhesion to ECM determines spindle orientation in both polarized and unpolarized systems. As reported in paragraph 1.3.1, HeLa cells plated on fibronectin orient the spindle in a β1-integrin-dependent manner (Toyoshima and Nishida, 2007). In addition, loss of β1-integrin in mouse epithelial cells causes spindle randomization (Lechler and Fuchs, 2005).

Several lines of evidence reported that intercellular junctions are maintained throughout divisions (Baker and Garrod, 1993; Reinsch and Karsenti, 1994; Théry *et al.*, 2005). In MDCK cells in monolayer and in keratinocytes *in vivo*, E-cadherins are maintained laterally (Baker and Garrod, 1993; Reinsch and Karsenti, 1994). Moreover, analysis of the junctional protein ZO-1 localization further confirmed these data, revealing that tight junctions are maintained during all stages of mitosis (Reinsch and Karsenti, 1994). In murine skin the absence of α-catenin causes the loss of cortical Par3 and LGN, randomizes NuMA localization at the cortex, and leads to spindle misorientation (Lechler and Fuchs, 2005). Consistently, experiments performed in MDCK cysts showed that several cell-cell junction molecules control spindle orientation, including the tight junctions molecule JAM-A (Junctional Adhesion Molecule-A), E-cadherin and Plexin/Semaphorin, whose depletion is associated to epithelial morphogenesis defects (den Elzen *et al.*, 2009; Tuncay *et al.*, 2015; Xia *et al.*, 2015; Pietro, Echard and Morin, 2016). In addition, studies in *Drosophila* uncover the role of tricellular junctions (TCJs, the point in which three cells take contacts) in guiding

spindle orientation independently of Gαi:LGN:NuMA pathway (Bosveld *et al.*, 2016) (Figure 11). Specifically, in fly pupal notum, Mud starts accumulating at TCJs from G2 phase. When the cell round-up, Mud position at the cortex is reminiscent of the position of Mud at TCJs in interphase, and acts as a polarity cue to instruct mitotic spindle orientation along the interphase cell shape. Notably, this mechanism cannot be transferred in vertebrates, where NuMA displays a nuclear localization in interphase, suggesting that alternative ways to link interphase positional cues with NuMA-containing force generators and the mitotic spindle axis exists.

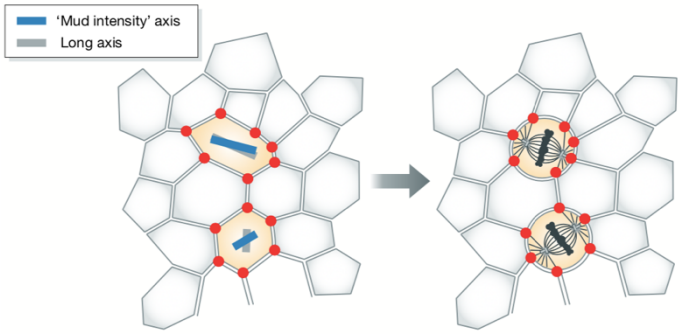

Figure 11 – Role of cell tension during interphase

Cartoon representing *Drosophila* notum epithelium. In epithelial cells, Mud accumulates at tricellular junctions (red dots) starting from G2 phase. The mitotic spindle aligns towards Mud clusters. The "Mud intensity axis" predicts the orientation of cell division. *Adapted from di Pietro F., EMBO reports, 2016.*

As the topic of this thesis concerns the characterization of NuMA:LGN interactions and the investigation of NuMA interaction with microtubules, in the last part of this introduction I will focus on the protein NuMA and on Aurora-A, a mitotic kinase we recently showed to be involved in regulating NuMA localization during mitosis.

1.5 NuMA

Human Nuclear Mitotic Apparaturs protein NuMA is a 238 kDa protein identified in 1980 as a high molecular mass component of the nuclear matrix. Notably, its nuclear functions are still largely unclear because most of studies focused on the mitotic activities of NuMA in complex with dynein (Lydersen and Pettijohn, 1980). In fact, during mitosis NuMA has been reported to localize at the spindle poles and at the cell cortex, where it contributes to mitotic spindle assembly and orientation.

1.5.1 NuMA in mitosis

NuMA is a master regulator of mitosis, and it is implicated not only in spindle orientation, but also in mitotic spindle assembly. After nuclear envelope breakdown, NuMA dissociates from importin-β in a Ran-dependent manner (see paragraph 1.2.2 for details), and drives the assembly of mitotic spindle close to the chromosomes (Nachury *et al.*, 2001). In the first stages of mitosis, NuMA contributes to spindle poles focusing and organization (Merdes *et al.*, 1996; Khodjakov *et al.*, 2003; Silk, Holland and Cleveland, 2009). Specifically, NuMA tethers spindle microtubules at the spindle poles working in association with cytoplasmic dynein, whose motor functions allows NuMA transport along the MTs. NuMA:dynein complexes crosslink parallel kinetochore MTs, and focus MTs minus ends at the spindle poles together with interpolar MTs (Khodjakov *et al.*, 2003). Studies in HeLa cells and *Xenopous* extracts demonstrated that NuMA acts independently of centrosomes in spindle pole focusing. Although NuMA acts redundantly to centrosomes in the early phases of spindle assembly, its activity becomes essential for spindle maintenance. Indeed, in HeLa cells and fibroblasts NuMA depletion results in defects in chromosome alignment, poles misorganization, and dissociation of centrosomes from MTs-minus ends (Merdes *et al.*, 1996; Haren *et al.*, 2009; Silk, Holland and Cleveland, 2009). Consistently, primary fibroblasts derived from mice depleted of exon-22 (see paragraph 1.5.2) displayed unfocused

spindle poles and centrosomes detachment from k-fibers (Silk, Holland and Cleveland, 2009). A recent work from the Doumont lab showed that NuMA is required for force generation at microtubules minus-ends, and that its knockdown impairs dynactin localization at the poles, suggesting that NuMA targets dynein/dynactin to minus-ends to cluster spindle MTs into poles (Hueschen *et al.*, 2017). Although in mitosis the bulk of NuMA localizes at the spindle poles, a pool of NuMA is recruited at cortical regions above the spindle poles via direct interaction with LGN and with the cell cortex (Du *et al.*, 2002; Seldin *et al.*, 2013; Kotak, Busso and Gönczy, 2014). Cortical NuMA is in turn responsible for dynein/dynactin recruitment, and regulates mitotic spindle orientation. The amount of NuMA at the cortex is tightly regulated by several phosphorylation events (Figure 12). We recently showed that in metaphase Aurora-A kinase regulates the balance of NuMA at the cortex and at the spindle poles by phosphorylating Ser1969 of NuMA in HeLa cells in metaphase. Consistently, Alanine-mutation of this phosphosite prevents NuMA cortical recruitment and results in its accumulation at the spindle poles (Gallini *et al.*, 2016). A second phosphorylation of NuMA by Aurora-A on Ser2047 seems to play a role in modulating cortical levels of NuMA, with a molecular mechanism that still remains unclear (Gallini *et al.*, 2016). Also Plk1 phosphorylates NuMA and dynein/dynactin to dissociate the complex (for details, see paragraph 1.2.2). In HeLa cells and mouse keratinocytes, the ABL1 kinase has been shown to regulate NuMA cortical localization through the phosphorylation of Tyr1774 (Matsumura *et al.*, 2012). This phosphorylation would favor NuMA recruitment by cortical LGN, through an unknown mechanism. Finally, a recent work from the Johnston lab showed that the Hippo-pathway kinase Warts phosphorylates Ser1868 within the coiled-coil of Mud and that this mechanisms might be conserved in vertebrates (Dewey, Sanchez and Johnston, 2015). Molecularly this Mud phosphorylation would relieve the interaction between the coiled-coil and the C-terminal portion of Mud, exposing the Pins binding domain, though no direct evidence for this mechanism have been provided.

In anaphase, NuMA amount at the cortex starts increasing, and results in an additional enrichment of cortical dynein/dynactin that promotes the generation of robust pulling forces for sister chromatids segregation and spindle elongation. Until metaphase, Cdk1-mediated phosphorylation of Thr2055 inhibits the direct association of NuMA with the lipids bilayer, possibly by electrostatic repulsion between negative charges of the phosphor-groups (Kotak, Busso and Gönczy, 2013; Zheng *et al.*, 2013; Kotak and Gönczy, 2014). Ckd1 activity is counterbalanced by the activity of the phosphatase PP2CA (Kotak, Busso and Gönczy, 2013). After metaphase to anaphase transition, cyclinB degradation results in Cdk1 inactivation. PP2CA remains instead active, dephosphorylating NuMA and promoting LGN-independent targeting at cortex.

Collectively, this evidence demonstrated that NuMA localization during mitosis in finely regulated, in order to achieve correct spindle assembly and positioning until metaphase and spindle elongation in anaphase.

1.5.2 NuMA domain structure

NuMA is a 2115 residues protein, composed by a N-terminal globular domain linked to the C-terminal unstructured tail region by a long coiled-coil domain (Figure 12). During mitosis, NuMA associates with dynein/dynactin through its N-terminal region (Kotak, Busso and Gönczy, 2012). Immunoprecipitation (IP) experiments show that the portion of NuMA encompassing residues 1-705 can co-IP both the dynein intermediate chain (DIC) of dynein and the $p150^{Glued}$ subunit of dynactin (Kotak, Busso and Gönczy, 2012). Notably, in HCT-116 cells light-induced cortical targeting of NuMA-1-705 results in dynein/dynactin recruitment at the cortex, but is not sufficient to generate pulling forces (Okumura *et al.*, 2018), suggesting that a supramolecular organization of force generators is required. Beside dynein/dynactin interaction, the functions of the N-terminal portion of NuMA are poorly characterized.

The C-terminal portion of NuMA has been instead extensively studied, and harbors lipid binding domains (Zheng *et al.*, 2013; Kotak, Busso and Gönczy, 2014), a nuclear localization signal (NLS) (Gueth-Hallonet, Weber and Osborn, 1996), two microtubules-binding domains (Du *et al.*, 2002; Gallini *et al.*, 2016), an LGN-binding region (Du *et al.*, 2002; Zhu *et al.*, 2011). and a 4.1-bindin region (Mattagajasingh, Huang and Benz, 2009). Studies from the Macara lab led to the initial identification of the region of NuMA involved in the interaction with LGN, encompassing residues 1892-1924 (Du *et al.*, 2002) (numbers refers to the long isoform-1 of human NuMA, which is 2115-residues long) . In a more recent work, the crystal structure of the LGN in complex with the shortest NuMA fragment retaining nanomolar affinity has been described, showing that residues 1899-1926 of NuMA binds to the to the inner groove of the TPR domain of LGN, and defining residues 15-350 as the determinants of the interaction (Zhu *et al.*, 2011) (see paragraph 1.2.1 for details). One of the most studied NuMA functions is its ability to interact with microtubules. Experiments performed with *Xenopous* extracts revealed that the C-terminus of NuMA encompassing residues 1994-2253 can induce the formation of MTs bundles (Merdes *et al.*, 1996). Later studies confirmed that a conserved region in the C-terminal part of human NuMA can directly associate with taxol-stabilized MTs through a region spanning residues 1914-1985, which has been identified as the minimal domain required for MTs binding (Du *et al.*, 2002; Haren and Merdes, 2002). Notably, this NuMA MTs-binding domain overlaps with the LGN-binding region, and suggested that LGN and MTs interactions are mutually exclusive, and raising the question of how they compete for NuMA binding. In the same study by Du and colleagues, co-sedimentation experiments with the fragment of NuMA encompassing residues 1580-2115 in the presence of the TPR domain of LGN indicated that binding of LGN to NuMA inhibits NuMA interaction with MTs. In addition, the ability of NuMA-1914-1985 to induce MTs bundling was inhibited by LGN-TPR, overall supporting the hypothesis of the mutually exclusive binding (Du *et al.*, 2002). The functional role of the MTs-binding domain was further analyzed in mouse and human cells by depleting a region

corresponding to the NuMA gene which encodes for the MTs binding domain (Silk, Holland and Cleveland, 2009; Gallini *et al.*, 2016; Seldin, Muroyama and Lechler, 2016). Analysis of primary cell lines derived from mice carrying an heterozygous mutation in the NuMA exon-22 revealed that the MT-binding region of NuMA identified by Merdes is required for spindle poles focusing, and MTs attachment to kinetochore, and that its depletion results in impaired NuMA localization at the poles and spindle misorientation (Silk, Holland and Cleveland, 2009; Seldin, Muroyama and Lechler, 2016). Depletion of the corresponding region in HeLa cells (exon-24 in human, encompassing residues 1944-2003) results in an impaired NuMA localization at the spindle poles (Gallini *et al.*, 2016). Recently, we reported that a second MT-binding region of NuMA exists at the C-terminus of the protein, that is compatible with concomitant binding of NuMA to LGN and to MTs, and efficiently promotes microtubules bundling, whose functions were still uncharacterized (Gallini *et al.*, 2016). Interestingly, while we were characterizing this newly identified MTs-binding region, Okumura and colleagues reported that this region of NuMA is required for the generation of pulling forces that allow to displace the mitotic spindle (Okumura *et al.*, 2018). Chang and colleagues reported that the interaction of NuMA with microtubules is suppressed by steric blockage of importin-β mediated by importin-α, which binds to a region of NuMA spanning residues 1970-2101 (Chang *et al.*, 2017).

Recent studies identified in the C-terminal portion of NuMA two phospholipid-binding domains that allow direct targeting of NuMA at the cortex during anaphase (Zheng *et al.*, 2013; Kotak, Busso and Gönczy, 2014). In particular, the region of NuMA encompassing residues 1996-2074 was first implicated in NuMA cortical localization in a Cdk1-dependent manner (Zheng *et al.*, 2013) (see paragraph 1.5.2). Functionally, direct binding of NuMA to the phospholipid membrane in anaphase would increase the accumulation of MT-pulling motors above the spindle poles to sustain spindle elongation and sister chromatid separation. Studies from the Cheeseman and Lechler laboratories identified a second region involved in NuMA targeting at the membrane, which spans residues 1788-1810, directly associating

with 4.1 R (Mattagajasingh, Huang and Benz, 2009; Kiyomitsu and Cheeseman, 2013; Seldin *et al.*, 2013). Consistently, FRAP experiments showed that a NuMA mutant lacking the 4.1 binding-domain displays increased mobility at the cell cortex (Seldin *et al.*, 2013). However, later studies by Kotak and colleagues revealed that loss of cortical NuMA upon 4.1 G/R depletion might result from indirect effects of cortical disruption. In the same study the authors proposed that the region containing the 4.1 G/R binding site, encompassing residues 1699-1876, is an additional phosphoinosities binding region (Kotak, Busso and Gönczy, 2014). More recently, studies from Okumura and Kiyomitsu uncovered the important function of the C-terminal portion of NuMA, encompassing residues 1700-1801, that in metaphase promotes NuMA assembly in specialized structures required to produce spindle pulling forces (Okumura *et al.*, 2018). Notably, this "clustering domain" of NuMA contains a Cdk1 consensus site which is highly conserved throughout species, whose mutation or depletion impairs NuMA clusterization and spindle orientation (Okumura *et al.*, 2018).

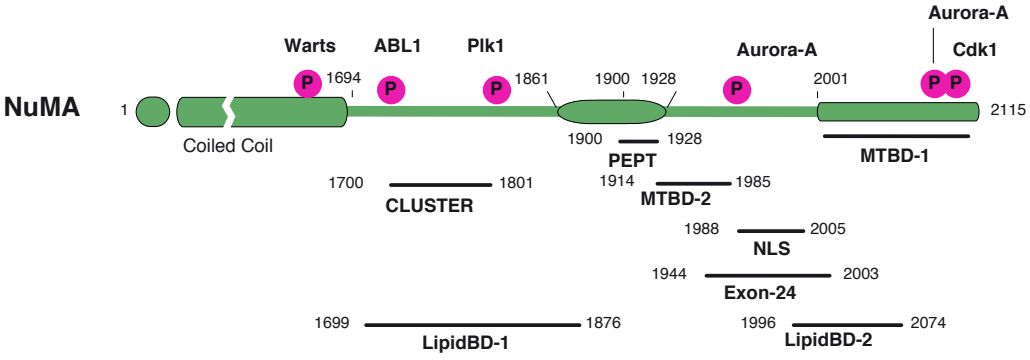

Figure 12 – Domain structure and phosphosites of human NuMA

ABL1 phosphosite on Tyr1774 (ABL1): Matsumura, Nat Commun, 2012

Aurora-A phosphosites on Ser1969 and Ser2047 (Aurora-A): Gallini, Curr Biol, 2016

Clusterization domain (CLUSTER): Okumura, eLife, 2018

Lipid binding domain (LipidBD–1): Kotak, EMBO J., 2014

Lipid binding domain (LIPIDBD–2): Zheng, MBoC, 2013

Nuclear localization signal (NLS): Gueth–Hallonet, Exp. Cell Res., 1996

NuMA Peptide (PEPT): Zhu, Mol. Cell, 2011

Microtubules binding domain (MTBD–1): Gallini, Curr Biol, 2016

Microtubules binding domain (MTBD–2): Du & Macara, Curr Biol, 2002

Plk1 phosphosite on Ser1833 and Ser1834 (Plk1): Sana, Life Sci Alliance, 2018
Warts phosphosite on Thr1677 (Warts): Dewey, Curr Biol, 2016

1.5.3 NuMA in interphase

During interphase NuMA localizes into the nucleus as a component of the nuclear matrix, with the exclusion of the nucleolar regions (Compton and Cleveland, 1993). However, a recent study showed that NuMA can relocalize to the nucleolus upon induced nucleolar stress, where it contributes in rDNA synthesis (Jayaraman *et al.*, 2017). In interphase, the localization of NuMA depends on importins activity, which binds to the NLS of NuMA (encompassing residues 1988-2005) mediating its nuclear translocation (Gueth-Hallonet, Weber and Osborn, 1996). In the nucleus, NuMA has been reported to show affinity for AT-rich specific DNA domains called MARS (matrix attachment regions), to which it seems to associate through its S\TPXX motifs present in the N- and C-terminal domain (Ludérus *et al.*, 1994). Moreover, NuMA plays a role in chromatin organization and DNA damage response by repairing double strand breaks in conjunction with the SWI/SNF chromatin remodeling complex (Vidi *et al.*, 2014). Electron microscopy studies revealed that NuMA organize oligomeric structures in the nucleus, forming multi-arm oligomers, suggesting that NuMA might play a structural role (Harborth *et al.*, 1999). Although very interesting, these findings are still rather preliminary, and NuMA molecular functions in interphase are still under debate.

1.6 Aurora-A

Aurora-A belongs to the family of Serine/Threonine kinases orchestrating mitotic progression. This family includes Aurora-A, B and C, whose activity peaks in mitosis and ensures proper bipolar spindle assembly, chromosomes segregation and cytokinesis (Vader and Lens, 2008; Nikonova *et al.*, 2013). From the end of the S-phase to the G1 phase of the

following cycle Aurora-A localize on duplicated centrosomes. This localization has been shown to be independent from microtubules, as treatment of *Xenopous* cells with the MTs-depolymerizing drug nocodazole does not change Aurora-A association with centrosomes (Roghi *et al.*, 1998). At mitotic entry Aurora-A is activated by several cofactors and kinases, including Cdk1 and TPX2 (Van Horn *et al.*, 2010; Zorba *et al.*, 2014). Binding of TPX2 to Aurora-A promotes Aurora auto-phosphorylation on Thr288, this way displacing the activation loop from the ATP-binding pocket, and providing access for Aurora-A substrates (Zorba *et al.*, 2014). Aurora-A functions in mitosis strictly correlate with its localization. In prometaphase, it localizes at the spindle poles and along spindle MTs, while from anaphase it accumulates to the central spindle (Nikonova *et al.*, 2013). At the spindle poles, Aurora-A contributes in centrosome maturation and bipolar spindle formation (Dutertre, Descamps and Prigent, 2002; Cowley *et al.*, 2009). Consistently, its depletion in HeLa cells leads to the formation of multipolar spindles and poles fragmentation (Marumoto *et al.*, 2003; Asteriti *et al.*, 2011). During metaphase, Aurora-A has been shown to regulate mitotic spindle orientation in both *Drosophila* and mammalian cells. In *Drosophila* neuroblast, Aurora-A activity promotes spindle orientation along the apico-basal polarity axis (Lee *et al.*, 2006). Its loss-of-function mutations cause aberrant symmetric divisions of neuroblasts and NBs expansion, resulting in a tumor-like proliferation (Lee *et al.*, 2006; Wang *et al.*, 2006). Studies in mammalian cells confirmed that Aurora-A functions in spindle orientation are conserved from invertebrates to mammals. Several studies indicated that chemical inhibition of Aurora-A with MLN8237 induces orientation defects in U2OS, HeLa and RPE-1 cells (Asteriti *et al.*, 2014; Gallini *et al.*, 2016). Notably, we showed that in HeLa cells the misorientation induced by Aurora inhibition can be ascribed to the altered NuMA distribution as the protein is lost from the cortex and accumulates at the poles (Gallini *et al.*, 2016). Aurora-A also works in late mitosis: in anaphase it is found associated to the central portion of the mitotic spindle, while during cytokinesis it localizes to the midbody (Nikonova *et al.*, 2013). The inhibition of Aurora-A during anaphase or the expression of a non-

phosphorylatable form of p150^{Glued} results in central spindle defects (Romé *et al.*, 2010; Reboutier *et al.*, 2013), confirming that Aurora plays a crucial role in controlling the activity of multiple MTs associated proteins.

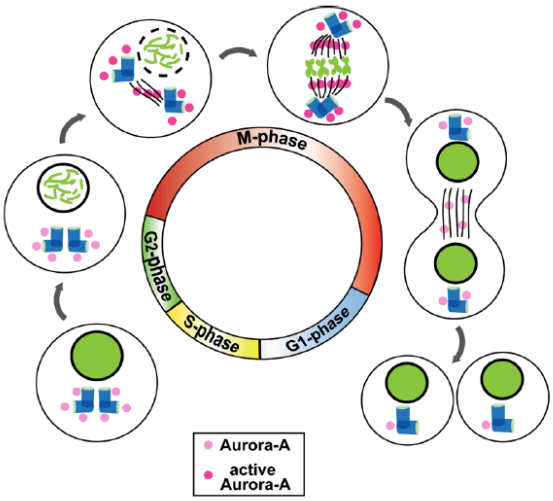

Figure 13 – Aurora–A coordinates mitotic progression

During S-phase, Aurora-A accumulates on duplicated centrosomes, and is activated during G2/M transition. In the first stages of mitosis, Aurora localizes at the spindle poles, while starting from anaphase it localizes on spindle MTs and at the spindle midzone. At the end of mitosis Aurora-A is ubiquitinated and degraded. *Adapted from Nikonova A. S, Cellular and molecular life sciences, 2013*

1.7 Aim of the project

Over the past years, many efforts have been made to elucidate how microtubule motors are recruited to the cell cortex in mitosis to promoting spindle orientation. However, the molecular mechanisms contributing to transduce cortical signals to the mitotic spindle apparatus still remain partially unclear. Converging evidence gathered in the last years indicate that in metaphase cells the core machinery responsible for cortical force generation consists of conserved trimeric Gαi:LGN:NuMA complexes, in which four membrane-bound Gαi proteins recruit the scaffold protein LGN, which in turns binds NuMA through its TPR domain. Biochemical and structural studies identified the minimal binding domains of the NuMA/LGN interaction, showing that the small stretch of NuMA encompassing residues

1900-1928 binds to the inner groove formed by the eight TPR repeats of LGN with nanomolar affinity. How such interaction supports and organizes the recruitment of NuMA:LGN complexes at the cortex to position the spindle still remains elusive. It is known that cortical NuMA instructs dynein/dynactin targeting, generating pulling forces on the astral microtubules, in order to position the spindle correctly. Recent optogenetic studies identified a clusterization domain in the C-terminal part of NuMA revealing that DDN (dynein-dynactin-NuMA) clusters are required to generate MT-pulling forces (Okumura *et al.*, 2018). In the same study it was shown that in HCT-116 cells spindle placement requires a 100-residues stretch in the C-terminal part of NuMA (spanning residues 2002-2115) that we recently identified to associate directly to microtubules (Gallini *et al.*, 2016). Whether and how these domains of NuMA contribute to spindle orientation in polarized cells still needs to be addressed.

Based on these findings, my PhD aimed at 1) investigating how cortical NuMA/LGN interactions spatially organizes dynein-based MT-motors to orient spindle in polarized and unpolarized epithelial cells, and 2) unveiling the functional role of the newly identified MT-binding domain of NuMA (residues 2002-2115) in spindle orientation.

2. MATERIAL AND METHODS

2.1 Cell culture

HeLa and 293T cells were cultured at 37 °C in a 5% CO_2 atmosphere, in Dulbecco's Modified Eagle Medium (DMEM) supplemented with 10% FBS, 1% L-glutamine and 50 μg/ml penicillin/streptomycin. For HeLa cells expressing the shRNA targeting NuMA, the medium was supplemented also with 0.5 μg/ml puromycin. For cells infected with pCDH vectors for stable expression, the medium was supplemented with 5 μg/ml hygromycin. For all the experiments, HeLa cells were plated on coverslips precoated with fibronectin (5 μg/ml, Roche) for 2 hours.

Caco-2 cells were cultured at 37 °C in a 5% CO_2 atmosphere, in DMEM supplemented with 20% FBS, 1% L-glutamine, 1% $NaHCO_3$, 1 % non-essential amino acid, and 50 μg/ml penicillin/streptomycin. For Caco-2 cells infected with pCDH vectors for stable expression, medium was supplemented with 3 μg/ml hygromycin.

2.1.1 Synchronization and cell treatment

HeLa cells were synchronized in mitosis with a single thymidine block. Briefly, cells were treated with thymidine (2.5 mM, Sigma T1895) for 24 hours, then released with 3 washes with PBS and fixed 9 hours after the release (Figure 14 A). To inhibit Aurora-A, HeLa cells were pre-synchronized by thymidine arrest/release and 50 nM MLN8237 (Selleck Chemicals) were added to the medium 5 hours after release. Cells were fixed after 9 hours from release (Figure 14 B).

For immunoprecipitation experiments, 293T cells were synchronized with Nocodazole treatment. Cells were treated with 330 nM Nocodazole (Sigma Aldrich) for 16 hours, to enrich the population of prometaphase cells, and then collected (Figure 14C).

Caco-2 cells grown in cysts were synchronized in mitosis with the ATP-competitor RO-3306, which is an inhibitor of the mitotic kinase Cdk1 (Sigma, SML0569). Briefly, 3-days

cysts were treated with 9 μM RO-3306 for 16 hours, released with three washes in PBS and then incubated with warm medium for 45 minutes prior to fixation (Figure 14 D).

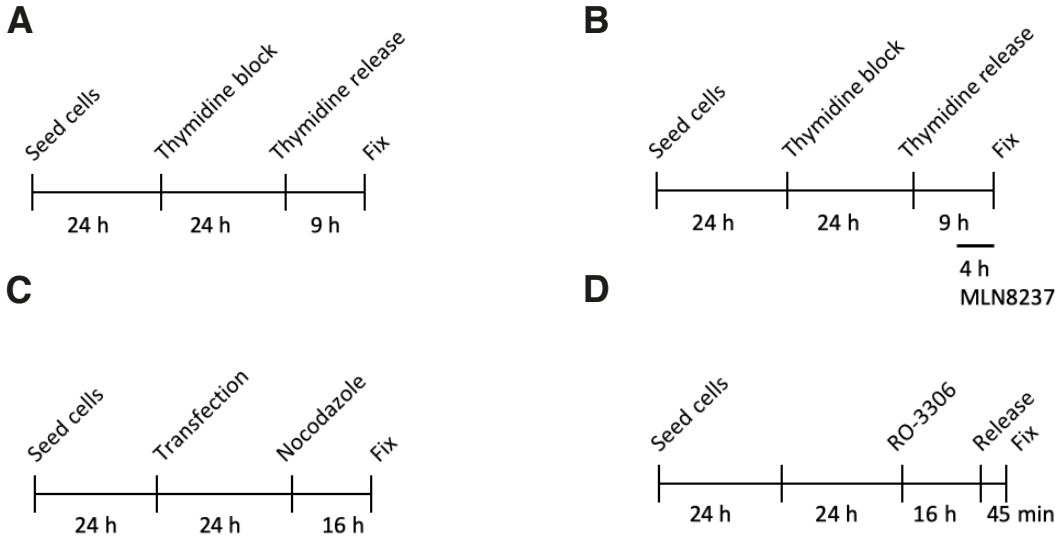

Figure 14 – Synchronization protocols of HeLa and Caco-2 cells

Schematic representation of protocols used to enrich HeLa and Caco-2 cells in mitosis for spindle orientation studies. (**A**) Single thymidine block. HeLa cells were treated with 2.5 mM thymidine for 24 and fixed 9 hours after the release. (**B**) Protocol for HeLa cell synchronization in Aurora-A inhibited conditions. After release from thymidine block, 50 nM MLN8237 were added to fresh medium for 4 hours prior to fixation. (**C**) Synchronization protocol of HeLa cells with nocodazole treatment. 24 hours post-transfection cells were treated with 330 nM nocodazole for 16hours and then collected (**D**) Protocol for 3-days Caco-2 cysts synchronization. At day 2 cysts were treated with 9 μM RO-3306 for 16 hours, and fixed 45 minutes after release.

2.1.2 Plasmids

To deplete LGN expression, two shRNAs were cloned into a pll3.7 vector carrying a GFP reporter, and used to generate stably interfered Caco-2 cell line. The most effective shRNA (GGATGTAGTGGGAAACAA) was used for the rescue experiments described in paragraph 3.2 of the results section. The same shRNA was used to generate a stable interfered HeLa cell line, and to perform the experiment shown in paragraph 3.3.2. Protein depletion was monitored by Western blot and immunofluorescence. To rescue LGN expression, a full-length LGN was cloned at the N-terminus of an mCherry tag into a pCDH

lentiviral vector carrying hygromycin resistance and under a Ubc promoter (Figure 15). To obtain the oligomerization deficient LGN mutant (LGN-ΔOLIGO), the LGN-mCherry cDNA was amplified by subsequent PCR reactions with phosphorylated primers, in order to remove the aminoacids 1-12 and 350-366. To knockdown NuMA in HeLa and 293T cells, I took advantage of the cell lines generated to study NuMA/Aurora-A crosstalk. Four pGFP lentiviral vectors (Origene technologies) carrying a GFP reporter and puromycin resistance and expressing shRNA sequences targeting NuMA were used to generate stable HeLa cell lines that were tested for knockdown efficacy (paragraph 3.3.4). The most effective shRNA-NuMA, carrying the sequence CATTATGATGCCAAGAAGCAGCAGAACCA, was used to generate also a 293T stable cell line. To rescue NuMA expression, full-lenght NuMA was cloned at the C-terminus of an mCherry tag into the pCDH-Ubc-Hygro used described above. To generate the NuMA-ΔOLIGO and NuMA-ΔLGNBD mutants, phosphorylated primers were used to amplify NuMA in order to deplete regions 1862-1899 and 1862-1928. The NuMA-ΔMT mutant was generated by introducing a stop codon at residue 2002 of NuMA using the Quikchange mutagenesis kit (Agilent), according to manifacture's guidelines.

To perform the immunoprecipitation experiment of paragraph 3.5.3, the NuMA fragment encompassing residues 1821-2115 was amplified and subcloned into the pCDH-Ubc-Hygro vector. For the IP experiment in paragraph 3.4.2, LGN-WT and LGN-ΔOLIGO were cloned in a pEGF-C1 vector, in frame with the GFP-tag. The same constructs were also cloned in a pCDH vector, with a C-terminal 3xFLAG tag.

To perform the experiment of paragraph 3.6.1, wild-type NuMA and the NuMA-ΔOLIGO mutant were cloned into a pCDH vector in frame with the GoLoco region of LGN spanning residues 369-677.

For the Proximity Ligation Assay experiment described in paragraph 3.4.1, LGN-WT and LGN-ΔOLIGO were inserted in a pLVX vector under the CMV promoter, in frame with a

C-terminal GFP tag. The same LGN molecules were also cloned in a pCDH-Ubc vector with a C-terminal 3xFLAG tag.

PRIMER NAME	PRIMER SEQUENCE	VECTOR NAME
Cell Biology		
LGN-1_FOR	GCGCGCGCTAGCACCATGAGAGAAGACCATTCTTTTC	pCDH-LGN-WT-mCherry
LGN-13_FOR	GCGCGCGCTAGCACCATGGAAGCTTCTTGCCTA	pCDH-LGN-ΔOLIGO-mCherry
LGN-677_REV	GCGCGCGGATCCATGGTCTGCCGATTTTTTC	pCDH-LGN-WT/ΔOLIGO-mCherry
LGN-368_FOR	GCGCGCGGATCCATGGTCTGCCGATTTTTTC	pCDH-LGN-ΔOLIGO-mCherry
LGN-350_REV	ATCCCCAACCTCTCTTGAAATTTC	pCDH-LGN-ΔOLIGO-mCherry
NuMA-stop2002_FOR	GGCCCGGGAACCCCCTAGTCCAAGAAGGCTACC	pCDH-mCherry-NuMA-ΔMT
NuMA-stop2002_REV	GGTAGCCTTCTTGGACTAGGGGGTTCCCGGGCC	pCDH-mCherry-NuMA-ΔMT
NuMA-1821_FOR	GCGCGCGGATCCAAGAAGCTAGATGTGGAA	pCDH-NuMA-1821-2215
NuMA-1901_FOR	TCCTTCTACATGGGAACCTGCCAG	pCDH-mCherry-NuMA-ΔOLIGO, GFP-NuMA-ΔOLIGO-GoLoco
NuMA-1928_FOR	CGTGTGTGCCCCCCTCACCTCAAG	pCDH-mCherry-NuMA-ΔLGN, GFP-NuMA-ΔLGN-GoLoco
NuMA-1861_REV	CAGACGAGCCAGGGACTGGGTAGA	pCDH-mCherry-NuMA-ΔOLIGO/ΔLGN
NuMA-2115_REV	GCGCGCGGCCGCCCCTTAGTGCTTTGCCTTGCCC	pCDH-NuMA-1821-2215
LIC1-1_FOR	GCGCGCGCTAGCACCATGGCGGCCGTGGGG	pCDH-FLAG-LIC1
LIC1-523_REV	GCGCGCGGATCCAGAAGCTTCTCCTTCCGTAGGAGA	pCDH-FLAG-LIC1
shLGN	GGATGTAGTGGGAAACAA	pll3.7-GFP-shLGN
shNuMA	CATTATGATGCCAAGAAGCAGCAGAACCA	pGFP-shNuMA
Immunoprecipitation		
LGN-1_FOR	GCGCGCGGATCCATGAGAGAAGACCATTCT	pEGFP-GFP-LGN-WT
LGN-13_FOR	GCGCGCGGATCCATGGAAGCTTCTTGCCTA	pEGFP-GFP-LGN-ΔOLIGO
LGN-677_REV	GCGCGCGTCGACTTAATGGTCTGCCGATTTTTT	pEGFP-GFP-LGN-WT/ΔOLIGO
FLAG_FOR	GCGCGCGGATCCGATTATAAGGATGACGATGACAAAG	pCDH-NuMA-3XFLAG, LGN-WT/ΔOLIGO-3XFLAG

FLAG_REV	GCGCGCGGCCGCGACTGATAGTGACCTGTTCG	pCDH-NuMA-3XFLAG, LGN-WT/ΔOLIGO-3XFLAG
PLA		
LGN-1_FOR	CGGTACCGCGGGCCCAAATGAGAGAAGACCATTCTTTTCA	pLVX-LGN-WT-GFP-
LGN-13_FOR	CGGTACCGCGGGCCCAAATGGAAGCTTCTTGCCTAGAGCT	pLVX-LGN-ΔOLIGO-GFP
LGN-677_REV	GATCCGGTGGATCCCTTAATGGTCTGCCGATTTTTTCCCT	pLVX-LGN-WT/ΔOLIGO-GFP

Figure 15 – Primer list

List of oligos used to clone LGN and NuMA constructs.

2.1.3 Transfections and infection

2.1.3.1 Spindle orientation experiment with NuMA constructs

To express NuMA in HeLa cells, transfections were performed using Lipofectamine 3000 (Life Technologies) according to manifacture's instructions. Specifically, NuMA-containing plasmids were transfected with Lipofectamine 3000 with a 1:1 ratio, using 2 μg of p3000 for each μg of DNA. For 12 well-plates, 1 μg NuMA DNA was transfected, while for 6-well plates 2 μg have been used.

2.1.3.2 Spindle rocking experiment

To overexpress LGN for the spindle rocking experiment of paragraph 3.3.3 HeLa cells were plated on fibronectin-coated coverslips in a 12-well plate, and transfected with 0.5 μg LGN-WT-mCherry or LGN-ΔOLIGO-mCherry using Lipofectamine 3000.

2.1.3.3 Immunoprecipitation

For the immunoprecipitation experiments, transfection of 293T cells was performed using Calcium Phosphate. For the experiment in paragraph 3.4.2, 0.25 μg pEGFP-LGN-WT and

10 μg pCDH-LGN-WT-3XFLAG or 0.25 μg pEGFP-LGN-ΔOLIGO and 10 μg LGN-ΔOLIGO-3XFLAG were co-transfected. The two expression vectors have been mixed with 61 ul $CaCl_2$ and water, and then added to a bubbling solution of HBS (Hank's Buffered Saline, 50 mM HEPES, 280 mM NaCl, 1.5 mM Na_2HPO_4). The transfection mix was added to fresh medium after ten minutes incubation.

For the IP experiment shown in paragraph 3.5.3, 10 μg pCDH-GFP-NuMA were co-transfected with 1 μg pCDH-NuMA-3XFLAG, following the protocol described above.

2.1.3.4 Proximity Ligation assay (PLA)

For PLA, HeLa cells were plated in a 12-well plate on fibronectin-coated coverslips and transfected with 0.5 μg pLVX-LGN-WT-GFP and 0.5 μg pCDH-LGN-WT-3xFLAG, or with 0.5 μg pLVX-LGN-ΔOLIGO-GFP and 0.5 μg pCDH-LGN-ΔOLIGO-3xFLAG using Lipofectamine 3000 according to manifacture's instructions.

2.1.3.5 Lentiviral production

For lentivirus production, 293T cells were transfected with 10 μg of the lentivector of interest together with vectors for lentiviral packing. Specifically, 4.5 μg PAX and 2 μg PMD were used. Transfection media was replaced 24 hours post-transfection with 5.5 ml fresh medium, in order to concentrate the virus. Infection of target HeLa, 293T or Caco-2 cells was performed in 6-well plates 24 hours after media replace. Selection drugs were added to the media 24 hours post infection.

2.2 Caco-2 cysts

2.2.1 Spindle orientation analysis

To produce cysts for spindle angle analysis, Caco-2 cells were split the day before single cells plating. To produce cysts, cells from 10 cm plates were washed two times with PBS, detached with trypsin and resuspended in a final volume of 12 ml. To obtain single cells, Caco-2 were strongly resuspended and filtered with a 70 µm strainer. For each well of a 8-well chamber slide, 120 µl of single cells diluted in complete medium supplemented with 40% matrigel were plated, at a final concentration of 60.000 cells/ml. To allow matrigel solidification, 8-well chamber slide were incubated at 37 °C, and 400 µl complete medium was added on top of the matrigel after 30 minutes. For orientation analysis, cysts are usually fixed at day 3 (Figure 16), as described by Jaffe *et al.*, 2008. Prior fixation, cells were synchronized in metaphase with RO-3306 (for details, see paragraph 2.1.1), fixed and immunostained.

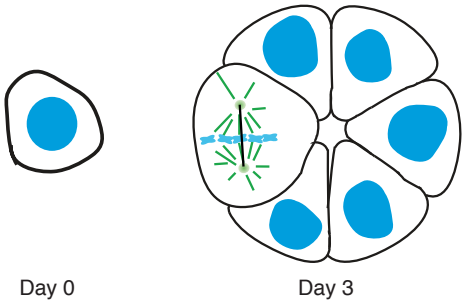

Figure 16 – Caco-2 cysts for spindle orientation analysis
Cartoon depicting growth of Caco-2 cyst by planar cell division. Caco-2 are plated as single cells in matrigel (day 0). For spindle orientation analysis, Caco-2 single cells are plated in matrigel and synncronized in metaphase by treating with 9 µM RO-3306. Cyst were usually fixed at day 3.

2.2.2 Multiple-lumen analysis

To produce cysts of Caco-2 cells for multi-lumen analysis, 8-well chamber slides were coated with 120 µl Matrigel 10 mg/ml using cold tips, and incubated at 37 °C to allow

matrigel solidification. Cells in plates were washed two times with PBS, detached with trypsin, dissociate to single cell as above, and resuspended in a final volume of 12 ml. For each well, 200 µl of single cells diluted in complete medium at a final concentration of 30.000 cells/ml were mixed with 200 µl of medium supplemented with 5% matrigel and plated. At day 5, to allow swelling of the central lumen for multilumen analyses, cysts were incubated with 0.1 µg/ml of Cholera-Toxin for 16 hours. At day 6, cysts were fixed and immunostained (Figure 17).

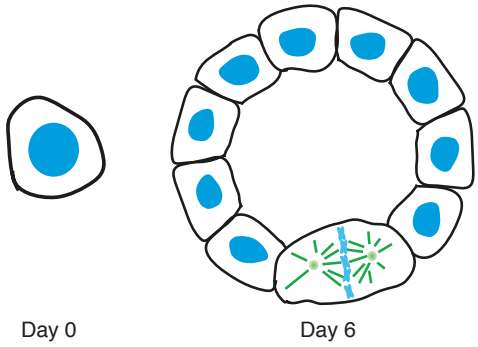

Figure 17 – Caco-2 cysts for multiple-lumen analysis

Cartoon depicting cysts of Caco-2 cells growing by planar cell division. Caco-2 single cells are plated on top of Matrigel-coated chamber slide (day 0). For multi-lumen analysis, cysts were usually fixed at day 6 after Cholera-Toxin treatment.

2.3 Immunofluorescence

2.3.1 HeLa cells

HeLa cells grown on fibronectin-coated coverslips were fixed as follows: absolute methanol at -20 ˚C to visualize NuMA and the p150 subunit of dynactin at the cortex, or 4% Paraformaldehyde (PFA) at room temperature to visualize LGN, α-tubulin, γ-tubulin. For cells fixed with PFA, permeabilization was performed with 0.3% Triton X-100 in PBS for 5 minutes at room temperature, followed by ten minutes of quenching with 0.1 M glycine. Permeabilized cells and cells fixed with methanol were blocked with 3% bovine serum

albumin (BSA) in PBS for 1 hour at room temperature. Primary antibody incubation was performed in blocking buffer supplemented with 0.05% Tween-20 for 2 hours at room temperature in a humidified chamber. Depending on the experiment, cells were stained with mouse anti-LGN (Mapelli lab, 1:5), mouse anti-NuMA (Mapelli lab, 1:3000), mouse anti-$p150^{Glued}$ (1:600 BD), rabbit anti-α-tubulin (1:50, Abcam), mouse anti-α-tubulin (1:200, Sigma-Aldrich), mouse-anti-FLAG (1:200, Sigma-Aldrich) or Cy3 conjugated anti-γ-tubulin (1:200, Sigma-Aldrich). Secondary antibody incubation was carried out for 1 hour at room temperature, in a dark humidify chamber. Cells were stained with anti-mouse or anti-rabbit AlexaFluor 647 or anti-mouse AlexaFluor 488 (1:300). DNA was stained with DAPI.

2.3.2 Caco-2 cyst

Caco-2 cysts grown in matrigel were washed two times with PBS and then fixed with 4% PFA for 30 minutes at room temperature, followed by quenching with 0.1 M glycine in PBS for 30 minutes. To permeabilize cells, cysts were incubated with 0.5% Triton X-100 in PBS for 30 minutes. After a 5 minutes wash with IF wash buffer (0.2% Triton X-100, 0.1% BSA and 0.05% Tween-20 in PBS), cysts were incubated with the blocking solution (5% BSA in IF buffer) for 1 hour and 30 minutes in a humidified chamber. Primary antibodies were diluted in IF wash buffer, and the incubation was carried out overnight at 4 °C. Secondary antibodies were diluted in IF wash buffer, and incubated for one hour at room temperature in humidified chamber. For spindle orientation analyses, cysts were stained with mouse anti α-tubulin (1:100, Sigma-Aldrich), followed by incubation with phalloidin-TRITC (1:1000) and anti-mouse AlexaFluor488 (1:100). For multi-lumen analysis cysts were stained with rabbit anti-ZO-1 (Invitrogen, 1:100) or with phalloidin-TRITC. DNA was stained with DAPI.

2.4 Live cell imaging

To monitor spindle rocking of HeLa cells overexpressing LGN wild-type or LGN-ΔOLIGO, cells were plated in a 12-well plate with glass bottom (Mattek), and transfected with 0.5 μg pCDH-LGN-WT-mCherry or pCDH-LGN-ΔOLIGO-mCherry using Lipofectamine 3000, as described in paragraph 2.1.3.2. Cells were synchronized with a single thymidine block, and released in warm medium. Images acquisition started 5 hours after the release. Images were acquired on a Nikon Eclipse Ti inverted with a 20X (Plan Apo λ 20X) objective. For the entire observation period, cells were kept in an incubated microscope stage at 37 °C and 5% CO_2. Differential interference contrast (DIC) frames were acquired every 3 minutes over 16/18 hours. For each frame, three Z-stacks were acquired in a 20 μm range.

2.5 Microscopy

Confocal images shown in Figure 25B, 26, 28, 29, 30, 33, 34A, 41 and 45 were acquired on a Leica SP2 AOBS confocal microscope controlled by Leica confocal software. For HeLa cells analysis, a 63X oil-immersion objective lens (HCX Plan-Apochromat 63X NA 1.4 Ldb Bl) was used. For Caco-2 cyst multi-lumen experiments, a 20X objective lens (HC PL FLUOTAR 20x 0.5 DRY) was used. Images shown in Figure 22, 23, 24, 25D, 31, 34B-C, 37, 38, 42, 43 and 44 were acquired on a Leica SP8 confocal microscope controlled by a Leica confocal software. For HeLa cells analysis, a 63X oil-immersion objective lens (HC PL Apochromat 63X NA 1.4 CS2) was used. For Caco-2, a 40X objective lens (HC PL Apochromat 40X NA 1.30 CS2) was used. All images were processed using the software Fiji.

2.6 Spindle orientation analysis

2.6.1 Spindle measurement in HeLa cells

Spindle orientation analysis was performed on HeLa cells plated on coverslips coated with fibronectin, which have been shown to divide with the spindle axis parallel to the substratum. To quantify the spindle angle, cells were stained with DAPI, to visualize the metaphase plate, and with γ-tubulin, to visualize the poles. Cells were imaged in x-z sections passing through the spindle poles. To determine the orientation of the spindle, the angle formed by a line passing through the poles and the substratum was measured using the angle tool of the software Fiji (Figure 18). Statistical analysis of spindle angles was performed with Prism, with the Krustal-Wallis test (Figure 26 and 29) and plotted as dot-plot distribution.

2.6.2 Spindle measurement in Caco-2 cysts

Spindle angle measurement of Caco-2 cells grown in 3D cysts were conducted as described by Jaffe (Jaffe *et al.*, 2008). Briefly, to quantify the spindle angle, cysts were stained with DAPI, to visualize the metaphase plate, with α-tubulin, to visualize the mitotic spindle and with phalloidin, to visualize the central lumen. Three x-y confocal sections of the equatorial region of the cyst were acquired and then merged, in order to visualize both the spindle poles when the metaphase cells are not oriented. To analyze the spindle axis orientation, the angle formed by a line passing through the spindle poles and the centroid of the cyst marked by Phalloidin was determined using the software Fiji (Figure 18). Statistical analysis of spindle angles was performed with Prism with the Krustal-Wallis test, and plotted as dot-plot distribution.

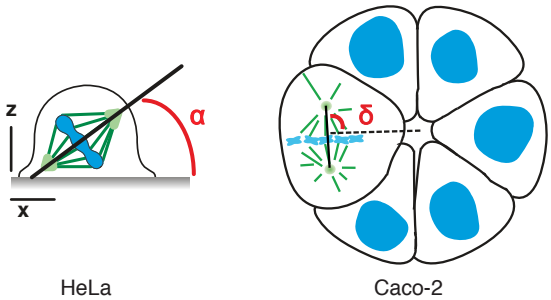

Figure 18 – Spindle angle measurement in HeLa and Caco-2

Left: Spindle angle measurement in metaphase HeLa cell imaged in x-z sections. The angle "α" was obtained by measuring the angle formed by a line passing through the spindle poles and the substratum. Right: Spindle angle measurement in Caco-2 cyst. The angle "δ" was obtained by measuring the angle formed by a line passing through the poles and the centroid of the cyst.

2.7 Image analysis and quantifications

2.7.1 Quantification of cortical signals

For the quantification of NuMA and $p150^{Glued}$ cortical levels, HeLa cells were fixed with absolute methanol, while for cortical LGN quantifications cells were fixed with 4% PFA. To quantify proteins signal at the cell cortex, confocal sections of metaphase cells were analyzed in Fiji with the following procedure. A 30-pixel-wide line was drawn from the spindle pole in focus to the cell cortex, to obtain the intensity profile along the line. Using the software Matlab, the amount of protein at the cortex was calculated by integrating the profile of a 10 pixel-wide area of the peak, while the amount of protein in the cytoplasm was calculated by integrating the 10 pixel-wide area, 5-pixel distant from the peak. The cortex to cytoplasm ratio was used to monitor cortical enrichment of the proteins.

To visualize dynein recruitment at the cortex, human dynein light-intermediate chain 1 (LIC1) was cloned in a pCDH lentiviral vector in frame with a 3xFLAG tag, and transfected in HeLa cells ablated of endogenous LGN and stably expressing LGN-WT or LGN-ΔOLIGO. Transfected cells were analyzed with the software Fiji, and classified on the basis that a crescent of LIC was visible or absent at the cortex.

2.7.2 Quantification of fluorescent signal at the poles

To evaluate the intensity of mCherry NuMA at the spindle poles, HeLa cells transfected with various NuMA constructs were fixed with 4% PFA, to preserve the total levels of the protein.

Confocal sections of metaphase cells stained with α-tubulin were acquired and analyzed with the software Fiji. In details, per each cell imaged, the α-tubulin signal of one pole in focus was used to build a tubulin mask, and the protein signal inside the mask was integrated. A tubulin mask of the same dimension was positioned in the cytoplasm to obtain the intensity in the cytoplasm. In Figure 30 and Figure 41 the pole/cytoplasm ratio of mCherry-NuMA constructs is shown.

2.7.3 Quantification of spindle oscillation

Spindle rocking measurement was performed as shown in Kotak et al. (Kotak, Busso and Gönczy, 2012) Briefly, HeLa cells stably expressing H2B-GFP were transfected with LGN and filmed as described above (paragraph 2.4). For each cell analyzed, six frames of a metaphase event were considered. Using the software Fiji, a line passing through the metaphase plate was drawn, in order to obtain the position of the metaphase plate in that frame. Once calculated the positions of all the six frames, the difference between the angle of the metaphase plate of two consecutive images was calculated. A difference higher than 10 degrees was considered "oscillation". The percentage of oscillation were calculated considering the number of oscillating events among the five values obtained in each individual mitotic event.

2.8 Western blot

For western blot analysis, HeLa and Caco-2 cells were synchronized with nocodazole, as described in paragraph 2.1.1, and collected 16 hours after nocodazole addition. Cells were lysed on ice in a lysis buffer containing 75 mM Hepes pH 7.5, 1.5 mM, EGTA, 1.5 mM MgCl2, 150 mM KCl, 0.1% NP40 and 15% glycerol and protease inhibitors (Calbiochem, 539134) for 30 minutes. 50 μg of cell lysates were resolved by SDS-electrophoresis and

transferred on a nitrocellulose membrane at 100 V for 1 hour and 30 minutes. Blocking was performed in TBS containing 0.1% Tween-20 and 5% low fat milk. Primary antibody incubation was performed at room temperature for 2 hours with the following dilutions: mouse anti-LGN (1:500, Mapelli lab), mouse anti-NuMA (1:200, Mapelli lab), mouse anti-Vinculin (1:10000, in-house IEO), mouse anti-α-tubulin (1:600, Abcam), rabbit anti-GFP (1:1000, in-house IEO), mouse anti-FLAG (1:8000, Sigma-Aldrich).

2.9 Immunoprecipitation

For the immunoprecipitation experiments of paragraph 3.4.2 and 3.5.3, 293T cells were grown in 10 cm plates in DMEM medium supplemented with 10% FBS and 1% L-glutamine. Cells were transfected as described in paragraph 2.1.3.3. 24 hours post-transfection cells were synchronized with 330 nM nocodazole treatment for 16 hours before harvesting. Cells were lysed on ice in lysis buffer containing 75 mM Hepes pH 7.5, 1.5 mM, EGTA, 1.5 mM MgCl2, 150 mM KCl, 0.1% NP40 and 15% Glycerol and protease inhibitors, for 30 minutes. For the experiment in paragraph 3.4.2, GFP-LGN-WT and LGN-WT-FLAG or GFP-LGN-ΔOLIGO and LGN-ΔOLIGO-FLAG (for details see paragraph 2.1.2) were co-transfected in the 293T stable cell line depleted of endogenous NuMA and expressing NuMA$^{1821-2115}$, with 0.25 μg pEGFP-LGN-WT and 10 μg pCDH-LGN-WT or 0.25 μg pEGFP-LGN-ΔOLIGO and 10 μg pCDH-LGN-ΔOLIGO. For the immunoprecipitation 300 μg of lysates were incubated with 10 μl α-GFP antibody conjugated to agarose beads (MBL) for 2 hours at 4 °C, with gentle agitation on the wheel.

For the experiment in paragraph 3.5.3 GFP-NuMA and NuMA-3xFLAG were cloned in a pCDH vector. 293T cells were co-transfected with 10 μg GFP-NuMA and 1 μg NuMA-3xFLAG. 500 μg of lysates were incubated with 10 μl α-GFP antibody conjugated to agarose beads, for 2 hours at 4 °C, with gentle agitation on the wheel. For both the experiments, after

unbound supernatant removal, beads were washed 4 times with 1 ml lysis buffer, followed by centrifugation at 2.000 rpm at 4 °C. After bead drying, Laemli buffer was added for SDS-PAGE and Western blot analysis.

2.10 Proximity Ligation Assay

Proximity Ligation Assay (PLA) is a technique that allow the detection of protein-protein interaction in cells, protein modifications and quantification of individual proteins (Figure 31). To test the existence of NuMA:LGN hetero-hexamers in cells by PLA, LGN-WT and LGN-ΔOLIGO were inserted in a pLVX vector in frame with a C-terminal GFP tag. The same LGN molecules were also cloned in a pCDH vector with a C-terminal 3xFLAG tag. HeLa cells were co-transfected with GFP and FLAG-tagged constructs (see paragraph 2.1.3.4 for details) and synchronized with a single thymidine block. Mitotic cells were fixed with 4% PFA at room temperature, washed and permeabilize with 0.1% Triton X-100 in PBS. Blocking was performed with the Duolink Blocking Solution for 1 hour at 37 °C, followed by primary antibody incubation. For PLA experiment we used mouse-anti-FLAG (1:200, Sigma-Aldrich) and rabbit-anti-GFP (1:1000, generous gift of Dr. Giorgio Scita) diluted in Duolink Antibody Diluent. Primary antibodies were incubated in a humidified chamber for 2 hours at room temperature, and washed two times in 1x "Wash Buffer A" for 5 minutes. Secondary antibodies (provided PLA probes) were diluted 1:5 in Duolink Antibody Diluent and mixed. For each reaction, 8 µl PLA probe MINUS, 8 µl PLA probe PLUS and 24 µl Antibody Diluent were used. PLA probes were incubated in a pre-heated humidified chamber for 1 hour at 37 °C. Probes incubation was followed by two washes in 1x Wash Buffer A, for 5 minutes. Ligation was performed for 30 minutes at 37 °C with 1 µl Ligase in 40 µl Duolink Ligation solution per reaction, followed by two washes in 1x Wash Buffer A, for 5 minutes. For probes amplification, 0.5 µl Polymerase was added to 40 µl Duolink Amplification Buffer per reaction. Coverslips were incubated in a pre-heated

humidity chamber for 100 minutes at 37 °C. Amplification was followed by two washes in 1x Wash Buffer B, for 10 minutes, and one quick wash with 0.01x Wash Buffer B. After removing the excess of wash buffer, cells were stained with DAPI (1:5000), washed in PBS and mounted in glycerol.

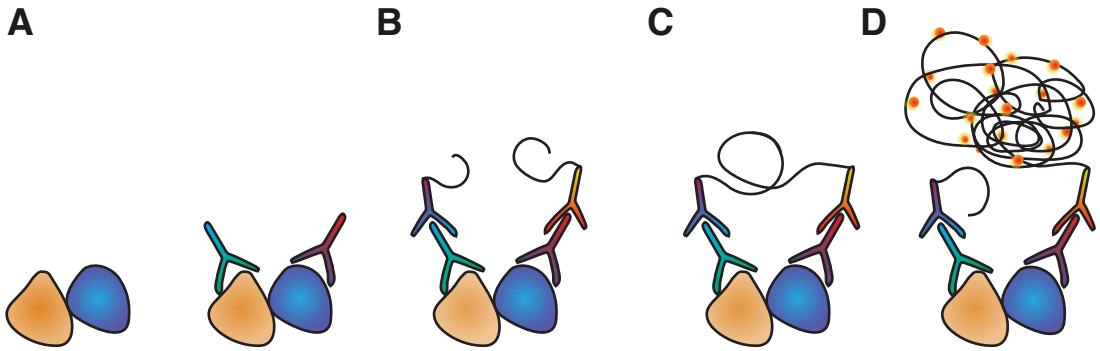

Figure 19 – Proximity Ligation Assay

Schematic representation of PLA protocol. After primary antibodies incubation (A) samples are incubated with PLA probes (B). Ligation of the probes (C) is followed by amplification (D) and signal detection.

2.11 Protocols for *in vitro* assays with purified proteins

In vitro assays with purified proteins were conducted collaboratively by Manuel Carminati and Francesca Rizzelli from my laboratory, and are briefly summarized in the following paragraph.

2.11.1 Proteins expression and purification

GST-LGN$^{1\text{-}350}$, GST-LGN$^{13\text{-}409}$, GST-LGN$^{1\text{-}409}$ (LGN^{TPR}), GST-LGN$^{7\text{-}367}$ and GST-NuMA$^{1861\text{-}1928}$ (NuMA^{LGNBD}) were cloned into pGEX-6P1 vector and expressed in BL21 Rosetta *E. coli* cells. Cells were lysed in 0.1 M Tris HCl pH 8.0, 0.3 M NaCl, 10% glycerol, 0.5 mM EDTA and 1 mM DTT, and cleared for 1 h at 100,000 x g. GST fusion proteins were purified by affinity on glutathione beads (GSH) and incubated with PreScission

protease overnight at 4 °C to remove the GST-tag. The cleaved constructs were eluted from GST beads in desalting buffer and loaded on a 6-ml Resource-Q ion exchange column. $NuMA^{1821-2115}$, $NuMA^{1821-2001}$ and $NuMA^{2002-2115}$ used in the MTs co-sedimentation assays and SEC analysis were cloned into pETM14 vector, expressed in BL21 Rosetta *E. coli* cells, and purified by nickel affinity and cation-exchange chromatography.

The NuMA-chimera construct was generated as follow: NuMA residues 1592-1694 were fused to residues 1821-2001 by an artificial linker of eight Thr-Gly-Ser (TGS) repeats. Deletion of the region encompassing residues 1695-1820 and linker insertion was achieved by PCR amplification of a pETM14-NuMA_1592-2001 template with 5' phosphorylated primers, each harboring a complementary sequence to the NuMA regions being joined of an overhang sequence coding for 4 TGS triplets. NuMA-chimera was expressed in BL21 Rosetta *E. coli* cells. Cells were lysed in 0.1 M Tris HCl pH 8.0, 0.3 M NaCl, 10% glycerol, 0.5 mM imidazole and 1 mM DTT, and cleared for 1 h at 100,000 x g, followed by incubation to remove the histidine-tag and purified onto a Resource-Q anion exchange column.

2.11.2 Size-exclusion-Chromatography

For SEC analysis of paragraph 3.1.1 and 3.5.4 LGN and NuMA were mixed in equimolar amounts (20 μM) loaded on a Superdex-200 Increase 3.2/300 column equilibrated in 20 mM Tris-HCl pH 8.0, 0.15M NaCl, 5% glycerol and 1 mM DTT, and eluted in 50 μl fractions. LGN^{TPR} and NuMAPEPT were combined in a 1:2 molar ratio. Eluted species were monitored by absorbance at 280 nm, and on Coomassie-stained SDS-PAGES.

2.11.3 Microtubules co-sedimentation assay

For microtubules co-sedimentation assay tubulin (Cytoskeleton Inc) was polymerized into stable microtubules in General tubulin buffer (80 mM PIPES pH 6.8, 1 mM $MgCl_2$, 1 mM

EGTA), supplemented with 1 mM GTP and 50 μM paclitaxel at 37 °C for 20 minutes. Microtubules were diluted to a final concentration of 9 μM in General tubulin buffer. For the experiments shown in paragraph 3.7.1 and 3.7.2, 1 μM NuMA C-terminal fragments were added to a final volume of 50 μl. Reactions were incubated at room temperature for 15 minutes and ultracentrifuged for 15 minutes at 400,000 x g at 25 °C. For the experiment of paragraph 3.7.2, to assess whether NuMA could associate simultaneously with MTs and with LGN, the co-sedimentation assay was repeated in presence of 1 μM LGN^{TPR}.

To remove the C-terminal tubulin tails, paclitaxel-stabilized microtubules were incubated with 200 μg/ml Subtilisin A at 30 °C for 30 minutes. The reaction was stopped with 10 mM PMSF. Microtubules with and without tails were incubated for 10 minutes at room temperature with 5 μM $NuMA^{2002\text{-}2115}$ or 1 μM $Ndc80^{Bonsai}$ (generous gift from Andrea Musacchio) in a final volume of 50 μl. Reactions were transferred onto 100 μl of cushion buffer (80 mM PIPES pH 6.8, 1 mM MgCl2, 1 mM EGTA, 50 μM paclitaxel, 50% glycerol) and ultracentrifuged for 15 minutes at 400,000 x g at 25 °C in a Beckman TLA100 rotor. Pellets and supernatants were analyzed by SDS-PAGE and visualized by Coomassie staining.

3. RESULTS

3.1 NuMA forms 3:3 complexes with LGN

3.1.1 LGN^{TPR} form high-order oligomers with $NuMA^{LGNBD}$

The core machinery responsible for cortical force generation consists of trimeric NuMA:LGN:Gαi complexes, connecting dynein/dynactin and astral microtubules to the cell cortex. LGN consists of a TPR domain joined to four GoLoco motifs by a linker region. All the minimal binding sites of known LGN interactors consists of about 32-40 residues peptides binding with a 1:1 stoichiometry to the inner concave surface of eight tetratricopeptide repeats (TPRs) (Culurgioni *et al.*, 2011; Yuzawa *et al.*, 2011; Zhu *et al.*, 2011; Carminati *et al.*, 2016). Each TPR consists of a couple of antiparallel helices organized in a concave super-helical array, in which the first helix-A of each TPR faces the inner side of the super-helix, while the second helix-B is positioned outside (Zhu *et al.*, 2011). A peculiar feature of the TPR domain of LGN is the presence of flanking extensions at the N-terminus and C-terminus which are predicted to adopt a helical conformation. Structural studies revealed that the elongated NuMA peptide encompassing residues 1900-1928 ($NuMA^{PEPT}$ hereon) lines the inner side of the helical N-terminal TPR scaffold of LGN, engaging in a nanomolar affinity interaction (Zhu *et al.*, 2011). Moreover, LGN has been reported to behave as a conformational switch, held inhibited by head-to-tail interactions (Du and Macara, 2004). What opens the conformational switch remains unclear. To start investigating the structural basis for NuMA:LGN:Gαi complexes assembly in metaphase, we decided to reconstitute the NuMA:LGN interaction. Human N-terminal LGN spanning residues 1-409 (LGN^{TPR} hereon, Figure 20A) and $NuMA^{PEPT}$ were expressed in bacteria and purified to homogeneity. These fragments were used to run an analytical size exclusion chromatography (SEC, see Materials and Methods for details), confirming the 1:1 binary interaction already described by Zhu and colleagues (Zhu *et al.*, 2011) (Figure 20B). However, we realized that when an extended NuMA fragment encompassing residues 1861-

1928 is run on a SEC column together with LGN^{TPR}, the complex elutes as a single peak at much higher molecular weight, suggesting that this longer NuMA fragment could form higher order oligomers with the TPR domain of LGN (Figure 20A-B). We then performed SEC analyses using the portion of NuMA encompassing residues 1861-1928 and several LGN fragments lacking the helices flanking the TPR. Depletion of both N-terminal and C-terminal helix of LGN results in a 1:1 interaction, confirming that NuMA 1861-1928 (NuMA-LGN-Binding-Domain, NuMA^{LGNBD} hereon) and LGN^{TPR} are the minimal binding fragments required for high-order oligomers formation (Figure 20C).

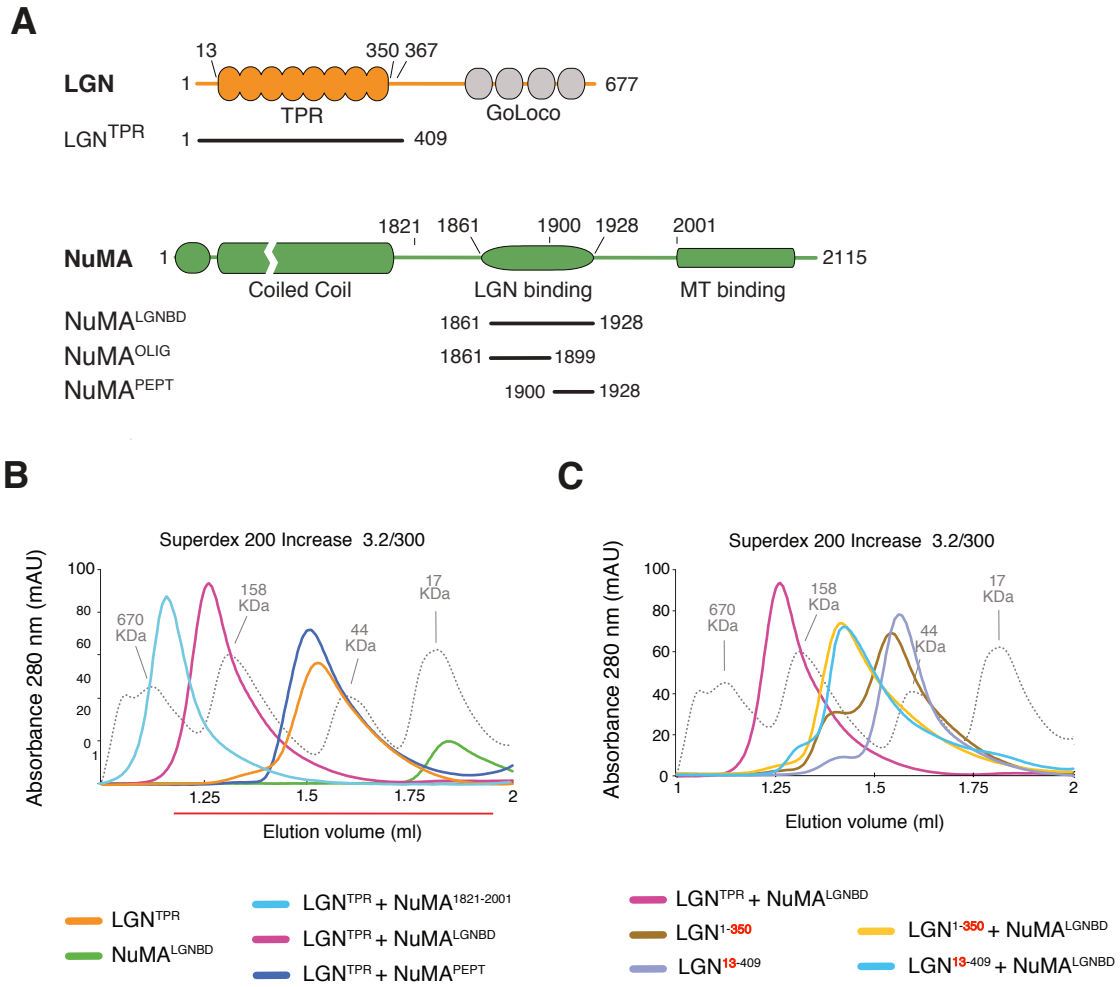

Figure 20 – LGN and NuMA form high-order oligomers

(**A**) Schematic representation of LGN and NuMA domain structures. Bold lines below the cartoons indicate proteins fragment used for the in vitro assay of figure B. (**B**) SEC elution profile of LGN^{TPR} (20 µM) in complex with NuMA$^{1821-2001}$ (20 µM, cyan), NuMA^{LGNBD} (20 µM, purple) or NuMA^{PEPT} (40 µM, blue). The early elution volume of LGN^{TPR}:NuMA^{LGNBD} indicates that they form higher

molecular weight species compared with the 1:1 stoichiometry of LGN^{TPR}:$NuMA^{PEPT}$. (**C**) SEC analysis conducted with LGN^{TPR} truncations and $NuMA^{LGNBD}$. Depletion of the residues 351-409 (yellow trace) or 1-12 (cyan trace) of LGN^{TPR} results in delayed elution compared to LGN^{TPR}:$NuMA^{LGNBD}$ (purple). Grey dotted lines indicate the run of globular molecular weight markers.

3.1.2 LGN and NuMA form hetero-hexameric complexes

To further characterize NuMA:LGN interaction, Simone Culurgioni from our lab and Sebastiano Pasqualato, head of the Biochemistry Unit at IEO, determined the crystal structure of the LGN-Binding-Domain of NuMA in complex with the TPR domain of LGN, that revealed an hetero-hexameric arrangement. The structure was solved at a resolution of 4.3 Å, with the final model including residues 7-367 of LGN and 1864-1928 of NuMA with a gap encompassing residues 1881-1897 (Figure 21). NuMA and LGN 3:3 complexes arrange in a donut-shaped architecture, whose backbone is formed by three TPR domains of LGN interacting in a head-to-tail way, forming a central triangular cavity. In the donut, the interface between the C-terminal stretch of the NuMA-LGNBD, spanning residues 1900-1928 and corresponding to $NuMA^{PEPT}$, and LGN^{TPR} is identical to the one observed in the crystal structure of the 1:1 complex between the $NuMA^{PEPT}$ and LGN^{TPR}, with the NuMA chain filling the groove formed by the TPR repeats of LGN. The additional flexible N-terminal stretch spanning residues 1892-1899 present in NuMA-LGNBD interacts with the two adjacent LGN molecules.

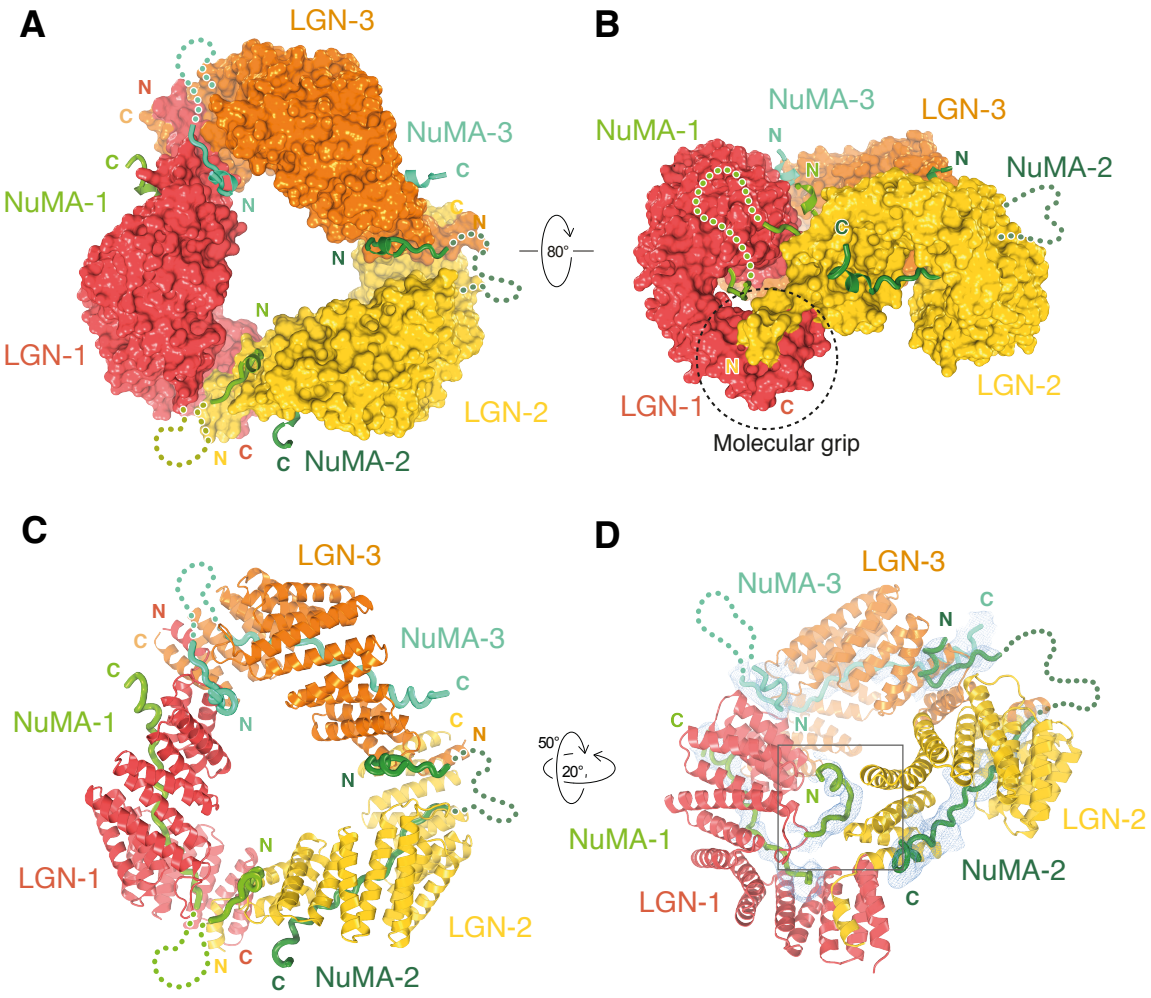

Figure 21 – Structure of the NuMA:LGN hetero-hexamers

(**A-B**) Surface representation of NuMA:LGN hetero-hexamer, with LGN depicted in red, orange and yellow and NuMA molecules as coils in different shades of green. Unstructured regions are represented with dotted lines. (**C-D**) Cartoon representation of NuMA:LGN hetero-hexamers. Panel C as the same orientation of A, while panel D highlight the hooking mechanisms of the NuMA^{LGNBD} to the adjacent LGN^{TPR} subunits.

3.2 NuMA:LGN oligomerization regulates spindle orientation during cystogenesis

3.2.1 Experimental setting to study spindle orientation in Caco-2 cells

During metaphase, the Gαi-bound pool of LGN recruits NuMA at the cell cortex via direct interaction. In a number of vertebrate systems, it has long been shown that knockdown LGN results in loss of cortical NuMA and spindle orientation defects (Peyre *et al.*, 2011b; Seldin *et al.*, 2013). To start investigating the relevance of NuMA:LGN oligomerization in cells, we first decided to rescue orientation defects caused by the loss of endogenous LGN by expressing an ectopic LGN unable to oligomerize. Based on the molecular information provided by the structure, I generated an LGN mutant depleted of the N-terminal region, encompassing residues 1-12, and the region downstream the TPR repeat (corresponding to the C-terminal helix of the TPR domain), encompassing residues 350-366. This mutant, hereon referred as LGN-ΔOLIGO, retains the ability to bind NuMA with 1:1 stoichiometry because it contains a proficient TPR domain, but cannot oligomerize (Figure 22A). As model system, we decided to use polarized Caco-2 cells. When plated as single cells in matrigel, Caco-2 cells divide with oriented planar divisions and give rise to monolayered epithelial spheres with a single lumen, with the apical side facing the inner lumen. Loss of LGN in this system causes misoriented divisions, and results in multi-lumen cysts. To address the role of the NuMA:LGN oligomerization in Caco-2 cells, I set out to rescue spindle orientation defects caused by the loss of endogenous LGN. First, I used two lentiviral vectors carrying short-hairpin RNAs targeting human LGN to generate Caco-2 cell lines stably interfered for LGN. Western blot analysis of these Caco-2 cell lines showed that both shRNA-LGN1-2 and shRNA-LGN3-4 efficiently knockdown LGN compared to control shRNA (Figure 22B). For the rescue experiment, I used a C-terminally mCherry-tagged version of LGN wild-type as positive control, and mCherry-tagged LGN-ΔOLIGO. LGN-WT-mCherry and LGN-ΔOLIGO-mCherry were cloned in a pCDH lentiviral vector and used to generate shLGN1-2 Caco-2 cell lines depleted of endogenous LGN and expressing the LGN rescue constructs. Western blot analysis confirmed that expression levels of the LGN rescue constructs were comparable with endogenous protein (Figure 22C). Moreover, to confirm

that the expression levels of LGN-WT and LGN-ΔOLIGO were similar, I also evaluated mCherry levels by imaging the Caco-2 cell lines grown in monolayer, confirming that the two constructs were expressed at comparable levels (Figure 22D).

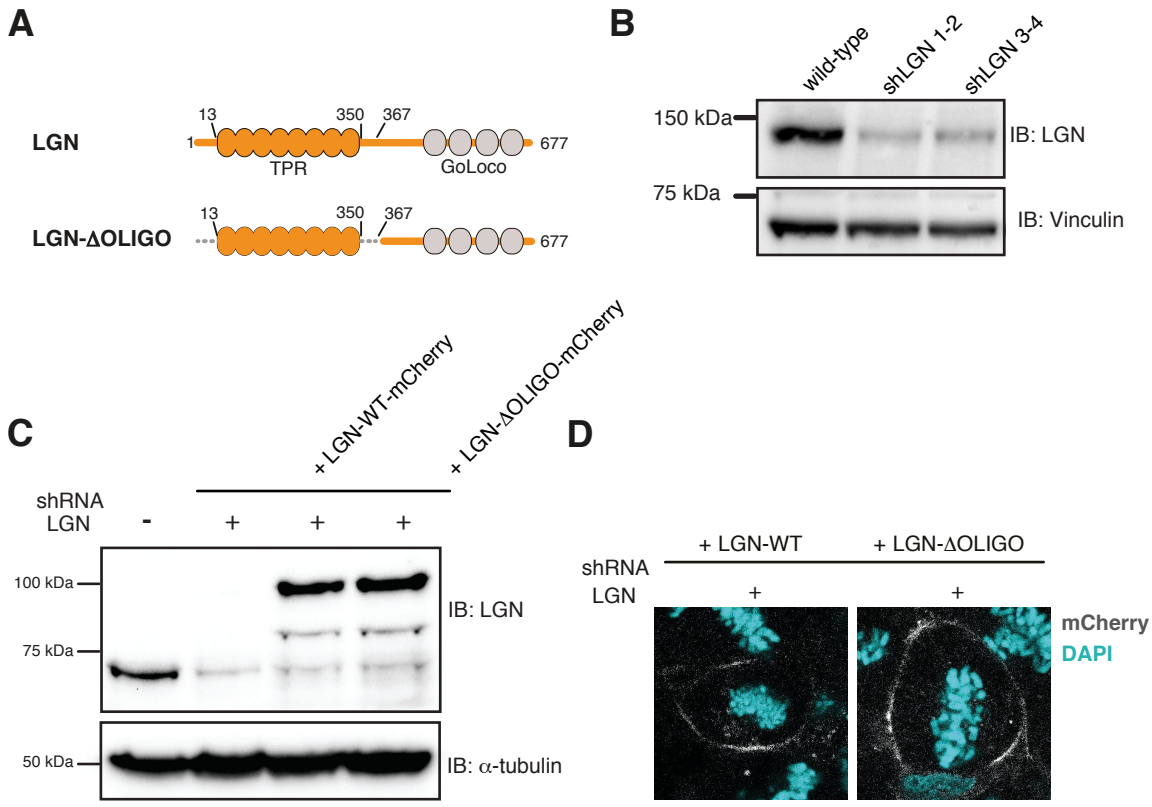

Figure 22 – Generation of Caco-2 rescue cell lines

(**A**) Schematic representation of the domain structure of wild-type LGN and LGN oligomerization-deficient (LGN-ΔOLIGO). Dashed grey lines indicate the residues deleted to generate the mutant construct. (**B**) Western blot of mitotic lysates of Caco-2 cells wild-type stably expressing shRNAs against LGN. Vinculin was used as loading control. (**C**) Western blot of mitotic lysates of Caco-2 cells stably depleted of endogenous LGN by shLGN1-2, and expressing LGN-WT-mCherry or LGN-ΔOLIGO-mCherry. α-tubulin was used as loading control. (**D**) Representative images of Caco-2 cells grown in monolayer interfered for LGN and expressing LGN-WT-mCherry or LGN-ΔOLIGO-mCherry. In the image, mCherry signal is shown. Cells were stained with DAPI to visualize the metaphase plate.

3.2.2 NuMA:LGN oligomerization is required for spindle orientation during cystogenesis

When plated in matrigel, Caco-2 cells divide through planar divisions, with the mitotic spindle aligned perpendicularly to the apico-basal axis. To evaluate mitotic spindle orientation of metaphase cells, I grew cysts from the Caco-2 cell lines described above, and synchronized them in mitosis with the Cdk1 inhibitor RO-3306 (see Material and Methods for details), in order to enrich the metaphase population. To quantify the spindle axis angle, per each cyst I acquired three confocal sections around the equatorial plane in order to visualize the mitotic spindle even in conditions in which the metaphase cell is not oriented (see Material and Methods for details), and measured the angle formed by a line passing through the spindle poles and the centroid of the cyst (Figure 23A). As expected, wild-type cells divide with the mitotic spindle perpendicular to the central lumen, with a mean spindle angle of 67˚. The knockdown of LGN induce spindle misorientation with a mean spindle angle of 43˚, in line with already reported in literature with LGN-depleted MDCK cysts. Ectopic expression of wild-type LGN-mCherry allowed to rescue the correct orientation, with a mean angle of 63˚, while expression of LGN-ΔOLIGO-mCherry did not, with metaphase cells dividing in a misoriented manner with an average angle of 42˚ (Figure 23B-C). These findings indicate that NuMA:LGN oligomerization is required for planar cell divisions during cystogenesis.

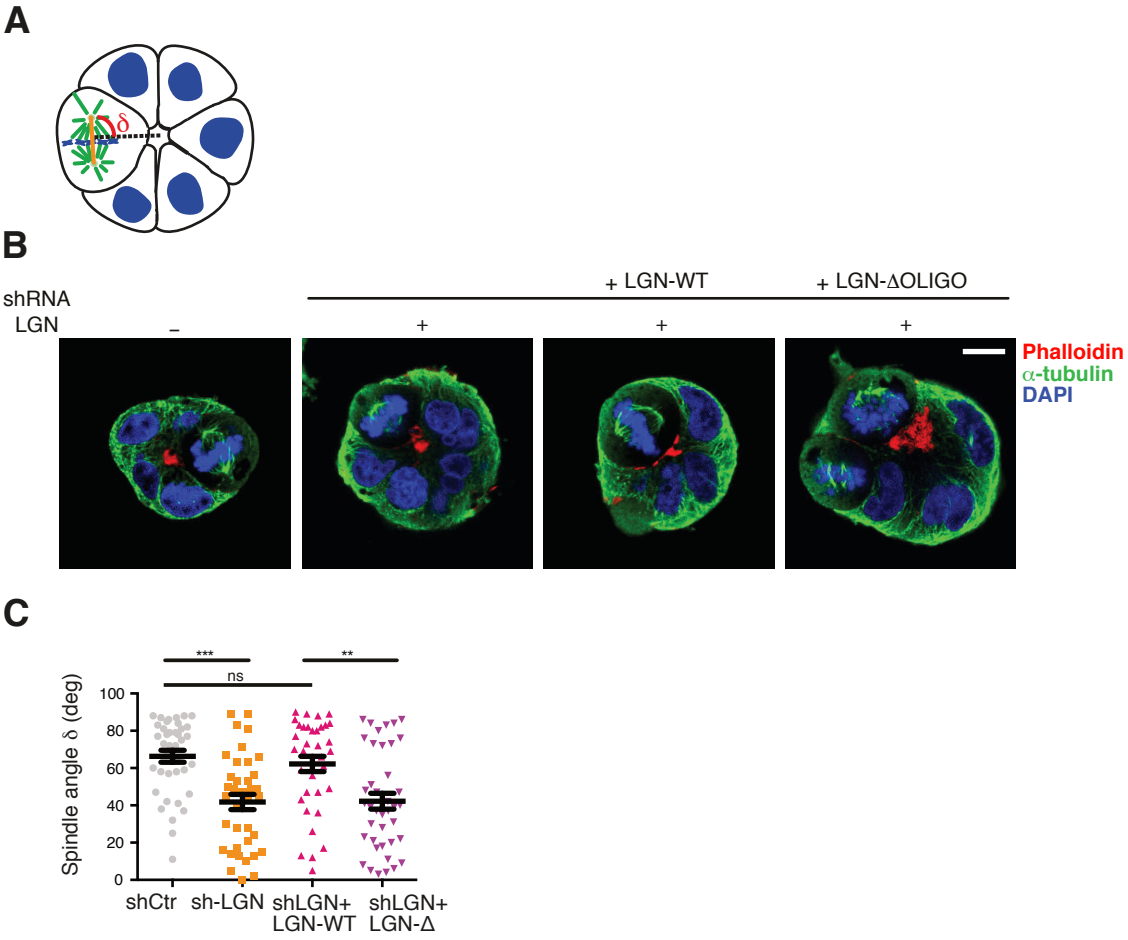

Figure 23 – NuMA:LGN oligomerization is required to orient the spindle during cystogenesis of Caco-2 cells

(**A**) Scheme depicting growing Caco-2 cyst during planar cell division. Spindle angle "δ" was obtained by measuring the angle formed by a line passing through the mitotic spindle axis (orange) and the metaphase plate (blue). (**B**) Confocal sections of Caco-2 cysts grown from cells wild-type or depleted with endogenous LGN and expressing the LGN-WT-mCherry or LGN-ΔOLIGO-mCherry rescue constructs. Cysts were stained with α-tubulin (green) to visualize the mitotic spindle, with Phalloidin (red) to visualize the apical lumen, and with DAPI to image DNA (blue). (**C**) Dot-plot showing spindle angle distribution of Caco-2 cells shown in B. Mean ± SEM are shown for three independent experiments, with n>36. The Krustal-Wallis test was applied. *** indicates $p<0.0001$, and ** indicates $p<0.01$.

3.2.3 Lack of NuMA:LGN oligomerization causes multiple-lumen Caco-2 cysts formation

During cystogenesis, cells dividing with planar divisions give rise to single lumen cysts, while cells undergoing misoriented divisions give rise to cysts with more than one lumen (Figure 24A). To test whether the misorientation phenotype observed in LGN-depleted Caco2 cysts expressing LGN-ΔOLIGO results in a multi-lumen phenotype, I set out to analyze morphology of cysts grown for 6 days, and to quantify the number of multi-lumen cysts. To this aim, at day 5 I treated cysts with cholera toxin, that enlarge the inner lumen making them more visible (for details, see Material and Methods). The majority of Caco-2 wild-type cells give rise to single lumen cyst, with a percentage of multi-lumen around the 30% (Figure 24B, left panel). As expected, the knockdown of LGN induced misorientation which reflects in the formation of multi-lumen cysts. In this LGN-depleted Caco-2 cells, expression of LGN-WT-mCherry rescued the control phenotype, with a percentage of multi-lumen under the 35%, while expression of LGN-ΔOLIGO-mCherry failed in organizing a single lumen, with a mean percentage of multi-lumen around 62% (Figure 24B-C).

It is known that polarity defects can induce misorientation and multilumen phenotype (Jaffe *et al.*, 2008). To confirm that polarity is preserved in LGN-depleted Caco-2 cysts, I stained 6 days-old cysts with ZO-1, a component of the tight junctions localizing to the apical surface of the cyst. Cysts stained with ZO-1 show an equivalent apical staining with dots at the tight junctions, fully supporting the notion that cysts lacking LGN or expressing LGN rescue constructs do not have polarity defects (Figure 24D).

Collectively, these results confirm that NuMA:LGN oligomerization is required for planar cell divisions and for correct epithelial cystogenesis.

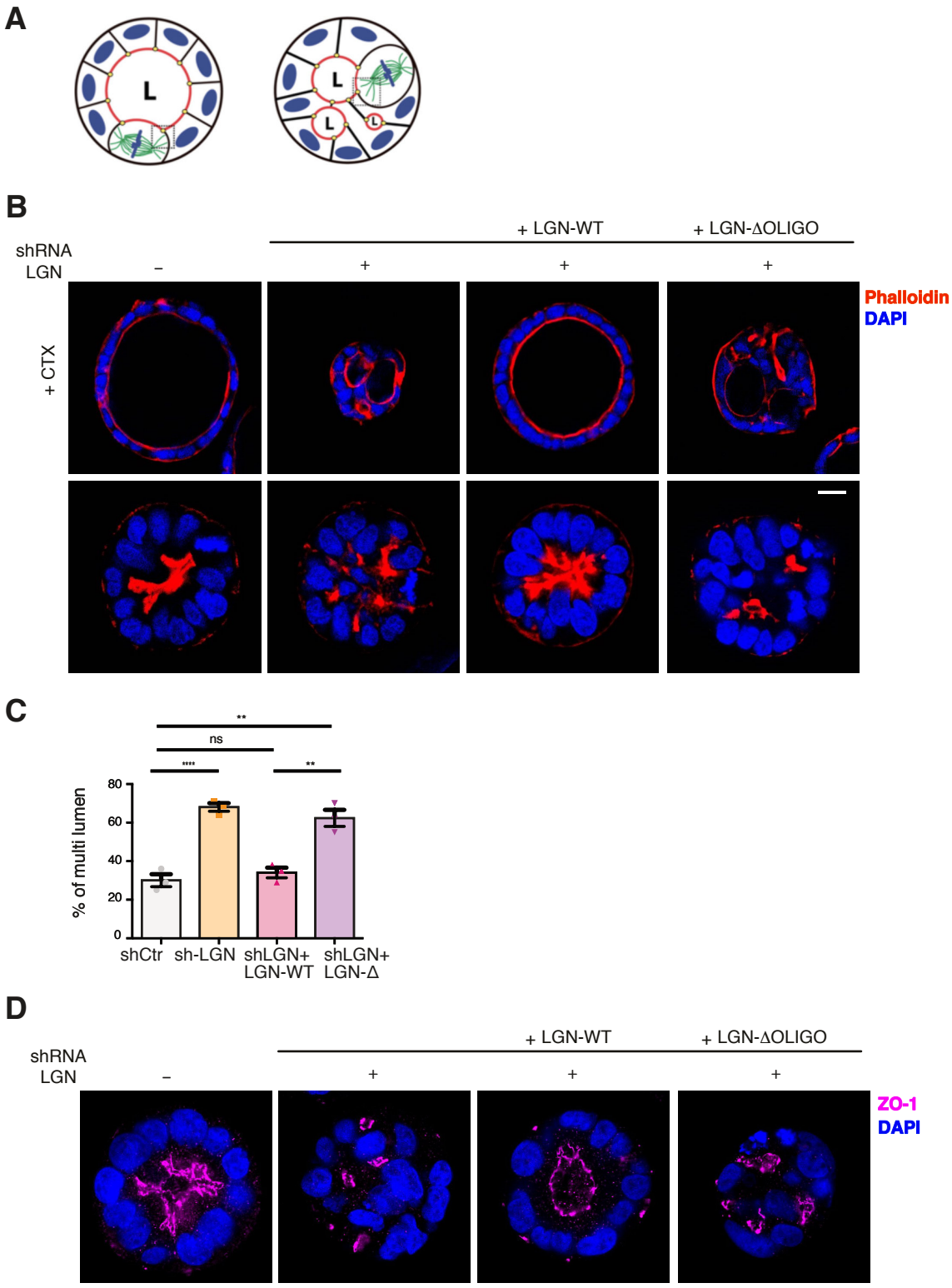

Figure 24 – NuMA:LGN oligomerization is required for single lumen cysts formation

(**A**) Cartoon depicting Caco-2 cells growing as single lumen or multi-lumen cysts highlighting oriented and misoriented divisions. (**B**) Confocal sections of 6-days Caco-2 cysts grown from cells wild-type or depleted of endogenous LGN and expressing LGN-WT-mCherry or LGN-ΔOLIGO-mCherry. In the top row, cholera toxin (CTX)-treated cysts are shown. Cysts were stained with Phalloidin (red) to visualize the apical lumen, and with DAPI to image DNA (blue). (**C**)

Quantification of cystogenesis of Caco-2 cells imaged in panel B. Histograms represent the percentage of multi-lumen cysts. Mean ± SD are shown for 3 independent experiments, with n>60. ***p<0.0001, **p<0.01, *p<0.05 by Fisher's exact test. (**D**) Representative images of Caco-2 cysts grown with wild-type or LGN-rescue cell lines analyzed in B. Cells were stained with ZO-1 (purple) and with DAPI (blue).

3.3 NuMA:LGN oligomerization is required for mitotic spindle orientation in HeLa cells

3.3.1 Setting the conditions to study spindle orientation in HeLa cells

To dissect the molecular mechanisms driving the misorientation phenotype caused by the oligomerization-deficient LGN-ΔOLIGO mutant in Caco-2 cysts, we set out to use HeLa cells, which are widely used as a model system to study spindle orientation, and are easier to image. Similarly to what I have done for Caco-2 cells, I first generated an HeLa cell line stably expressing the shRNA targeting LGN previously used for the experiments with Caco-2 cells, and evaluate efficiency knockdown by Western blot. I also produced a HeLa cell line expressing a control shRNA to use as negative control. Western blot analysis confirmed that the shLGN1-2 efficiently knockdown LGN in HeLa (Figure 25A). To validate this result, I also evaluated LGN levels at the cortex in HeLa cells expressing the shLGN1-2 compared to control cells. Immunofluorescence analysis showed that LGN was not present at the cortex only in cells expressing the shRNA 1-2, confirming the knockdown efficiency (Figure 25B). To perform spindle orientation assays, I used the same pCDH lentiviral vector containing LGN-WT-mCherry and LGN-ΔOLIGO-mCherry to generate stable HeLa cell lines depleted of endogenous LGN and expressing the rescue constructs. Western blot analysis showed that expression levels of rescue constructs were comparable between each other, and that they were equal to endogenous LGN (Figure 25C). Moreover, I imaged the mCherry signal of

HeLa cells expressing the rescue constructs, and confirmed that LGN-WT-mCherry and LGN-ΔOLIGO- mCherry were expressed at similar levels (Figure 25D).

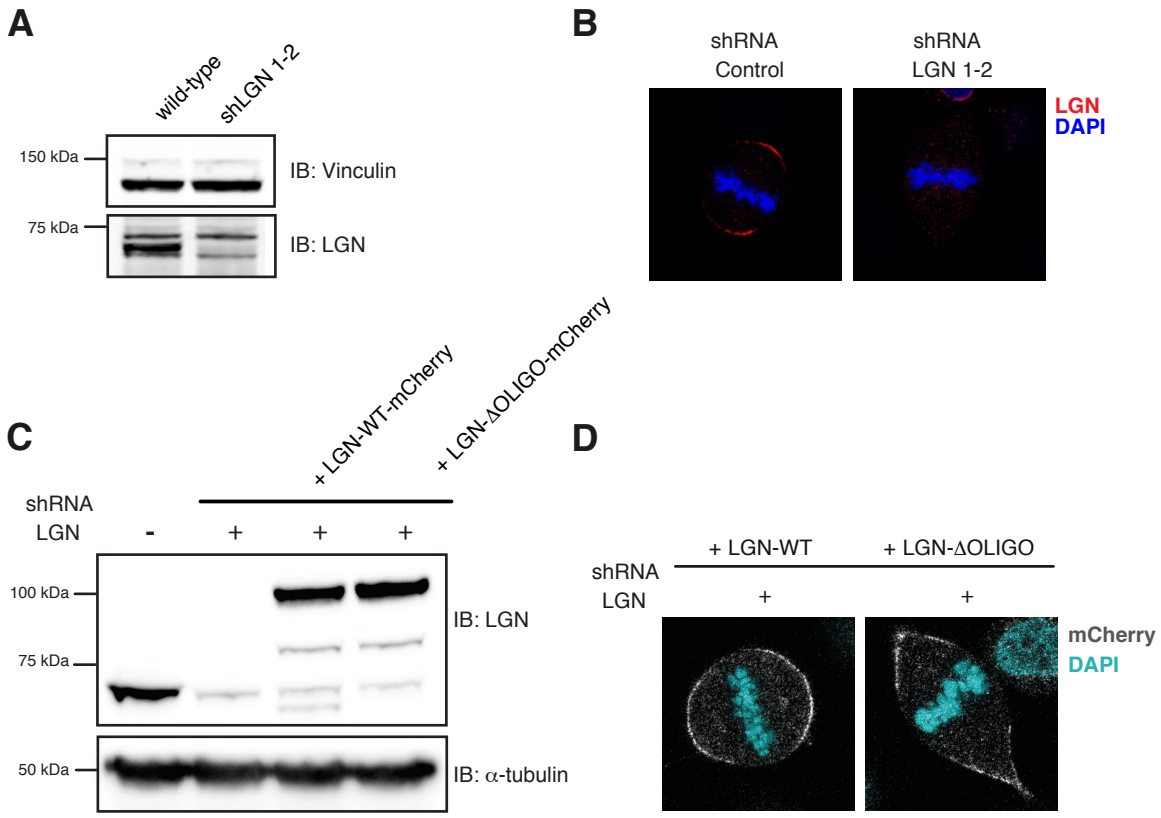

Figure 25 – Generation of HeLa rescue cell lines

(**A**) Western blot of mitotic lysates of HeLa cells stably expressing Control shRNA or shLGN 1-2. Per each lane, 50 μg of lysates were loaded. Vinculin was used as loading control. (**B**) Confocal sections of HeLa cells synchronized in metaphase stably expressing the shRNAs against LGN tested in A. Cells were stained with anti-LGN (red) to verify protein depletion and with DAPI (blue). (**C**) Western blot of mitotic lysates of HeLa cells stably depleted of endogenous LGN, and expressing LGN-WT-mCherry or LGN-ΔOLIGO-mCherry. Per each lane, 30 μg of lysate were loaded. α-tubulin was used as loading control. (**D**) Representative images of HeLa cells stably interfered for LGN and expressing LGN-WT-mCherry or LGN-ΔOLIGO-mCherry. In the image, mCherry signal is shown. Cells were stained with DAPI to visualize the metaphase plate.

3.3.2 NuMA:LGN oligomerization is required to orient the spindle in HeLa cells

When plated on fibronectin-coated coverslips, HeLa cells divide with the mitotic spindle aligned to the substratum, in a β1-integrin dependent manner. To evaluate the extent of spindle orientation defects caused by LGN impairment, I quantified the mitotic spindle angle

taking advantage of method developed by Théry *et al.*, 2005 and Toyoshima and Nishida, 2007, already imported in the lab.

Briefly, to perform spindle orientation assays, I plated HeLa cells on fibronectin-coated coverslip and synchronize them by single thymidine block (see Material and Methods for details), in order to enrich the population of cells in metaphase (Figure 26A). Then, I imaged cells stained with γ-tubulin and DAPI with x-z confocal sections passing through the pole-to-pole axis and quantified the angle "α" formed by a line passing through the spindle poles and the substratum (Figure 26B). This analysis confirmed that HeLa cells expressing the control shRNA divide by with the spindle parallel to the substratum, with a mean spindle angle of 5˚. In line with what observed in Caco-2 cysts and with known literature, knockdown of LGN misorients the spindle to about 13˚. Expression of LGN-WT fully rescued the correct orientation, while expression of LGN-ΔOLIGO did not, with cells dividing with a mean angle of 13˚ (Figure 26B-C).

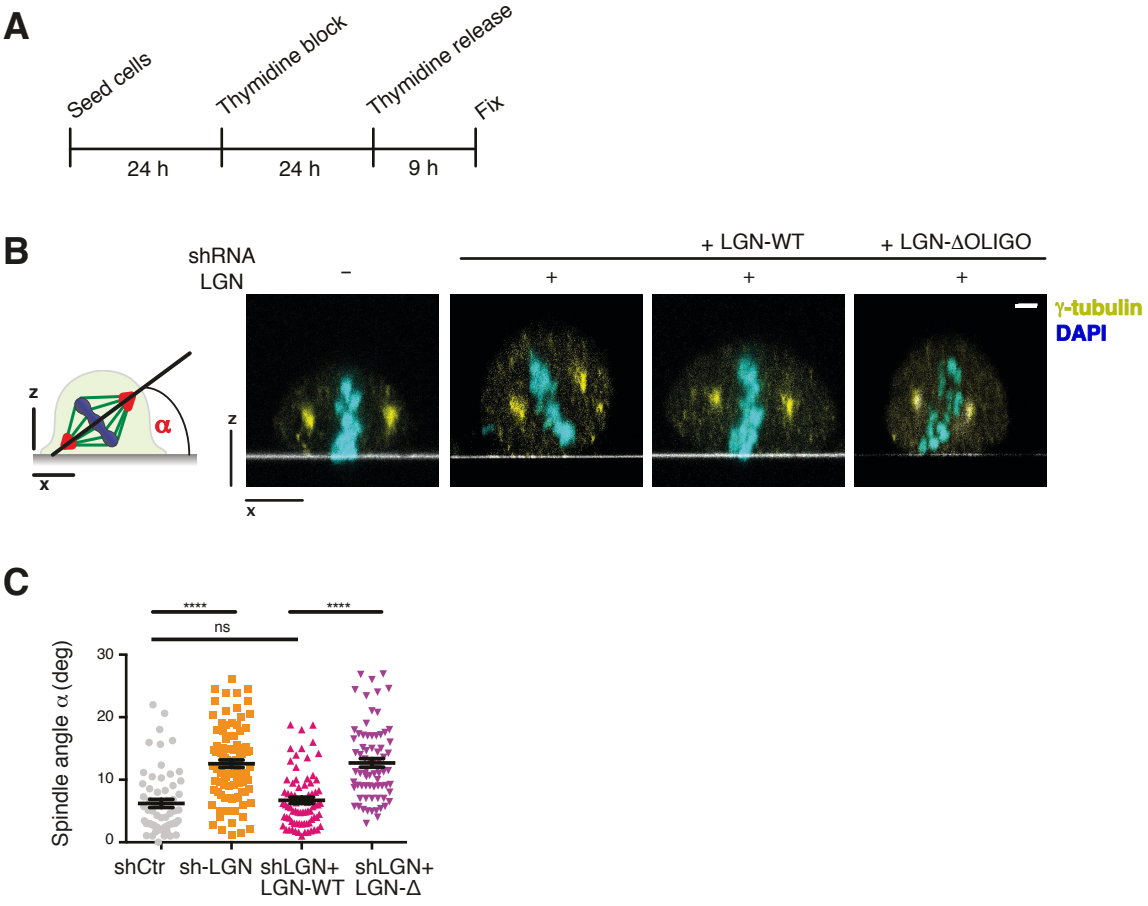

Figure 26 – NuMA:LGN oligomerization is required for spindle orientation in HeLa cells
(**A**) Schematic representation of the synchronization protocol used to study spindle orientation in HeLa cells. (**B**) Left: cartoon depicting a metaphase HeLa cell. The spindle angle "α" is the angle formed by a line passing through the spindle poles (red) and the substratum. Right: confocal x-z sections of HeLa cells depleted of endogenous LGN and expressing LGN-WT-mCherry or LGN-ΔOLIGO-mCherry. Cells were stained with γ-tubulin to visualize the spindle poles (yellow), and with DAPI to visualize the metaphase plate (cyan). The substratum is visible as a white line. (**C**) Dot-plot showing the distribution of spindle axis angles of HeLa cells imaged in panel C. Mean ± SEM are shown for four independent experiments, with n=61 for control cells, n= 94 for shRNA-LGN, n=78 for LGN-depleted cells expressing LGN-WT and n=74 for LGN-depleted cells expressing LGN-ΔOLIGO. **** indicates $p<0.0001$, by the Krustal-Wallis test.

These results confirmed that NuMA:LGN oligomerization is required to orient the mitotic spindle also in HeLa cells, paving the way for a dissection of the molecular mechanism driving the misorientation in this system.

3.3.3 Overexpression of LGN-ΔOLIGO cause spindle rocking in HeLa cells

Elegant time-lapse experiment in HeLa cells reported that the overexpression of LGN and Gα cause spindle rocking in metaphase, due to an increased recruitment of spindle motors at the membrane. To assess whether an excess of LGN can overcome the requirement of NuMA:LGN oligomerization in generating pulling forces to orient the spindle, I set out to perform a spindle rocking experiment by overexpressing LGN-WT and LGN-ΔOLIGO in HeLa cells. To test the effects of excessive ectopic expression of LGN rescue constructs, I transfected HeLa cells stably expressing GFP-H2B with 10 μg LGN-WT and LGN-ΔOLIGO in order to express the two proteins at much higher levels than endogenous LGN (Figure 27A). 28 hours after transfection, I filmed the cells to analyze metaphase plate movements as described in (Kotak, Busso and Gönczy, 2012). Briefly, cells were filmed with 3-minute frames. Spindle rocking was calculated considering "oscillation" when the metaphase plate rotates more than 10˚ between two consecutive frames. As expected, time-lapse recording

showed that the frequency of oscillation of the metaphase plate of HeLa cells expressing LGN-WT was three-times higher compared to wild-type HeLa cells, and that overexpression of LGN-ΔOLIGO triggers spindle rocking to the same extent (Figure 27B). We reasoned that this result is not completely unexpected because the rescue constructs were massively overexpressed, presumably bypassing the regulatory mechanisms governing spindle positioning under physiological conditions.

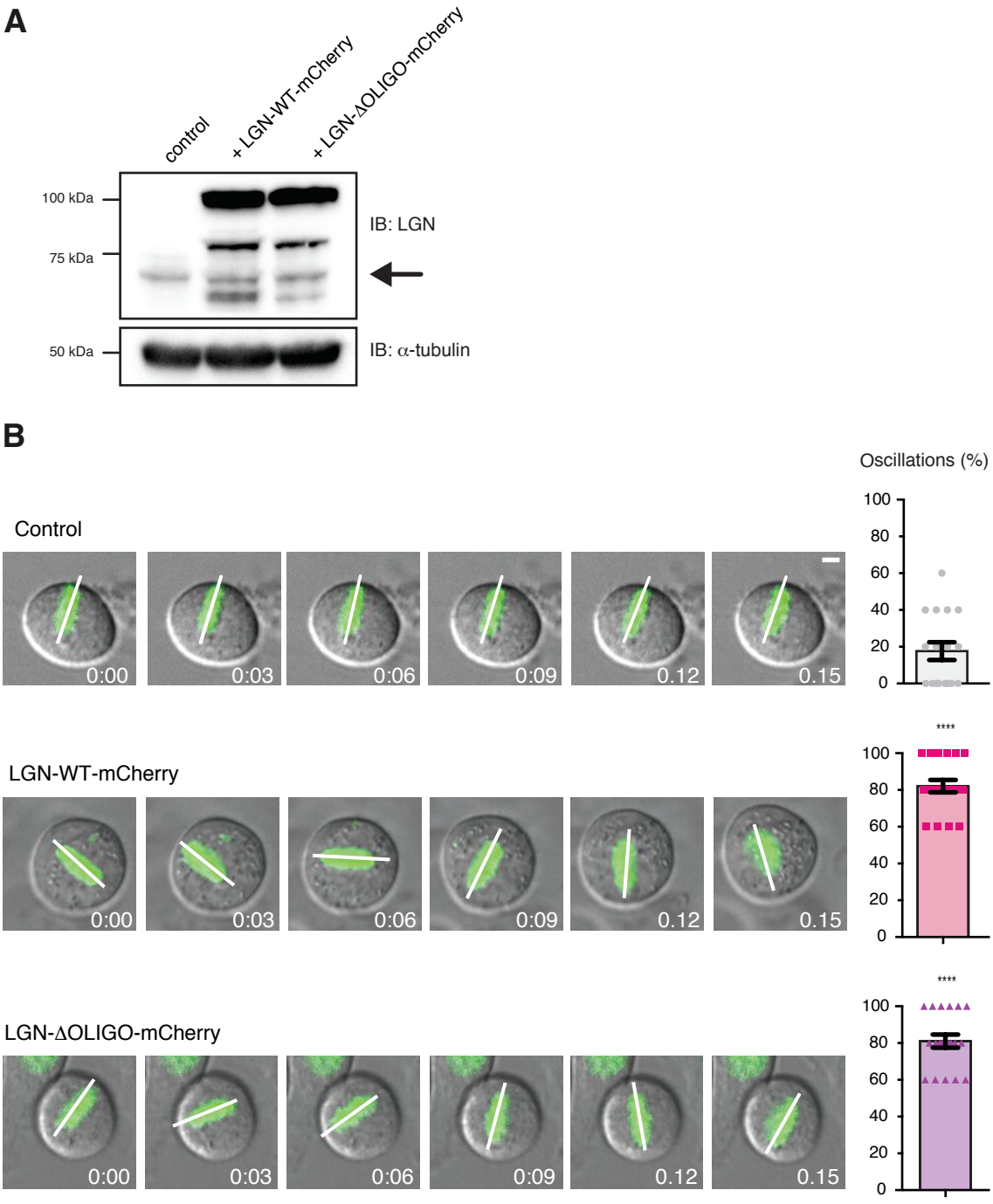

Figure 27 – LGN overexpression cause spindle rocking in HeLa cells

(**A**) Western blot of mitotic lysates of HeLa cells wild-type or transiently transfected with LGN-WT-mCherry or LGN-ΔOLIGO-mCherry. Per each lane, 30 μg of lysate was loaded. α-tubulin was used as loading control. The black arrow indicated endogenous LGN. (**B**) Left: representative frames of the time-lapse experiment of HeLa cells stably expressing H2B-GFP transiently transfected with LGN rescue constructs. The H2B-GFP signal (green) is overlayed with DIC. The white line indicates the position of the metaphase plate. Frames were acquired every three minutes, with 10 cells per condition acquired in two independent experiments. Right: quantification of oscillation frequency. **** indicates $p<0.0001$, by two-tailed Student's test. Scale bars, 5 μm.

3.3.4 Setting the conditions to rescue NuMA expression in HeLa cells

To confirm the results obtained with the LGN mutant from the NuMA side, we exploited again the information provided by the crystal structure to generate a NuMA construct unable to oligomerize. To this aim, I depleted the region of NuMA encompassing residues 1862-1899, that fits between the two LGN^{TPR} molecules of the hexameric donut, generating a NuMA mutant unable to form high-order oligomers, but still retaining the capability to interact with LGN with a 1:1 stoichiometry, hereon defined as NuMA-ΔOLIGO (Figure 28A). I cloned the NuMA-ΔOLIGO construct in a pCDH lentiviral vector in frame with a mCherry tag. I also generated a second NuMA mutant, depleted of the entire LGN-binding domain (encompassing residues 1862-1928, hereon referred as NuMA-ΔLGNBD) to be used as negative control, while the full-length NuMA construct in frame with mCherry was also inserted in the same pCDH vector to be used as positive control. To perform spindle orientation assays, I used the same NuMA-depleted HeLa cell line that we generated to analyze the cross-talk between NuMA and Aurora-A (Gallini *et al.*, 2016) (Figure 28B-C). The large size of the NuMA gene does not allow the generation of stable cell lines expressing NuMA by lentiviral infection as the viral packing is not efficient. Thus, we decided to transiently transfect the mCherry-NuMA constructs in HeLa cells expressing the shRNA-NuMA-D with Lipofectamine 3000, a reagent suitable for transfection of large-size genes.

Western blot analysis confirmed that the NuMA constructs were well expressed in the NuMA-depleted HeLa cells, at much higher amounts than endogenous NuMA (Figure 28D). Since it has been reported that NuMA overexpression cause mitotic defects (Brüning-Richardson *et al.*, 2012), I set out to quantify the fluorescent signal of mCherry-NuMA wild-type in order to define a threshold over which NuMA itself causes misorientation. To this aim, I synchronized transfected HeLa cells in metaphase and stained them with DAPI to identify metaphase cells. Then, I imaged cells in x-z sections passing through the spindle poles and quantified the mCherry fluorescence intensity coming from misoriented cells expressing mCherry-NuMA-WT, and define an intensity threshold (Figure 28E). The highest intensity of the mCherry signal that does not couse misorientation, was used as a threshod for the spindle orientation assays described in the following section.

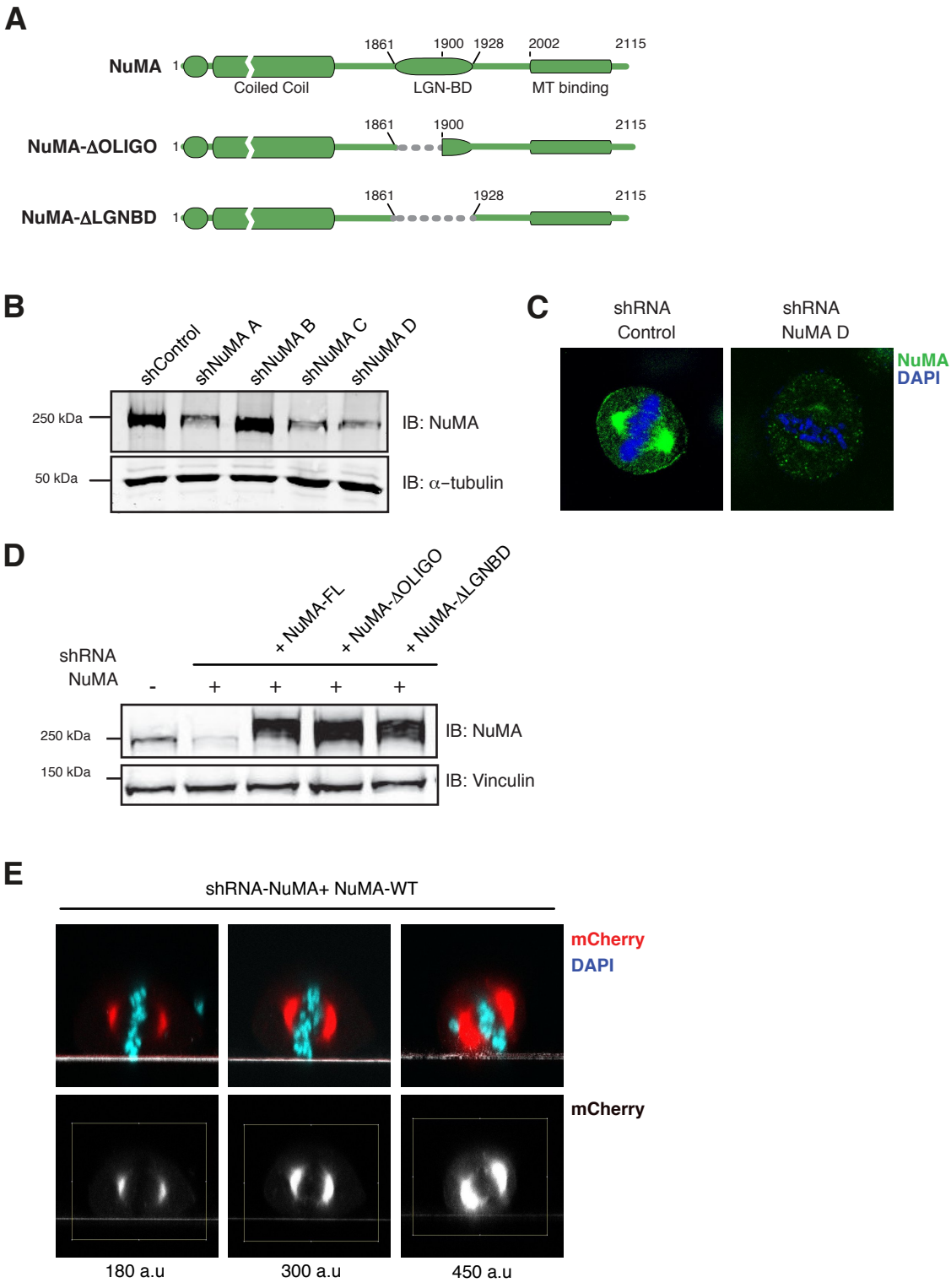

Figure 28 – Setting the conditions to study a NuMA oligomerization-deficient mutant in HeLa cells

(**A**) Schematic representation of the domain structure of wild-type NuMA, NuMA-ΔOLIGO and NuMA-ΔLGNBD. Dashed grey lines indicated the regions depleted to generate the mutant constructs. (**B**) Western blot of mitotic lysates of HeLa cells wild-type stably expressing shRNAs against NuMA. Per each lane, 50 µg of lysate were loaded. α-tubulin was used as loading control. (**C**) Confocal sections of HeLa cells synchronized in metaphase stably expressing the shRNA-

NuMA-D tested in B. Cells were stained with NuMA (green) to verify protein depletion and with DAPI (blue). (**D**) Western blot of mitotic lysates of HeLa cells stably depleted of endogenous NuMA, and transiently transfected with mCherry-NuMA-WT, mCherry-NuMA-ΔOLIGO or mCherry-NuMA-ΔLGNBD. Per each lane, 50 μg of lysate was loaded. Vinculin was used as loading control. (**E**) HeLa shRNA-NuMA stable cell line transfected with mCherry-NuMA-WT. mCherry signal included in the ROI marked as a box in the bottom panels was quantified with the software Fiji. An intensity of 450 a.u was defined as threshold for the rescue experiments.

3.3.5 The oligomerization domain of NuMA is required for spindle orientation

To evaluate the spindle orientation of HeLa cells depleted of endogenous NuMA and expressing the rescue constructs, I applied the same protocol used for the orientation experiment with the LGN mutants in paragraph 3.3.2, plating HeLa cells on fibronectin and synchronizing them by single thymidine block. Cells depleted of endogenous NuMA showed orientation defects, with an average spindle axis angle of 14˚. Expression of mCherry-NuMA-WT fully rescued the control phenotype, while NuMA-ΔOLIGO did not, showing a mean angle of division of about 12˚. As expected, also NuMA-ΔLGNBD, which cannot bind LGN, did not rescue the correct orientation of the spindle (Figure 29A-B). We concluded that the stretch of NuMA oligomerizing with LGN, i.e. residues 1892-1899 are required for correct spindle orientation.

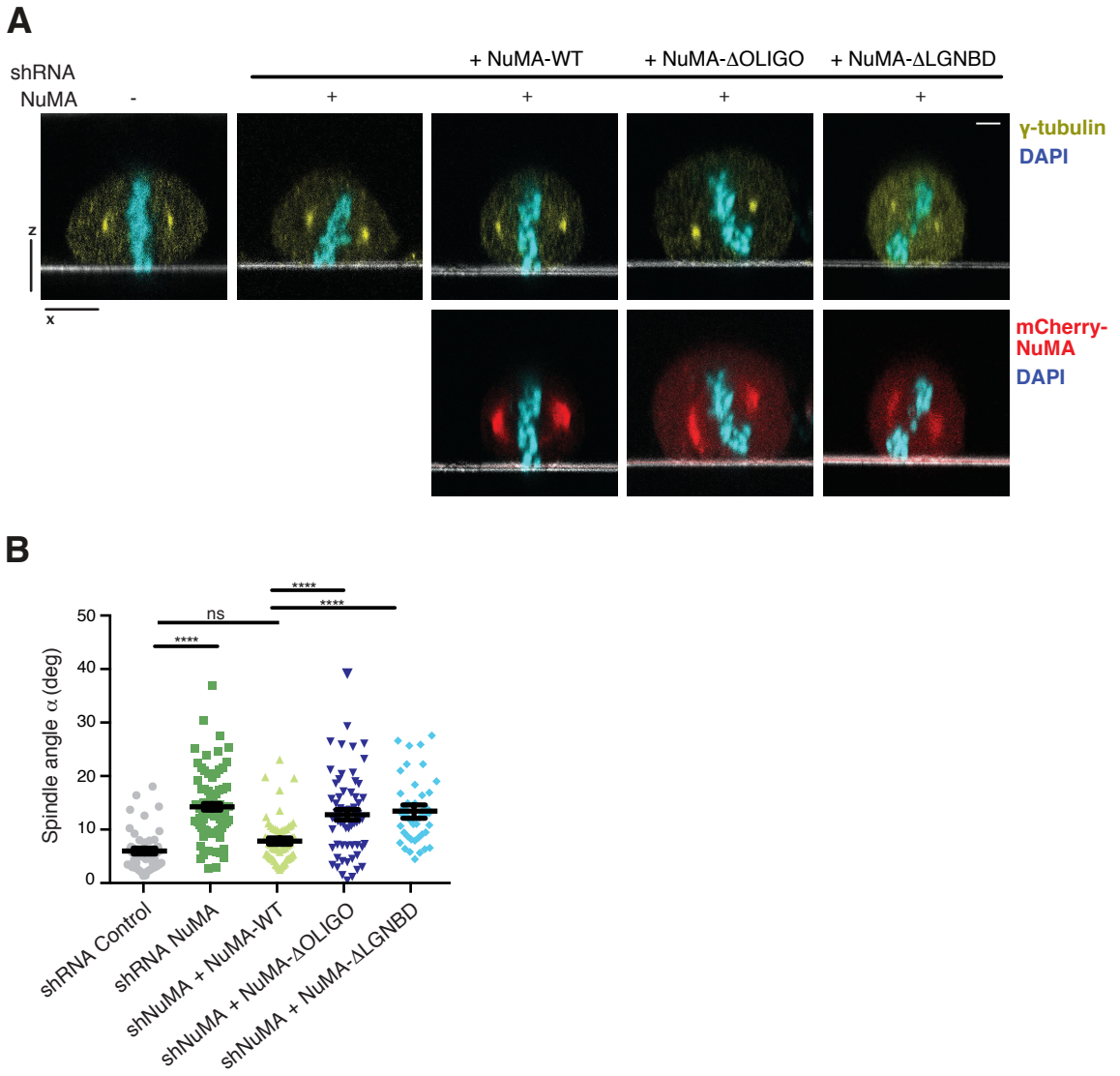

Figure 29 – NuMA-ΔOLIGO does not rescue mitotic spindle orientation

(**A**) Confocal x-z sections of HeLa cells depleted of endogenous NuMA and transfected with mCherry-NuMA-WT, mCherry-NuMA-ΔOLIGO or mCherry-NuMA-ΔLGNBD. Cells were stained with γ-tubulin (yellow) to visualize the spindle poles, and with DAPI to visualize the metaphase plate (cyan). The substratum is visible as a white line. (**B**) Dot-plot showing the distribution of HeLa cells imaged in panel A. Mean ± SEM are shown for four independent experiments, with n=51 for control cells, n= 71 for shRNA-NuMA, n = 56 for NuMA-depleted cells expressing NuMA-WT, n=63 for NuMA-depleted cells expressing LGN-ΔOLIGO and n=45 for NuMA-depleted cells expressing NuMA-ΔLGNBD. **** indicates $p<0.0001$, by the Krustal-Wallis test. Scale bars, 5 μm.

3.3.6 NuMA-ΔOLIGO localize less at the spindle poles

The orientation analysis performed with the NuMA constructs confirmed the results obtained with the LGN mutant, somehow suggesting a requirement of the NuMA:LGN

oligomerization to orient the spindle. However, I noticed a defective localization of the NuMA-ΔOLIGO and NuMA-ΔLGNBD mutants at the spindle poles compared to NuMA WT, as they seemed to localize less at the poles. To confirm this hypothesis, I set out to quantify NuMA localization at the spindle poles of cells expressing the mCherry-NuMA constructs (for details, see Material and Methods). Quantification of mCherry fluorescence intensity confirmed a 2-fold decrease in the levels of NuMA-ΔOLIGO at the poles, while NuMA-ΔLGNBD showed a 3-fold decrease compared to NuMA-WT (Figure 30A-B). Since proper NuMA localization at the poles is a prerequisite for the correct organization of the mitotic spindle, we decided that we could not fully ascribe the misorientation phenotype observed NuMA-ΔOLIGO expressing cells to the lack of NuMA cortical activity, as this phenotype could be caused by spindle assembly defects.

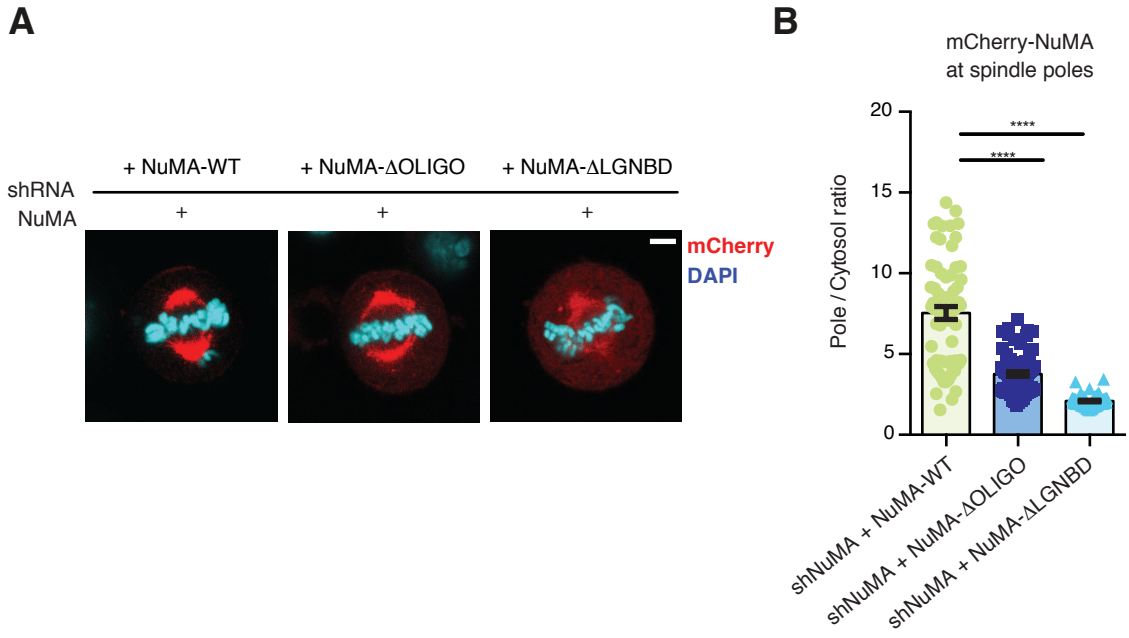

Figure 30 – NuMA-ΔOLIGO and NuMA-ΔLGNBD localize less at the spindle poles

(**A**) Confocal images of HeLa cells depleted of endogenous NuMA and transfected with mCherry-NuMA-WT, mCherry-NuMA-ΔOLIGO or mCherry-NuMA-ΔLGNBD. Cells were stained with DAPI (cyan) to visualize the metaphase plate. (**B**) Quantification of mCherry fluorescence intensity at the poles, with histograms representing the poles-to-cytoplasm fluorescent ratio. Mean ± SEM are shown for four independent experiments, with n>60. **** indicates p<0.0001, by the Krustal-Wallis test. Scale bars, 5 μm.

3.4 NuMA and LGN form proteins network

3.4.1 Studying NuMA:LGN oligomerization in cells

With the aim to understand how NuMA and LGN promote spindle orientation, we started investigating whether NuMA:LGN hetero-hexamers form in cells. To test this hypothesis, we developed a strategy to co-transfect LGN wild-type or the oligomerization-deficient LGN-ΔOLIGO with different tags, in order to induce the assemble of a ”donut” containing at least two differentially-tagged LGN molecules**,** and monitor the presence of the two tags in the donut performing a Proximity Ligation Assay (PLA). PLA is a technique that allow the detection and the quantification of protein-protein interaction in cells, when they belong to the same complex and hence are closer than 40 nm. (see Methods for a detailed description). Our idea was to prove that differentially tagged wild-type LGN molecules could give PLA signals as they engage in the same hetero-hexamer with NuMA, while LGN-ΔOLIGO could not because they are far apart on different NuMA molecules.

To use the PLA technique, I first cloned LGN-WT and LGN-ΔOLIGO in a pLVX vector in frame with a C-terminal GFP tag. Then, I cloned the same LGN molecules in a pCDH vector with a C-terminal 3xFLAG tag. To perform PLA, two primary antibodies from different species were needed. For this experiment, I tested primary antibodies against the LGN tags, in order to set the best working conditions and to check that the tagged-LGN constructs correctly localize at the cortex. Immunofluorescence analysis of HeLa cells transfected with LGN-WT-3xFLAG and GFP-LGN-WT showed that both FLAG and GFP-tagged LGN correctly localize at the cortex, and that the double-staining with primary antibodies required for PLA worked properly (Figure 31A). I next carry out various negative-controls required to test that PLA results were genuine and not due to cross-reactivity of the antibodies. I performed a co-transfection of the GFP and FLAG-tagged LGN and stained HeLa cells with primary antibodies and PLA probes together or in combination, before proceeding with the PLA protocol. The control experiment confirmed that all the primary and secondary

antibodies worked well, with no major signal coming from the cells (Figure 31B). PLA experiment showed that GFP-LGN-WT and LGN-WT-3xFLAG interacts in HeLa cells, showing a punctate signal within the transfected cells (Figure 31C). However, I could observe a punctate signal also in cells co-transfected with GFP-LGN-ΔOLIGO and LGN-ΔOLIGO-3xFLAG. Since for this experiment we worked by transfection of high amount of proteins, we reasoned that these results could be due to the excessive of LGN expressed in cells, that in some way become in close proximity. We did not pursued the experiment any further and tried to develop an alternative and more robust strategy to assess the presence of NuMA:LGN hetero-hexamers in cells.

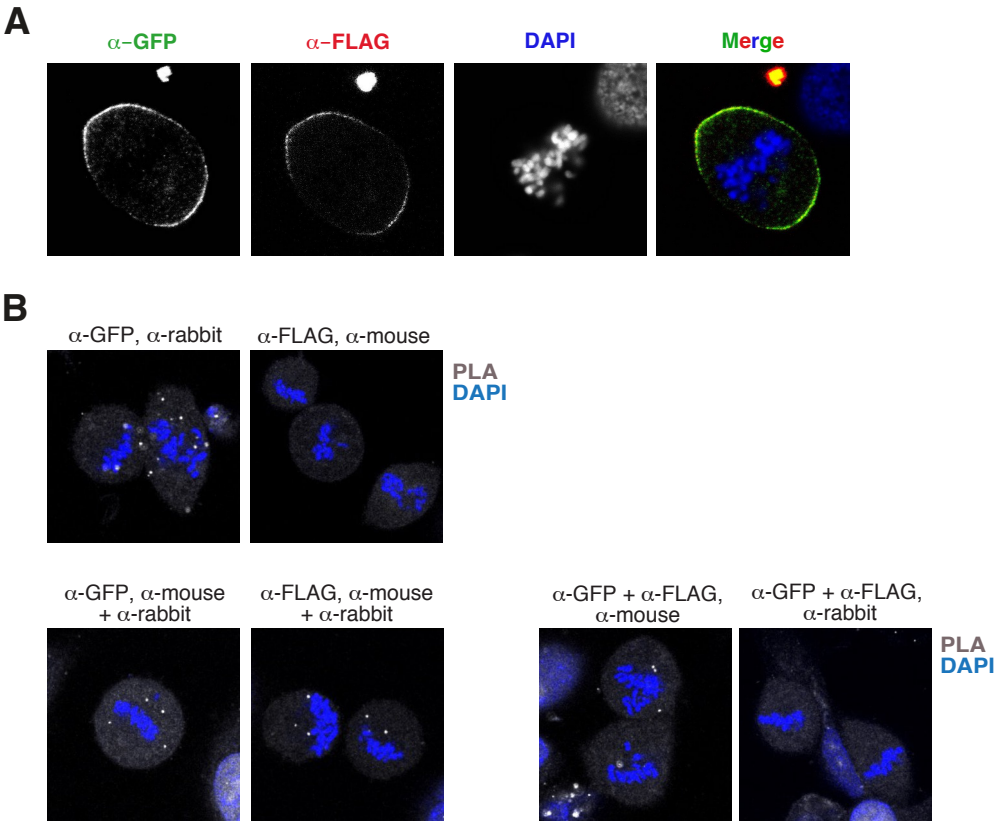

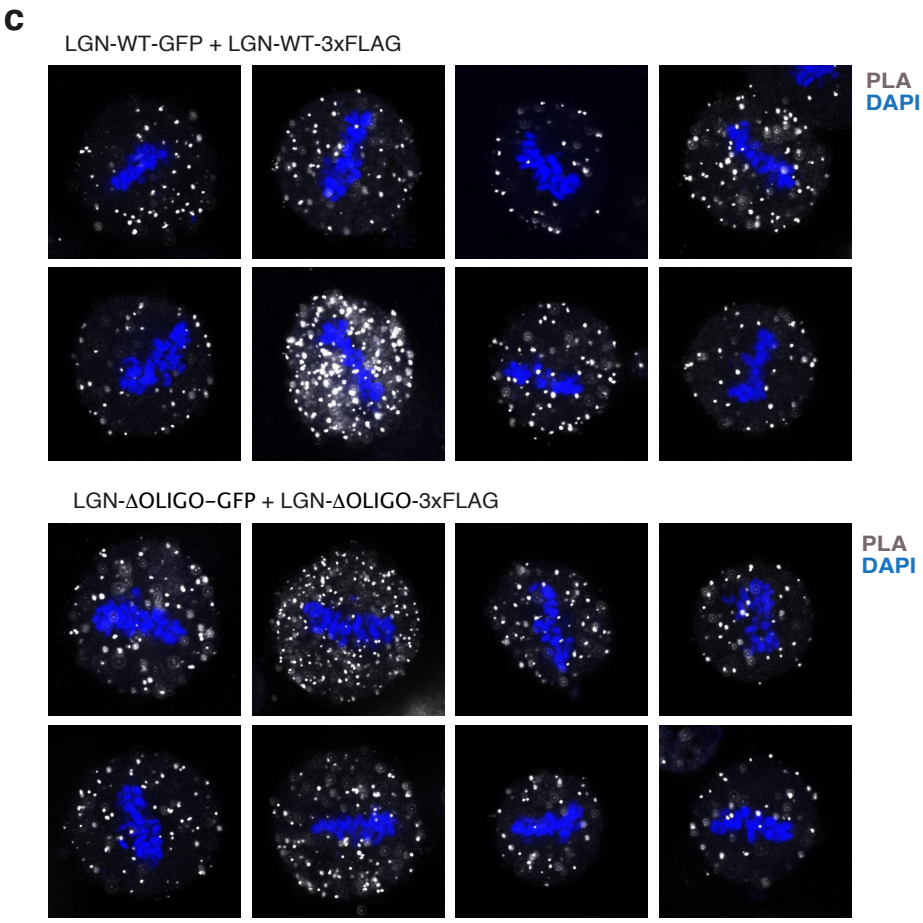

Figure 31 – Both LGN-WT and LGN-ΔOLIGO give PLA signal in cells

(**A**) Representative image of HeLa cells co-transfected with GFP-LGN-WT and LGN-WT-3xFLAG. Cells were stained with GFP and FLAG antibodies and with DAPI. (**B**) Representative image of HeLa cells co-transfected with the constructs indicated above and stained with primary antibodies (GFP and FLAG) and PLA probes (mouse or rabbit), alone or in combination. PLA signal is shown in white. DNA was stained with DAPI (blue). (**C**) Top: representative image of HeLa cells co-transfected with GFP-LGN-WT and LGN-WT-3xFLAG. Bottom: representative image of HeLa cells co-transfected with GFP-LGN-ΔOLIGO and LGN-ΔOLIGO-3xFLAG. PLA signal is shown in white. DNA was stained with DAPI (blue).

3.4.2 NuMA and LGN form hetero-hexamers in cells

As a complementary approach to PLA, we decided to implement a co-immunoprecipitation experiment co-transfecting differentially-tagged LGN molecules, as performed in the previous paragraph. Specifically, we planned to use a GFP-tagged LGN to perform the immunoprecipitation and a FLAG-tagged LGN to check the co-immunoprecipitated interactors. Because LGN:LGN interactions requires NuMA, we expected to find among the

GFP-LGN interactors NuMA and FLAG-LGN, meaning that an hetero-hexameric structure assembled in cells (Figure 32A). As negative control for this co-IP experiment we planned to co-transfect LGN-ΔOLIGO with GFP and with FLAG tags. In this case, we expected to IP GFP-LGN and find only NuMA among the co-immunoprecipitated molecules, because of the binary interaction between NuMA and LGN preserved even in absence of NuMA:LGN oligomerization (Figure 20). Importantly, we know that endogenous NuMA contains a long coiled-coil domain which induces the self-dimerization. We therefore reasoned that performing the IP experiment in presence of a full-length NuMA would represent an obstacle, since endogenous NuMA immunoprecipitating with LGN could dimerize with another NuMA molecule bound to another LGN even in the absence of NuMA:LGN oligomerization. To overcome this problem, I generated a 293T cell line depleted of endogenous NuMA, taking advantage of the same shRNA-NuMA used to knockdown NuMA in HeLa cells (see paragraph 3.3.4). I then cloned the monomeric C-terminal portion of NuMA downstream of the coiled-coil, encompassing residues 1821-2115, in a pCDH vector, and infected the 293T-shRNA-NuMA cell line to obtain a stable expression of the rescue construct. Western blot analysis confirmed that the C-terminal NuMA construct was expressed in 293T cell depleted of the endogenous protein, with about a 3-fold enrichment (Figure 32B). To perform the co-IP experiment, first I cloned LGN-WT and LGN-ΔOLIGO in a pEGFP vector in frame with a N-terminal GFP tag. For FLAG-tagged LGN, I used the vector described in paragraph 3.4.1. To confirm that all constructs were efficiently expressed in cells at comparable levels, I set the conditions to co-transfect the GFP-tagged and the FLAG-tagged form of wild-type LGN in 293T cells stably expressing shRNA-NuMA and $NuMA^{1821-2115}$ ($NuMA^{Cter}$) (Figure 32C).

Co-immunoprecipitation experiment conducted with anti-GFP antibodies confirmed that only the wild-type GFP-LGN can co-immunoprecipitate LGN-WT-3xFLAG and $NuMA^{1821-2115}$. Conversely, GFP-LGN-ΔOLIGO co-IPs only $NuMA^{1821-2115}$, and in lower amount compared to the wild-type protein (Figure 32D). This results fully support the notion that

NuMA and LGN can assemble high-order oligomers in cells, and that mutations affecting the NuMA:LGN oligomer formation in vitro also impairs the oligomerization in cells. Moreover, this evidence suggests that NuMA:LGN oligomerization occurs independently of NuMA self-assembly, and that the hetero-hexamers we characterized in vitro are the key event in multivalent NuMA:LGN interactions in mitosis.

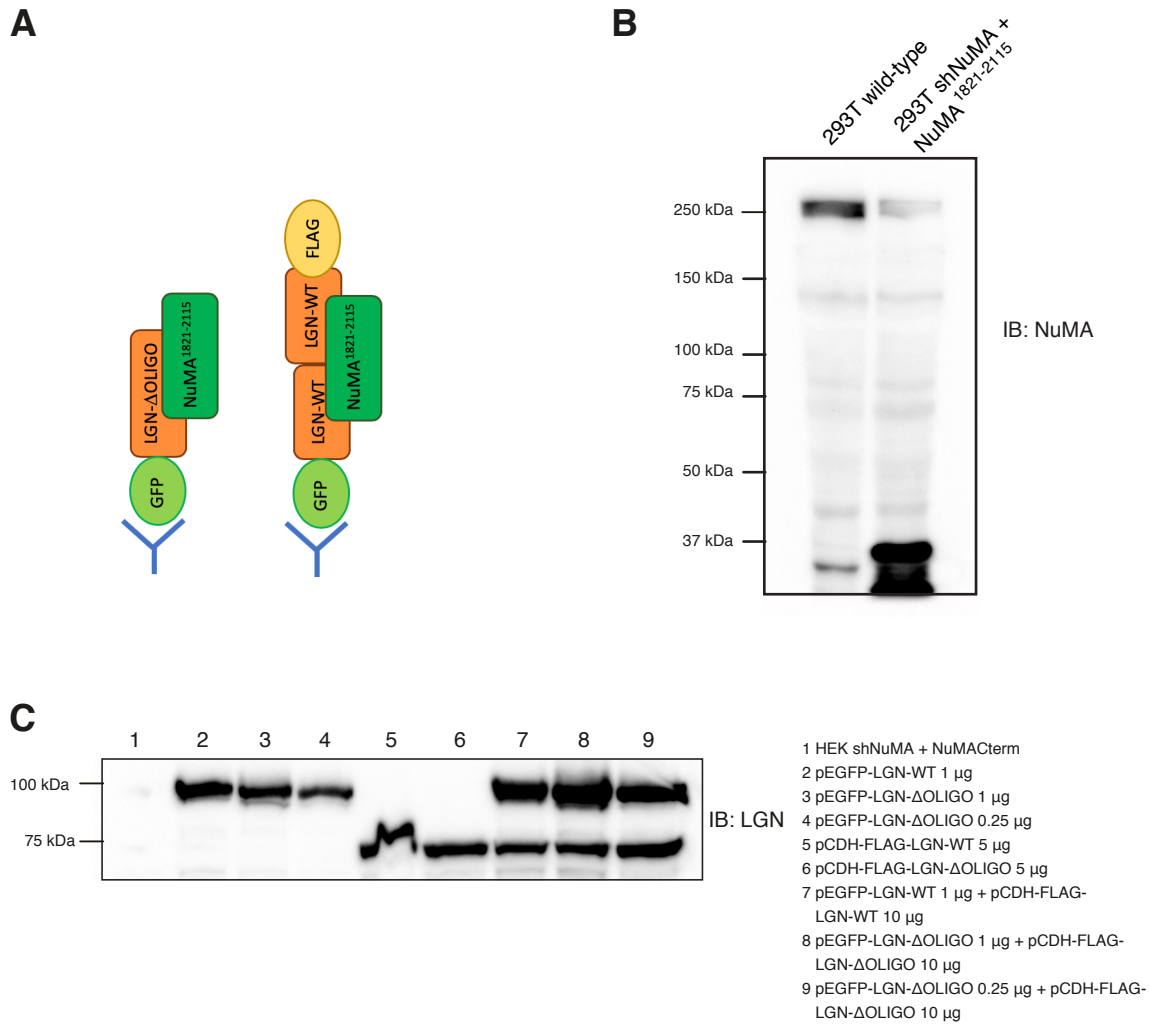

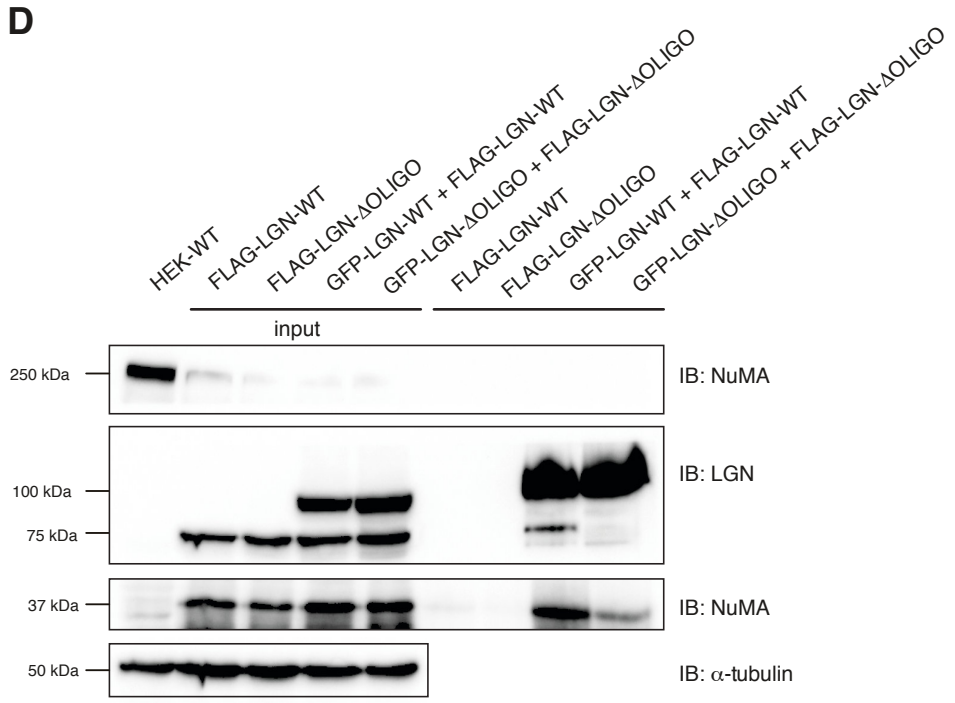

Figure 32 – LGN and NuMA form hetero-hexamers in cells

(**A**) Cartoon depicting different IP scenarios. In presence oligomerization-proficient NuMA and LGN proteins, GFP-LGN-WT can engage in hetero-hexamers with LGN-WT-3xFLAG and NuMA$^{1821\text{-}2115}$. Conversely, performing IP experiments with the oligomerization-deficient GFP-LGN-ΔOLIGO mutant results in a co-immunoprecipitation of NuMA$^{1821\text{-}2115}$ alone, because of the 1:1 binary interaction between NuMA and LGN. (**B**) Western blot of mitotic lysates of 293T cell lines stably depleted of endogenous NuMA and expressing NuMA$^{1821\text{-}2115}$. (**C**) Western blot to set the pEGFP-LGN-WT/ΔOLIGO and pCDH-FLAG-LGN-WT/ΔOLIGO co-transfection. 50 μg of mitotic lysates of 293T shNuMA+NuMA$^{1821\text{-}2115}$ transfected with the indicated constructs were loaded. α-tubulin was used as loading control. (**D**) Western blot of mitotic lysates of 293T cell lines stably depleted of endogenous NuMA and co-transfected with GFP-LGN-WT and LGN-WT-3xFLAG or with GFP-LGN-ΔOLIGO and LGN-ΔOLIGO-3xFLAG. Cell transfected LGN-WT-3xFLAG and LGN-ΔOLIGO-3xFLAG were used as control for the IP, and wild-type cells were loaded to monitor NuMA depletion and NuMA$^{1821\text{-}2115}$ expression (IB anti-NuMA at 250 kDa for the endogenous protein and 37 kDa for NuMA C-terminal construct). α-tubulin was used as loading control for the inputs.

3.5 Force generators are recruited at the cell cortex independently of NuMA:LGN oligomerization

3.5.1 NuMA:LGN oligomerization is not needed for LGN and NuMA cortical recruitment in metaphase

According to the current model, in vertebrate cells in metaphase LGN is recruited at the cell cortex by binding of its C-terminal GoLoco motifs to Gαi proteins, while the N-terminal TPR domain directly interacts with NuMA (Du, Stukenberg and Macara, 2001). In turn, the cortical pool of NuMA promotes the cortical recruitment of dynein/dynactin, this way regulating mitotic spindle orientation. In trying to understand why the LGN-ΔOLIGO mutant cannot sustain spindle orientation, we first hypothesized that NuMA:LGN oligomerization could promote protein clustering at the cell cortex. To test this possibility, I analyzed the cortical recruitment of spindle orientation proteins in the HeLa cell lines depleted of endogenous LGN and expressing the rescue constructs. First, I performed an immunofluorescence to evaluate cortical levels of LGN wild-type or LGN-ΔOLIGO in metaphase. Line-scan analysis (see Material and Methods for details) confirmed that the cortical pool of LGN was lost in the shRNA-LGN cell lines, while both LGN-WT and LGN-ΔOLIGO localize at the cortex and to the same extent of the endogenous protein (Figure 33A). This result was expected, since the mutated LGN-ΔOLIGO construct lacks part of the N-terminal region, while the GoLoco domain required for the interaction with Gα is unaffected. To evaluate whether the expression of the LGN oligomerization-deficient mutant impacts on NuMA accumulation at the cortex, I performed an immunofluorescence against NuMA on the same cell lines described above, and quantified amount of protein at the cortex. As expected, depletion of LGN abolish NuMA recruitment at the membrane compared to control cells, while in cells expressing the mCherry-LGN-WT the amount of NuMA at the cortex was fully rescued (Figure 33B). The cortical pool of NuMA was rescued also in cells expressing the LGN-ΔOLIGO mutant with no significant difference with what observed in

cells expressing LGN wild-type. This result was somehow unexpected, and suggests that NuMA:LGN oligomerization is dispensable for NuMA recruitment at the cortex, and that the binary interaction of NuMA with LGN suffices to recruit correct levels of NuMA at the cortex.

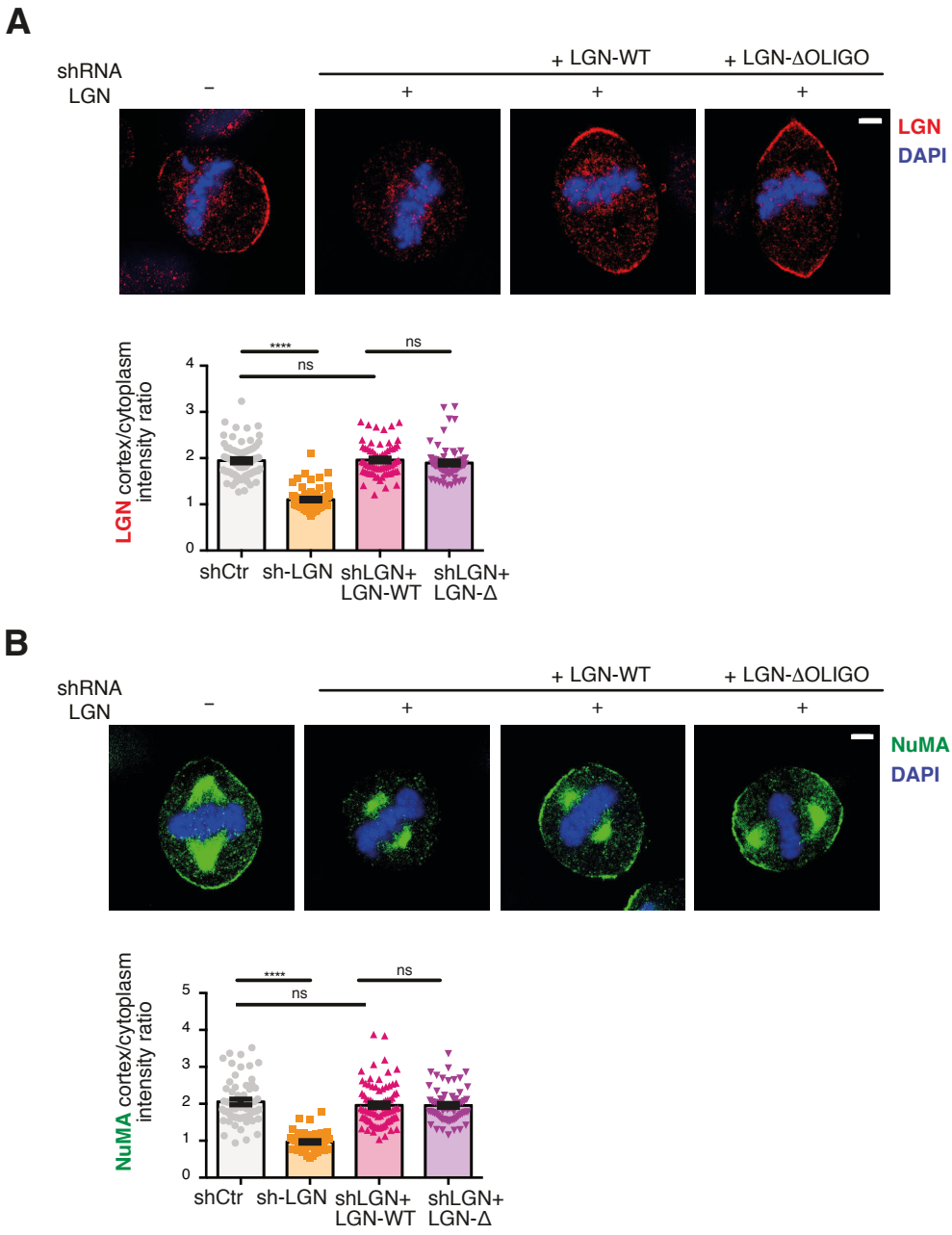

Figure 33 – LGN and NuMA localize at the cortex regardless of NuMA:LGN oligomerization

(**A**) Top: confocal images of HeLa cells depleted of endogenous LGN and expressing LGN-WT-mCherry or LGN-ΔOLIGO-mCherry. Cells were stained with LGN (red) and DAPI (blue). Bottom: quantification of cortical signals, with histograms representing the cortex-to-cytoplasm fluorescence ratio. Mean ± SEM are shown for three independent experiments, with n>69. (**B**) Top: confocal

images of HeLa cells expressing the LGN rescue constructs. Cells were stained with NuMA (green) and DAPI (blue). Bottom: quantification of cortical signals. Mean ± SEM are shown for three independent experiments, with n>60. **** indicates p<0.0001, by the Krustal-Wallis test. Scale bars, 5 μm.

3.5.2 Motor proteins are recruited at the cortex in absence of NuMA:LGN oligomerization

To endorse the results obtained with the analysis of NuMA cortical localization, we decided to analyze the recruitment of spindle motors, whose cortical clustering could be affected by the lacks of NuMA:LGN oligomerization. I first focus on the dynactin-subunit $p150^{Glued}$, which is widely considered a valid readout to evaluate the recruitment of the dynactin complex. Consistently with the notion that in metaphase cortical pool of NuMA recruits dynein/dynactin complexes, loss of NuMA from the cortex in cells depleted of endogenous LGN abrogates cortical dynactin. On the other hand, dynactin recruitment in the LGN rescue HeLa cell lines reflects NuMA behavior, with no major differences in the cortical amount of $p150^{Glued}$ after the expression of LGN-WT or ΔOLIGO compared to wild-type cells (Figure 34A). To confirm the results obtained with dynactin also with the dynein, I set out analyze dynein distribution in the HeLa rescue cell lines. Despite I tried several fixation and permeabilization protocols, and different blocking conditions, I could detect only very weak dynein cortical signals from the region above the spindle poles (Figure 34B), which were not reliable for a quantification. Therefore to visualize cortical dynein we decided to adopt a different strategy, and analyze the localization of the ectopically expressed dynein-subunit Light Intermediate Chain 1 (LIC1). Specifically, I cloned FLAG-tagged LIC1 in a pCDH vector under the Ubc promoter, used the vector to transfect the HeLa cell lines described above, and stain for the FLAG tag, in order to visualize the distribution of LIC1. LIC1-FLAG localized in cortical region above the spindle poles in control conditions, while no cortical LIC1 was detectable in HeLa cells depleted of LGN. Upon re-expression of both

LGN-WT and LGN-ΔOLIGO, LIC1 accumulated back at the cortex (Figure 34C). Since also under these transfection conditions the levels of LIC1 at the cortex were not easy to detect and the amount of transfected construct could be significantly different than endogenous LIC, I decided to simply count the percentage of cells with a visible cortical signal (Figure 34C, bottom), instead to adopt the line-scan quantification. Collectively, these results indicate that NuMA:LGN oligomerization is not required for NuMA and dynein/dynactin recruitment at the cell cortex during metaphase.

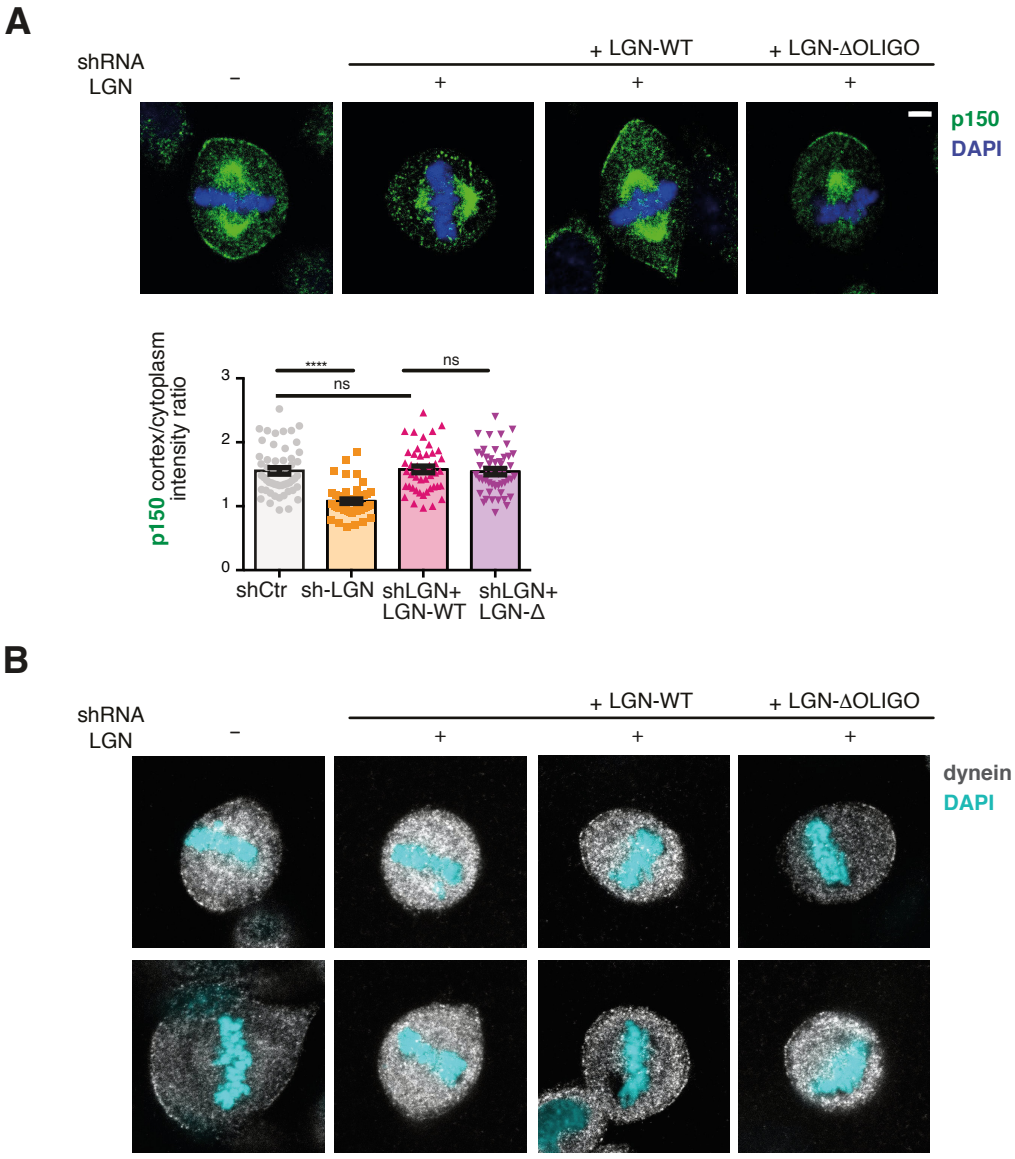

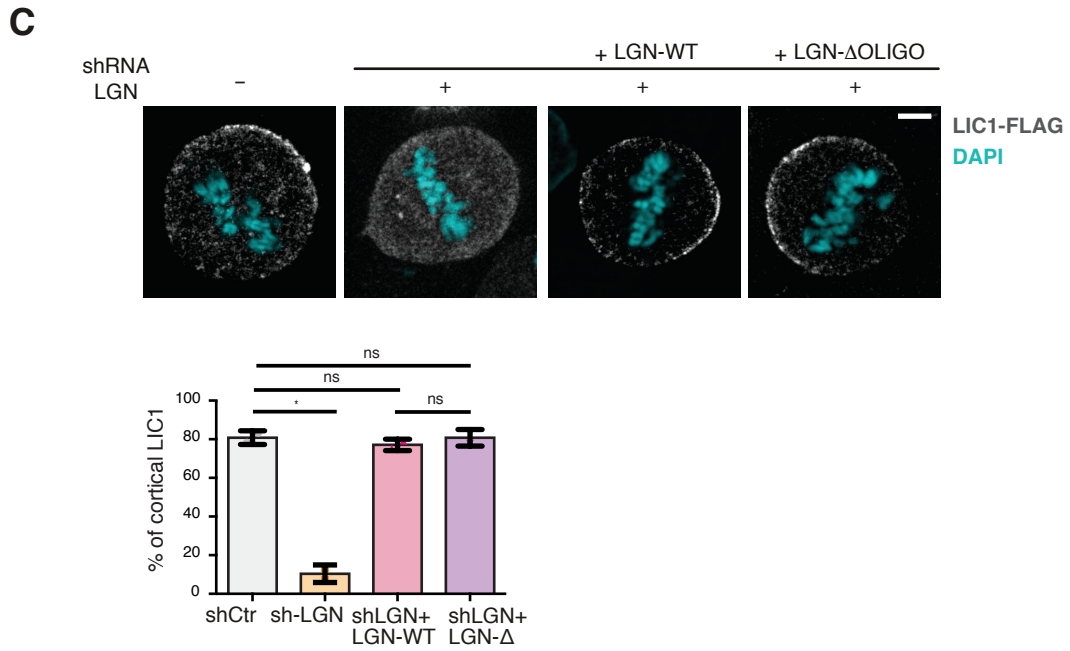

Figure 34 – Dynein and dynactin are recruited at the cortex regardless of NuMA:LGN oligomerization

A) Top: confocal images of HeLa cells depleted of endogenous LGN and expressing LGN-WT-mCherry or LGN-ΔOLIGO-mCherry. Cells were stained with $p150^{Glued}$ (green) and DAPI (blue). Bottom: quantification of cortical signals, with histograms representing the cortex-to-cytoplasm fluorescence ratio. Mean ± SEM are shown for three independent experiments, with n>47. **** indicates p<0.0001, by the Krustal-Wallis test. (**B**) Representative images of HeLa cells expressing the LGN rescue constructs. Cells were stained with dynein (white) and with DAPI (cyan). (**C**) Top: confocal images of HeLa cells expressing the LGN rescue constructs and transfected with FLAG-LIC1. Cells were stained with anti-FLAG antibody (white) and with DAPI (cyan). Bottom: quantification of signals at the cortex, with histograms representing the percentage of cells displaying cortical FLAG. Mean ± SD are shown for two independent experiments, with n>32. * indicates p<0.05, by the Fisher's exact test. Scale bars, 5 μm.

3.5.3 NuMA self-dimerize through its coiled-coil domain

To gain insight into the role of NuMA:LGN hetero-hexamers during mitosis and their role in spindle orientation, we started reasoning about NuMA capability to self-dimerize and how this can be combined with the 3:3 stoichiometry of the NuMA:LGN interactions. To confirm NuMA self-assemble in cells, I cloned full-length NuMA in a pCDH vector in frame with a GFP tag or a FLAG tag, and co-transfect the two constructs in 293T cells.

Immunoprecipitation experiments performed on synchronized cells showed that GFP-NuMA co-immunoprecipitates with NuMA-3xFLAG, confirming NuMA self-assemble in mitotic cells (Figure 35A). We then characterized the precise oligomeric state of NuMA *in vitro*. Specifically, we designed a construct encompassing residues 1592-1694, which is predicted to be the C-terminal portion of the coiled-coil of NuMA, and experimentally showed by Static-Light-Scattering analysis that the purified construct forms homodimers in solution (Figure 35B).

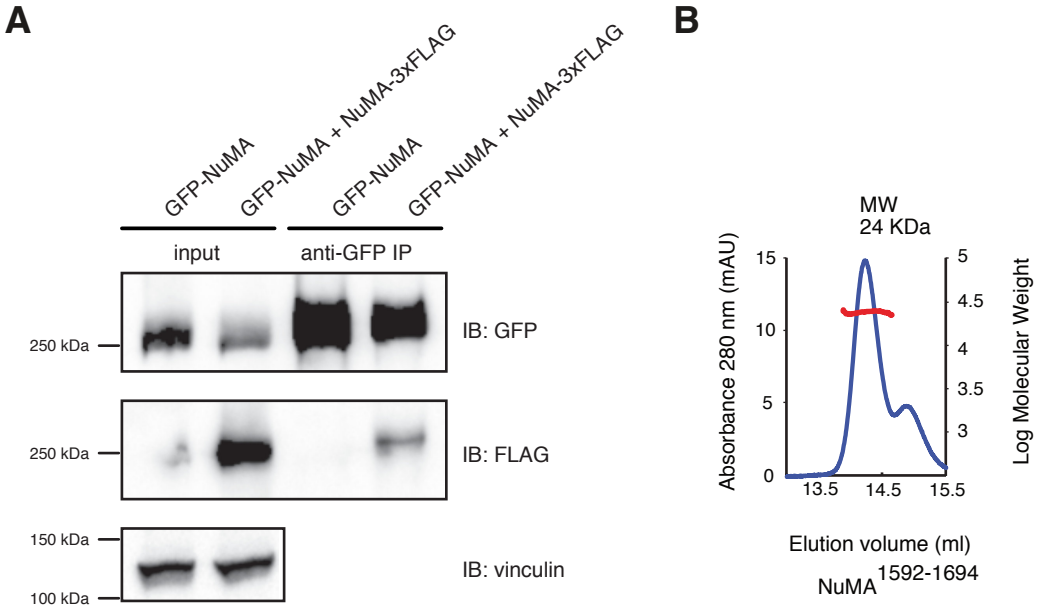

Figure 35 – NuMA self-assemble in cells

(**A**)Western blot of mitotic lysates of 293T cells co-transfected with GFP-NuMA and NuMA-3xFLAG. Cells transfected with GFP-NuMA alone were used as control for the GFP IP experiment. Vinculin was used as loading control for the input. (**B**) SLS profile of NuMA1592-1694 showing an average molecular mass of 24 kDa along the peak, as expected for a dimeric construct.

3.5.4 Binding of NuMA to LGN^{TPR} generate proteins network *in vitro*

We then reasoned that the combination of full-length NuMA homo-dimers with the 3:3 stoichiometry of the NuMA:LGN hexamers could promote the assembly of large protein networks. The minimal assembly satisfying all the interactions would be represented by a couple of NuMA:LGN donut in which two NuMA chains from each donut interacts with one other and one NuMA chain from one donut interacts with the NuMA molecule from the

other (Figure 36A, left). Alternatively, extended protein networks can form, in which NuMA dimers contribute one NuMA chain to different donuts (Figure 36A, right).

As the NuMA fragment 1592-2001 resulted to be insoluble (data not shown), to test the formation of multimeric assemblies in vitro we decided to generate a NuMA chimeric construct in which the dimerizing coiled-coil region tested in paragraph 3.5.3 (encompassing aa 1592-1694) and the LGN-binding fragment of NuMA (spanning aa 1821-2001) were connected by an artificial linker of Thr-Gly-Ser repeats (NuMA-chimera hereon, Figure 36B). The NuMA chimeric construct was soluble and could be purified to homogeneity. Size-exclusion-chromatography experiments analogous to the one performed in paragraph 3.1.1 revealed that upon incubation NuMA-chimera and LGN^{TPR} eluted at high molecular weight but out of the void volume of the column (Figure 36C). The same experiment performed with the NuMA-chimera and an LGN construct lacking the helices flanking the TPR ($LGN^{TPR\text{-}\Delta OLIGO}$, encompassing residues 13-350) resulted in a complex eluting towards lower molecular weights (gold trace). All together, these results indicate that the binding of dimeric NuMA moieties to LGN^{TPR} results in multivalent protein assemblies that based on the structural evidence are formed by hetero-hexameric $NuMA^{LGNBD}$:LGN^{TPR} donuts connected by flexible elongated coiled-coil regions of NuMA.

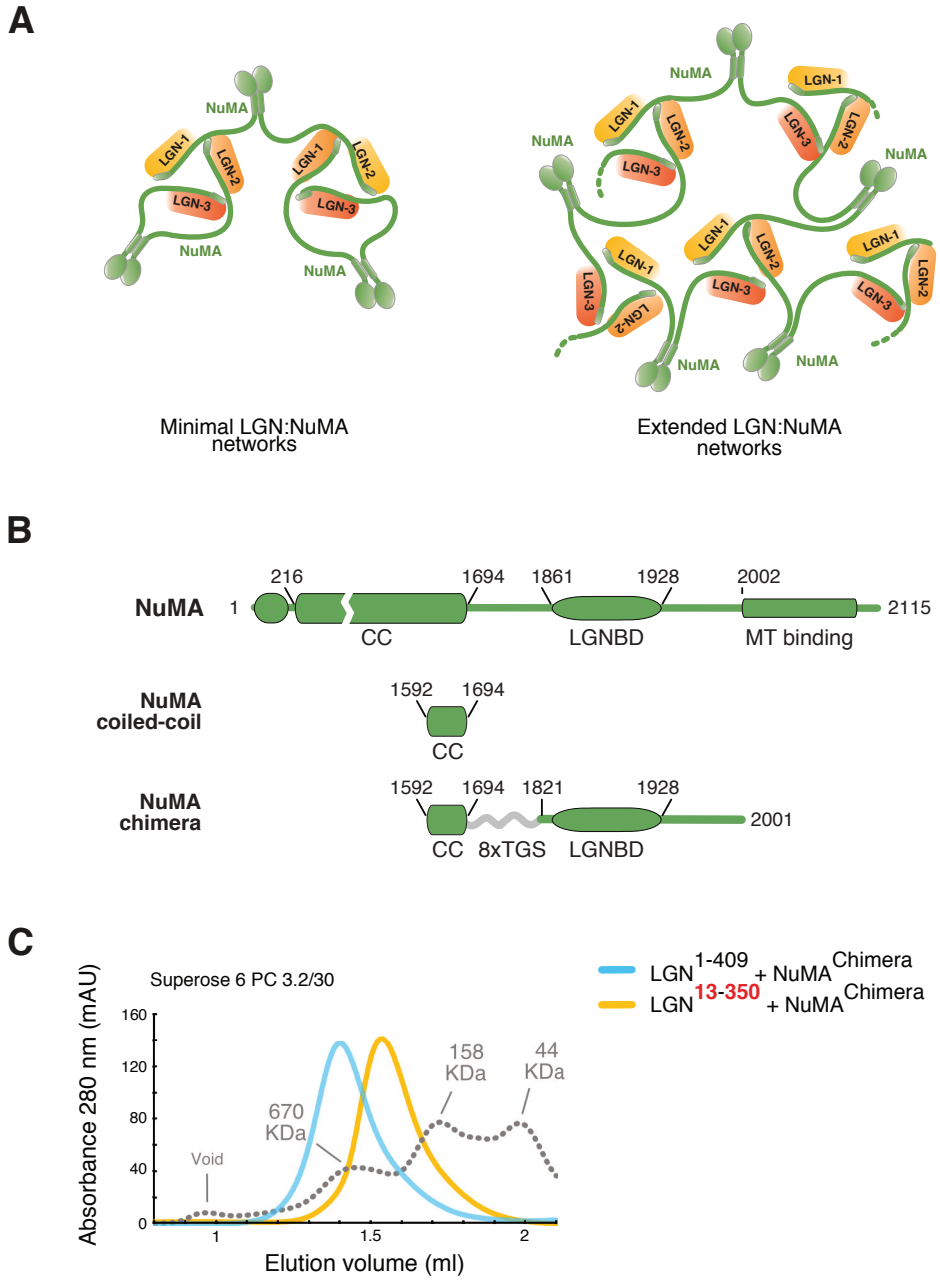

Figure 36 – NuMA-chimera and LGN^{TPR} form protein networks *in vitro*

(**A**) Cartoon illustrating different possible oligomers resulting from the assembly of full-length NuMA with LGN^{TPR}. The minimal stoichiometry of dimeric NuMA engaged in hetero-hexamers with LGN^{TPR} is 6:6 (left). When each NuMA chain of a dimer binds a NuMA from a different donut, higher order protein networks with different stoichiometry are possible (right). (**B**) Schematic representation of NuMA wild-type, the C-terminal part of the coiled-coil and the NuMA-chimera. (**C**) SEC elution profile of NuMA-chimera with LGN^{TPR} (LGN$^{1-409}$, blue trace) and with LGN$^{TPR-\Delta OLIGO}$ (LGN$^{13-350}$, yellow trace). Complexes of the NuMA-chimera with the oligomerization-deficient LGN$^{TPR-\Delta OLIGO}$ elute later indicating they have and average molecular weight lower than complexes formed with LGN^{TPR}. Grey dotted lines indicate the run of globular molecular weight markers.

3.6 NuMA:LGN cortical protein networks are essential to promote spindle orientation

3.6.1 Rescue of spindle orientation phenotype by targeting NuMA at the cortex

Since we characterized the multivalent protein network organized by NuMA and LGN oligomerization, we reasoned that precisely this supra-molecular interaction could be the key event in clustering dynein/dynactin motors and sustaining the activation of pulling forces orienting the spindle. Therefore, we set to develop a strategy to prove that NuMA: LGN hetero-hexamers at the cortex are essential for spindle orientation.

To this aim, we exploit the knowledge previously generated in the lab regarding the mitotic relationship between NuMA and Aurora-A (Gallini *et al.*, 2016), that I will briefly describe as it sets the stage for our experiments on NuMA:LGN-mediated cortical protein networks. Aurora-A is a mitotic kinase localizing at the spindle poles, where it phosphorylates the C-terminal part of NuMA, regulating its dynamic exchange between the spindle poles and the cells cortex. We showed that HeLa cells treated with 50 nM of the Aurora-A specific inhibitor MLN8237 display orientation defects, and loss of the cortical pool of NuMA (Figure 37A), without affecting LGN localization. These results indicated that Aurora-A inhibition causes spindle misorientation by impairing NuMA localization at the cortex. To prove the ideas, we considered studies from the Cheeseman laboratory (Kiyomitsu and Cheeseman, 2012) showing that the C-terminal fusion of NuMA to the GoLoco region of LGN in sufficient to target NuMA at the plasma membrane. To investigate whether the ectopic targeting of NuMA could bypass the requirement of Aurora-A activity in spindle orientation, we generated a fusion protein in which the full-length NuMA was fused with the GoLoco motif of LGN (encompassing residues 359-677), in frame with a GFP tag (hereon GFP-NuMA-WT-GoLoco). As negative control, we used a GFP-NuMA-WT construct cloned in a pCDH vector (Figure 37B). First, we tested the localization of the constructs in metaphase with or without MLN8237 treatment. The GFP-NuMA construct

localized at the spindle poles and at the cell cortex, recapitulating endogenous NuMA localization. As expected, the treatment with MLN8237 abolished cortical localization and increased the amount of NuMA at the spindle poles (Figure 37C). The GFP-NuMA-WT-GoLoco fusion protein localized uniformly at the cortex, at higher levels compared to the GFP-NuMA, and displayed weak localization at the poles. Cells expressing GFP-NuMA-WT-GoLoco treated with MLN8237 accumulates at the poles, similarly to cells expressing GFP-NuMA, but maintain the pool of membrane bound protein. Interestingly, analysis of the spindle orientation of HeLa cells expressing these constructs revealed that cortical targeting of NuMA is sufficient to rescue spindle orientation in MLN8237-treated cells (Figure 37D). As expected, HeLa cells transfected with GFP-NuMA recapitulate endogenous NuMA behavior, and after Aurora-A inhibition displayed orientation defects compared to DMSO-treated cells. Cells expressing GFP-NuMA-WT-GoLoco divide in an oriented manner. Interestingly, cells expressing the GFP-NuMA-WT-GoLoco construct treated with MLN8237 still divide with oriented spindles, confirming that ectopic targeting of NuMA at the cortex is sufficient to achieve correct spindle orientation in conditions in which Aurora-A is inhibited and endogenous NuMA aberrantly sequestered at the spindle poles (Figure 37D).

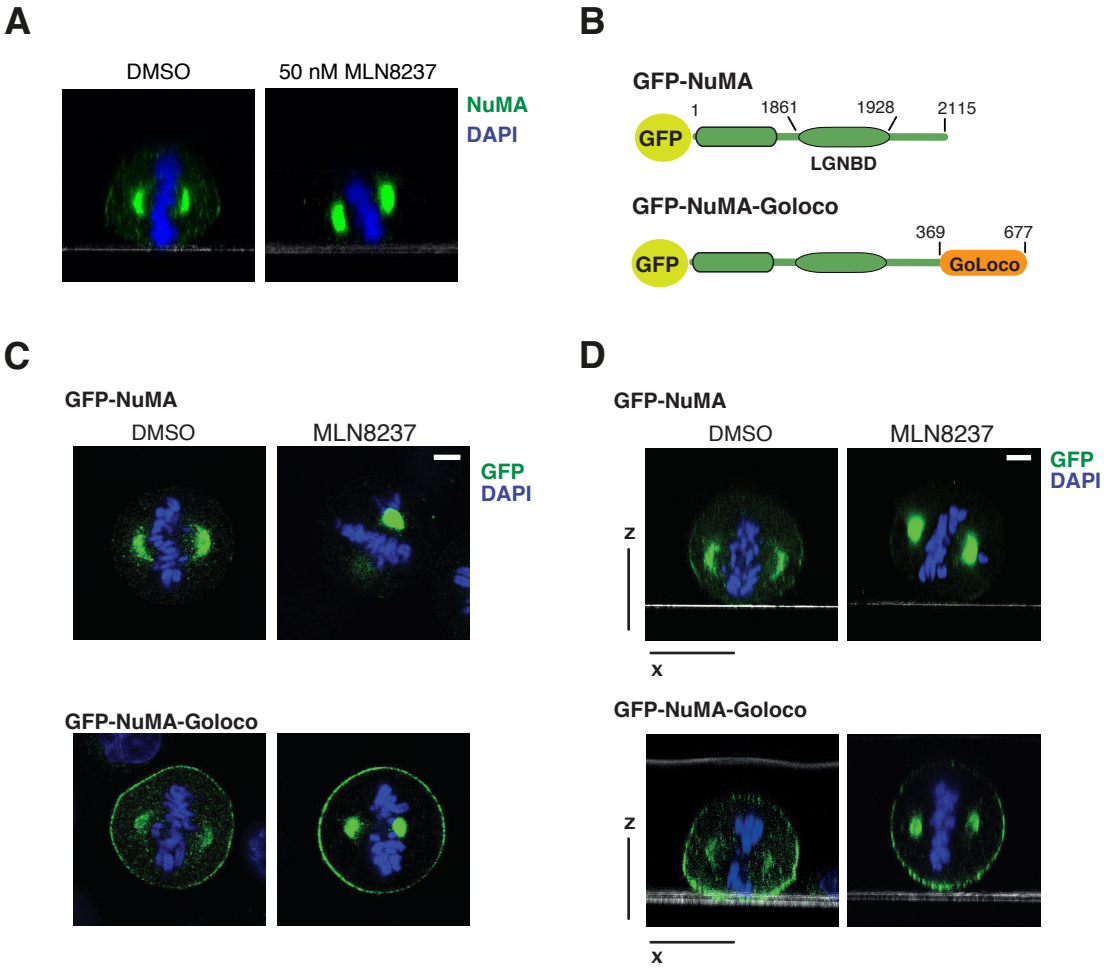

Figure 37 – Ectopic targeting of NuMA at the cortex is sufficient to rescue the misorientation induced by Aurora-A inhibition

(**A**) Representative x-z sections of HeLa cells treated with DMSO or 50 nM MLN8237. Cells were imaged with GFP-NuMA (green) and DAPI (blue). The coverslip is visible as a white line. (**B**) Schematic representation of GFP-NuMA-WT and GoLoco fusion protein used for targeting NuMA at the cortex. (**C**) Confocal images of HeLa cells transfected with GFP-NuMA or GFP-NuMA-GoLoco, treated with DMSO or 50 nM MLN8237. (**D**) Confocal x-z sections of HeLa cells transfected with GFP-NuMA or GFP-NuMA-GoLoco, treated with DMSO or 50 nM MLN8237. Cells were stained with DAPI. Scale bars, 5 μm.

3.6.2 Cortical protein networks are required to orient the spindle

With the aim to understand if NuMA:LGN protein networks are required for correct spindle orientation regardless of the levels of NuMA and LGN protein at the cortex, I cloned the oligomerization-deficient NuMA-ΔOLIGO mutant (see paragraph 3.3.4) in the pCDH-GFP vector described above in frame with the GoLoco motif. This GFP-NuMA-ΔOLIGO-

GoLoco mutant binds to LGN in a 1:1 stoichiometry, is unable to oligomerize with LGN, and is targeted at the cell cortex by direct binding to Gαi. As the fusion protein GFP-NuMA-GoLoco, GFP-NuMA-ΔOLIGO-GoLoco localizes at the cell cortex in both DMSO and MLN8237 treated cells (Figure 38A). Spindle orientation experiments showed that cells expressing this construct divide in an oriented manner under physiological conditions, but when the oligomerization-deficient GFP-NuMA-ΔOLIGO-GoLoco is probed in HeLa treated with MLN8237, cells are not able to rescue the misorientation induced by loss of cortical endogenous NuMA despite NuMA-ΔOLIGO-GoLoco is recruited at the cortex at the same levels of the oligomerization-proficient NuMA-WT-GoLoco (Figure 38A-B).

For the sake of completeness, since NuMA-ΔOLIGO-GoLoco lacks a ~ 40 aminoacid stretch, we reasoned that its inability to rescue the misorientation caused by MLN8237-induced loss of cortical NuMA could be ascribed to some additional uncharacterized function beside the NuMA:LGN oligomerization. For this reason, we decided to analyze astral microtubules organization and dynein recruitment at the cell cortex in cell treated with MLN8237 and expressing the NuMA-GoLoco rescue constructs. Immunofluorescence analysis of cells stained with α-tubulin showed that MLN treatment did not perturb astral microtubules organization (Figure 38C). To assess the cortical levels of dynein, I transfected LIC1-FLAG (see paragraph 3.4.2) and stain with anti-FLAG antibody. Again, I did not observed major differences in LIC1-FLAG distribution at the cortex when NuMA-ΔOLIGO-GoLoco was expressed in Aurora-A inhibited conditions (Figure 38D).

Collectively, this evidence suggests that cortical NuMA and dynein recruitment is not sufficient to orient the spindle, and that NuMA:LGN oligomerization at the cortex is essential to organize dynein-based spindle motors in a way that astral microtubule pulling forces can effectively orient the spindle.

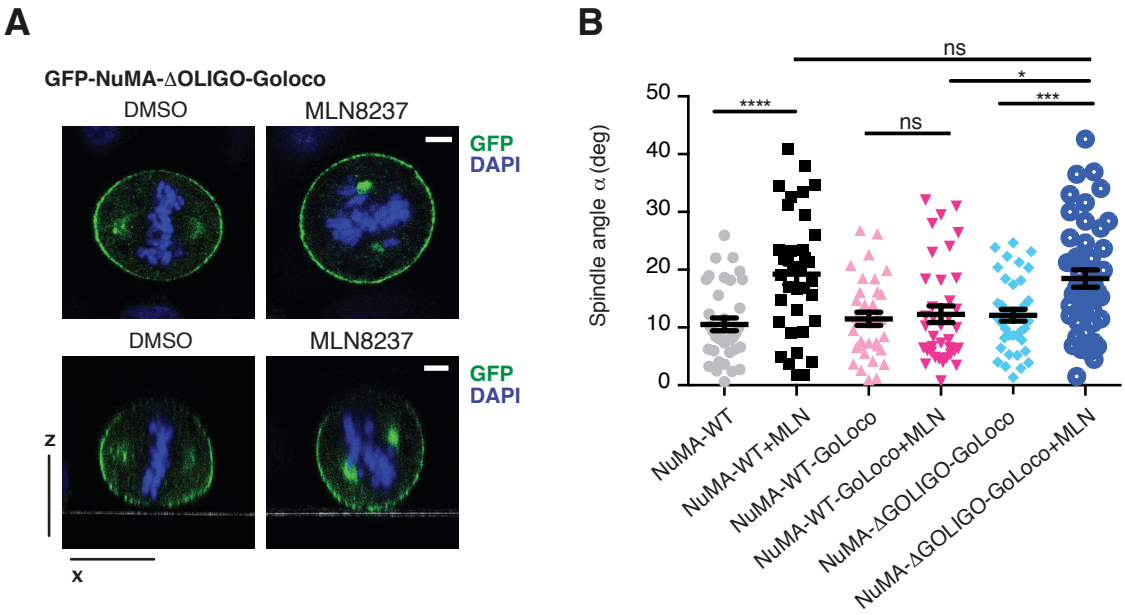
A
GFP-NuMA-ΔOLIGO-Goloco
DMSO
MLN8237
GFP
DAPI
DMSO
MLN8237
GFP
DAPI
z
x
B
ns
*
***
****
ns
Spindle angle α (deg)
50
40
30
20
10
0
NuMA-WT
NuMA-WT+MLN
NuMA-WT-GoLoco
NuMA-WT-GoLoco+MLN
NuMA-ΔGOLIGO-GoLoco
NuMA-ΔGOLIGO-GoLoco+MLN

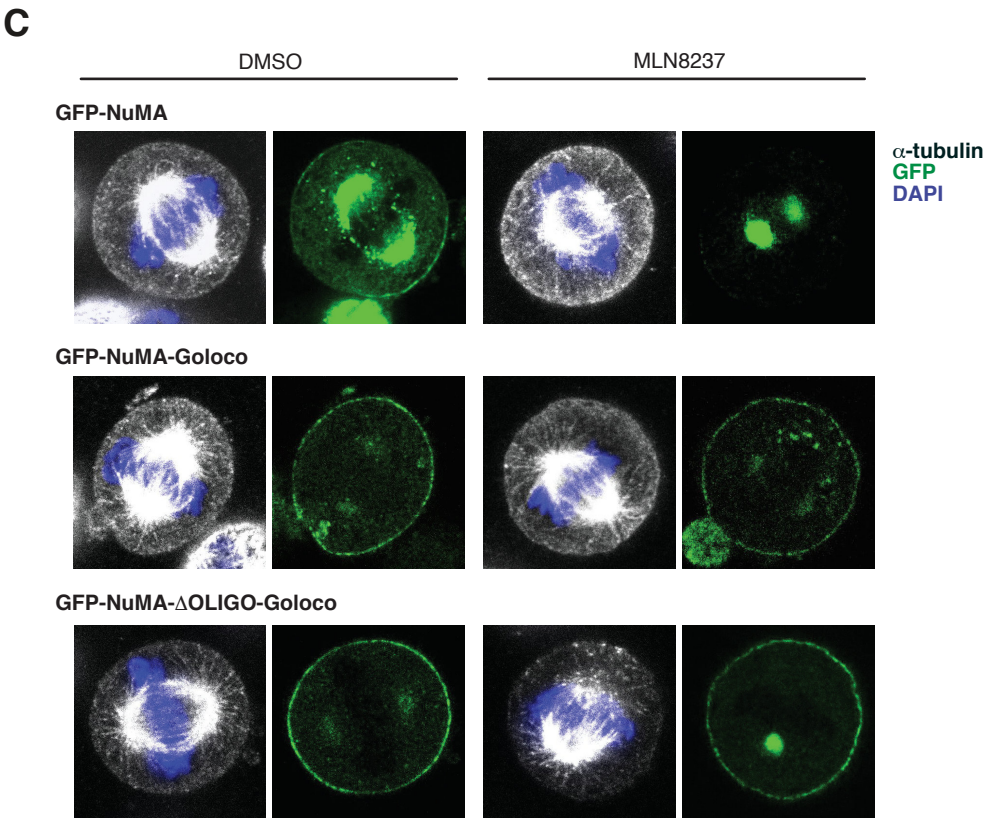
C
DMSO
MLN8237
GFP-NuMA
α-tubulin
GFP
DAPI
GFP-NuMA-Goloco
GFP-NuMA-ΔOLIGO-Goloco

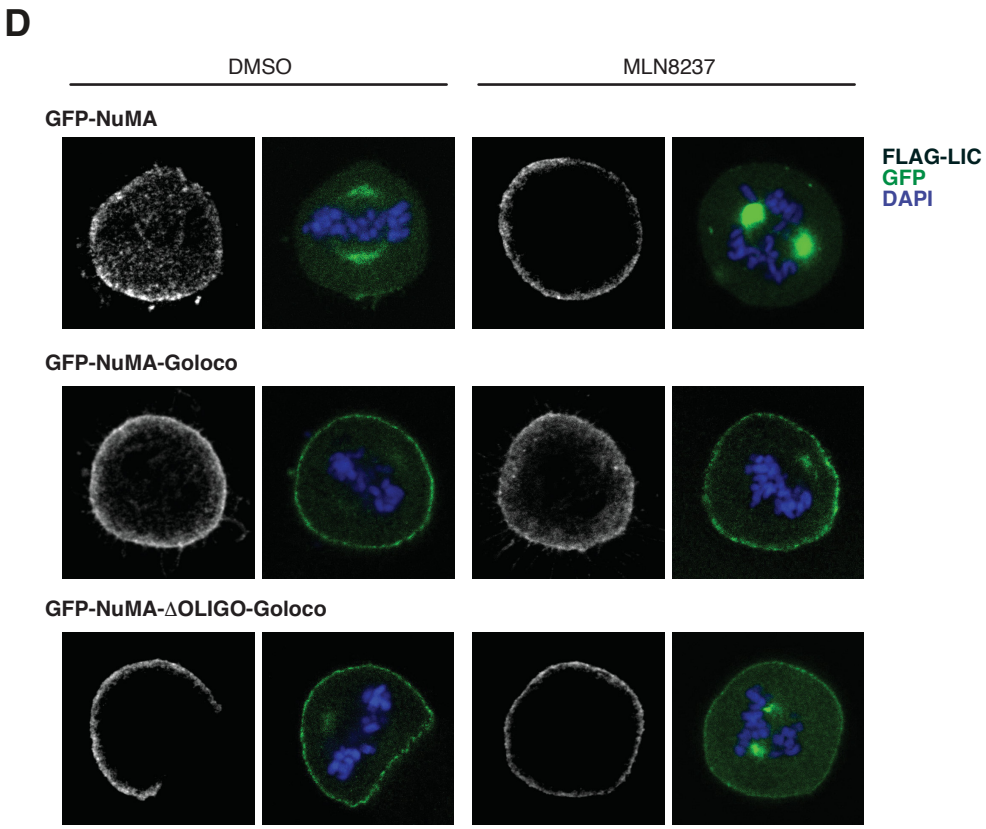

Figure 38 – NuMA:LGN oligomerization at the cortex is required for spindle orientation of HeLa cells in metaphase

(**A**) Top: confocal images of HeLa cells transfected with GFP-NuMA-ΔOLIGO-GoLoco treated with DMSO or 50 nM MLN8237. Bottom: x-z sections of HeLa cells transfected with GFP-NuMA-ΔOLIGO-GoLoco treated with DMSO or 50 nM MLN8237. Cells were stained with DAPI. Scale bars, 5 μm. (**B**) Dot-plot showing the spindle angle axis distribution of HeLa cells imaged in panel B. Mean ± SEM are shown for three independent experiments, with n>56. **** p<0.0001, ***p<0.001, *p<0.05 by Krustal-Wallis test. (**C**) Representative images of HeLa cells expressing GFP-NuMA rescue constrcuts, treated with DMSO or 50 nM MLN8237. Cells were stained with α-tubulin (white) and with DAPI (blue). GFP signal distribution (green) is shown on the right side. (**D**) Representative images of HeLa cells co-transfected with GFP-NuMA rescue constructs and FLAG-LIC1, treated with DMSO or 50 nM MLN8237. Cells were stained with anti-FLAG (white) and with DAPI (blue). GFP signal distribution (green) is shown on the right side.

3.7 NuMA and microtubules

3.7.1 NuMA can bind microtubules and LGN concomitantly

Recently, we identified an Aurora-A phosphosite lying in the C-terminal part of NuMA, on Ser-1969, involved in the regulation of NuMA localization at the poles, which overlapped with the region of NuMA previously predicted to bound the microtubules (Du *et al.*, 2002; Gallini *et al.*, 2016). With the aim to assess whether Aurora-A could perturb NuMA microtubules-binding activity, Manuel Carminati performed microtubules-bundling experiments with two fragments of the NuMA C-terminal part, encompassing residues 1821-2001 and 2002-2115, which revealed that the $NuMA^{2002\text{-}2115}$ efficiently promote microtubules bundling, whereas $NuMA^{1821\text{-}2001}$ did not (data not shown), suggesting that a different microtubules-binding region of NuMA could exists. The microtubules-binding region of NuMA we identified lies is the C-terminal part of the protein, downstream the LGN binding domain, rather than overlapping with it as previously reported (Du *et al.*, 2002; Haren and Merdes, 2002). This finding opened the possibility that NuMA could simultaneously form hetero-hexamers with LGN and interact with microtubules, supporting our hypothesis of a cortical protein network interacting with the astral microtubules of the mitotic spindle to regulate the orientation. To investigate whether NuMA could concurrently bind microtubules and LGN, we performed a co-sedimentation assay using the C-terminal portion of NuMA ($NuMA^{1821\text{-}2115}$), and the two complementary portion used in the bundling assay ($NuMA^{1821\text{-}2001}$ and $NuMA^{2002\text{-}2115}$) in presence of equimolar amount of LGN^{TPR}. $NuMA^{2002\text{-}2115}$ co-sediments with the microtubules, leaving LGN^{TPR} in the supernatant, while $NuMA^{1821\text{-}2001}$ was found in the supernatant (Figure 39). The whole NuMA C-terminus co-sediments with microtubules together with LGN^{TPR}, confirming that NuMA could associate simultaneously with LGN and with the microtubules.

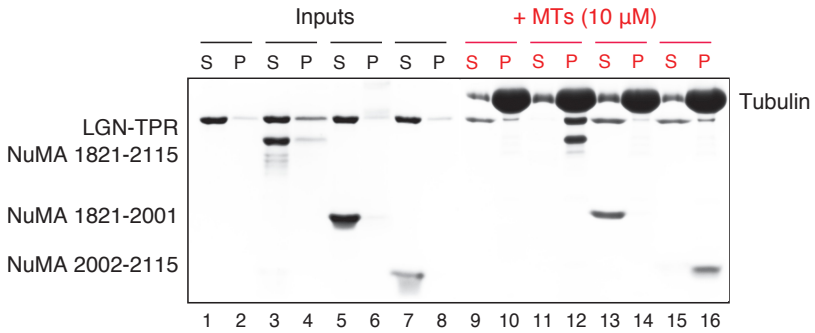

Figure 39 – NuMA$^{1821-2115}$ can bind microtubules and LGN simultaneously

Co-sedimentation of 2 µM NuMA C-terminal fragments with 10 µM polymerized tubulin and 1 µM LGN^{TPR}. Supernatant (S) and pellet (P) fractions were separated by SDS-PAGE and Coomassie stained.

3.7.2 NuMA binds to tubulin core

To further characterize NuMA capability to associate with microtubules *in vitro*, we performed a co-sedimentation assay with the fragment of NuMA we identified as microtubules binding domain (NuMA$^{2002-2115}$) using microtubules deprived of the tubulin tails. Briefly, stabilized microtubules were treated with Subtilisin A, a non-specific protease which removes C-terminal tails from β and α-tubulin, and then incubated with NuMA$^{2002-2115}$. For this experiment, the kinetochore protein Ndc80 was used as negative control, since tubulin tail removal with subtilisin treatment abolish its association with microtubules *in vitro* (Ciferri *et al.*, 2008). Co-sedimentation assays showed that NuMA$^{2002-2115}$ can pellet with microtubules with or without tubulin tails, indicating that NuMA directly recognize microtubule lattice (Figure 40).

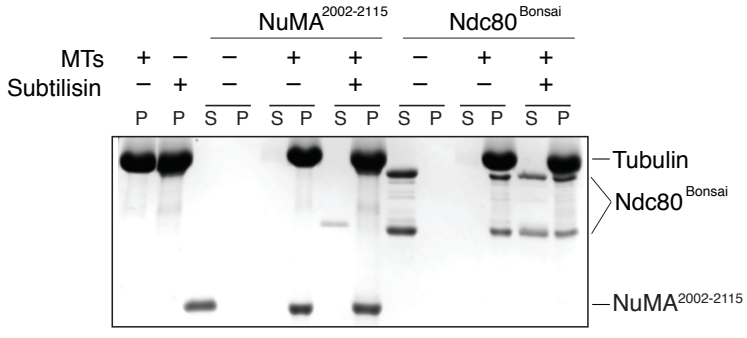

Figure 40 – NuMA$^{2002-2115}$ binds tubulin with and without tails

Co-sedimentation assay performed with 9 μM paclitaxel-stabilized microtubules with or without tubulin tails and 5 μM NuMA$^{2002-2115}$. Supernatant (S) and pellet (P) fractions were separated by SDS-PAGE and Coomassie stained.

3.7.3 Depletion of NuMA microtubules-binding region affects localization at the poles

To investigate the relevance of the newly identified microtubule-binding domain of NuMA in cells, I set out to analyze spindle poles distribution of a NuMA mutant lacking this region. To generate a truncated NuMA mutant unable to bind microtubules (NuMA-ΔMT hereon, Figure 41A), I inserted a stop codon at residue 2002 of NuMA wild-type cloned in the pCDH-mCherry vector. Then, I transiently transfected mCherry-NuMA-WT and mCherry-NuMA-ΔMT in HeLa cells depleted of endogenous NuMA as in paragraph 3.3.4 (Figure 41B), and analyzed the localization of the two constructs in metaphase. While wild-type NuMA decorates the microtubules emanating from the spindle poles with a sort of "umbrella shaped" distribution, the NuMA-ΔMT mutant retains the localization at the centrosome with a smaller and rounded distribution, possibly being excluded from the microtubules (Figure 41C). This phenotype becomes more visible upon overlaying the NuMA mCherry signal with a tubulin mask (that we use to quantify the mCherry signal from the poles). While wild-type NuMA completely fills the tubulin mask, the NuMA-ΔMT mutant displays an empty mask, likely due to the loss of interaction with microtubules. Quantification of polar signal endorsed these observations, since that NuMA-ΔMT poles/cytosol fluorescence intensity ratio was half than the NuMA-WT (Figure 41D). These results indicate that NuMA binding to microtubules is required for spindle poles localization.

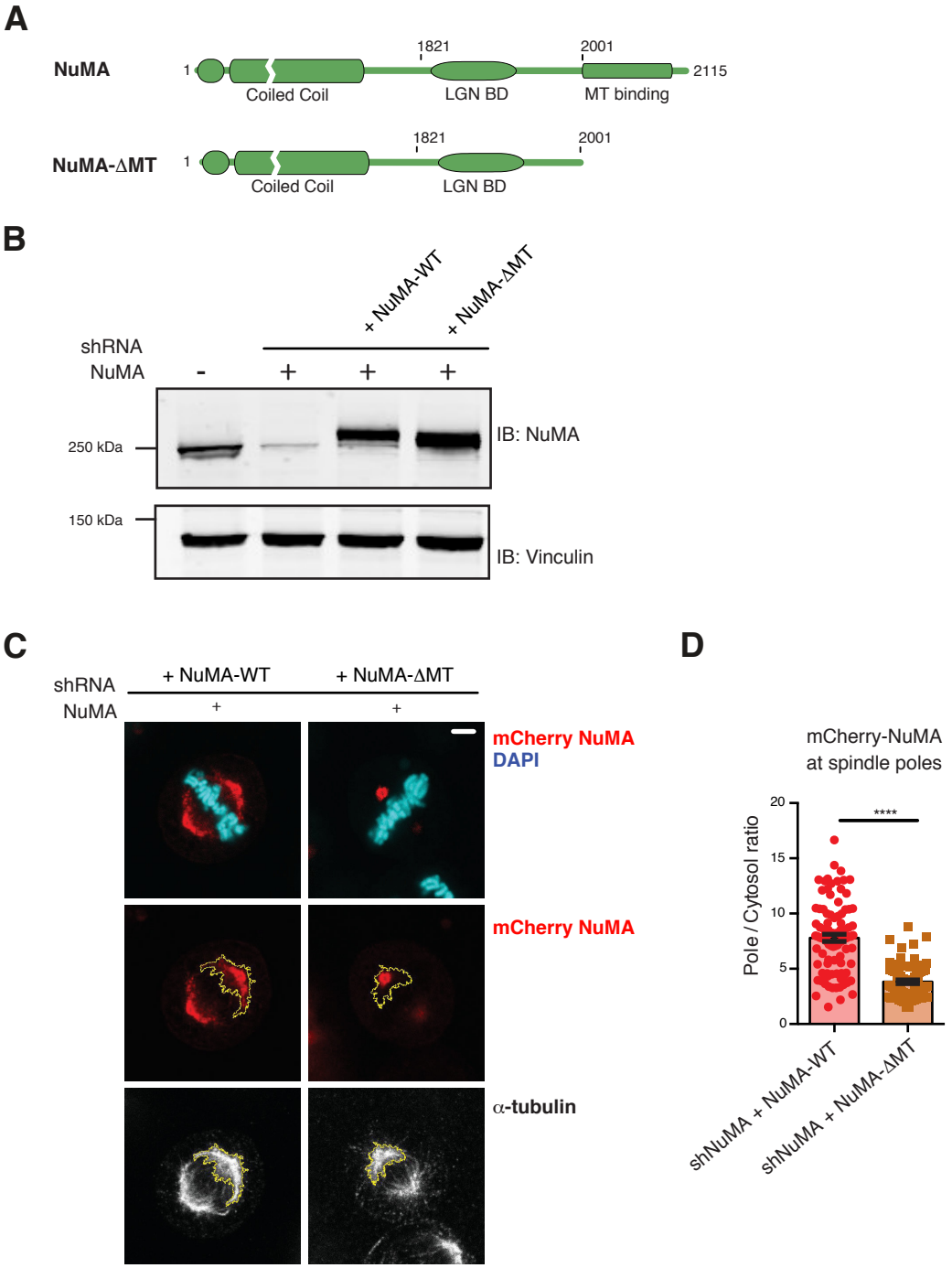

Figure 41 – NuMA-ΔMT localize at the poles with a rounded distribution

(**A**) Schematic representation of the domain structure of NuMA wild-type and NuMA-ΔMT. (**B**) Western blot of mitotic lysates of HeLa cells stably depleted of endogenous NuMA and transfected with mCherry-NuMA-WT and mCherry-NuMA-ΔMT. Vinculin was used as loading control. (**C**) Confocal images of HeLa cells depleted of endogenous NuMA and expressing mCherry-NuMA-WT and mCherry-NuMA-ΔMT. Cells were stained with α-tubulin (white) to visualize the mitotic spindle and with DAPI (cyan). The signal of α-tubulin was used to draw a mask (yellow) around the spindle poles to quantify the mCherry-NuMA signal. (**D**) Quantification of mCherry-NuMA at the poles, with histograms representing the poles-to-cytoplasm fluorescent ratio. Means ± SEM are shown for four independent experiments, with n>66. **** p<0.0001 by Mann-Whitney test. Scale bars, 5 μm.

3.7.4 The NuMA microtubule-binding domain is required for cortical recruitment

3.7.4.1 NuMA-ΔMT does not localize at the cortex

To evaluate whether depletion of the microtubules-binding region of NuMA affects its localization at the cell cortex, I decided to analyze NuMA cortical recruitment in HeLa cells depleted of the endogenous protein and transfected with NuMA-WT and NuMA-ΔMT. Depletion of endogenous NuMA in these experiments is required to prevent dimerization of the rescue constructs with the endogenous protein. To avoid cortical mCherry signal bleaching during acquisition, I stained cells with α-NuMA antibody, and with DAPI, to identify metaphase cells. As expected, wild-type NuMA localize at cortical regions above the spindle poles, while NuMA-ΔMT did not enrich at the cortex, and maintained only the spindle poles localization (Figure 42A). Quantification of cortical signals with line-scan analysis confirmed this observation, showing that in the NuMA-ΔMT mutant the cortex/cytosol ratio has 1-fold decrease (Figure 42B).

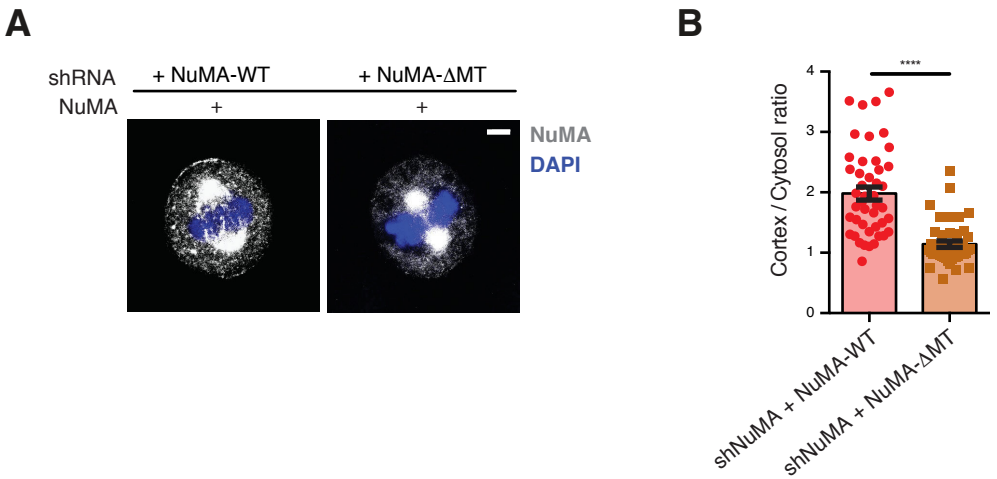

Figure 42 – NuMA-ΔMT is not recruited at the cell cortex in metaphase

(**A**) Representative images of HeLa cells depleted of depleted of endogenous NuMA and transfected with mCherry-NuMA-WT and mCherry-NuMA-ΔMT. Cells were stained with NuMA (white) to visualize cortical signal and with DAPI (blue). (**B**) Quantification of NuMA cortical signal, with histograms representing the cortex-to-cytoplasm fluorescent ratio. Means ± SEM are shown for three independent experiments, with n>45. **** p<0.0001 by Mann-Whitney test. Scale bars, 5 μm.

3.7.4.2 LGN localizes at the cell cortex when NuMA-ΔMT is expressed

The fact the NuMA-ΔMT mutant cannot localize at the cell cortex was unexpected, since in metaphase NuMA is recruited at the cortex by interaction with LGN, and we only depleted the region involved in microtubules binding, and not the LGN binding domain (Figure 41A). To understand whether NuMA-ΔMT did not localize at the cortex because its expression in some way affected LGN distribution, we decided to check LGN localization by immunofluorescence in cells expressing NuMA-WT or NuMA-ΔMT. In both cases, transient transfection of the NuMA-WT or NuMA-ΔMT constructs did not affect LGN localization at the cell cortex, which maintained the distribution in the regions above the spindle poles (Figure 43A-B). This result indicates that loss of cortical pool NuMA in the mutant unable to bind the microtubules was not due to change in LGN localization.

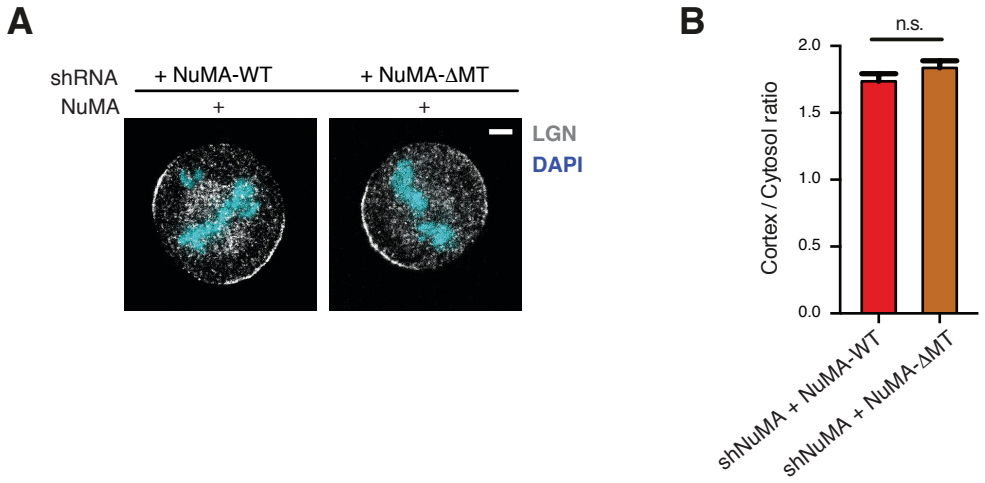

Figure 43 – LGN localization is not affected by NuMA-ΔMT expression

(**A**) Representative images of HeLa cells depleted of depleted of endogenous NuMA and transfected with mCherry-NuMA-WT and mCherry-NuMA-ΔMT. Cells were stained with LGN (white) to visualize cortical signal and with DAPI (cyan). (**B**) Quantification of LGN cortical signal, with histograms representing the cortex-to-cytoplasm fluorescent ratio. Means ± SEM are shown for three independent experiments, with n>50. The Mann-Whitney test was applied.

3.7.4.3 Astral microtubules depolymerization does not affect NuMA cortical recruitment

Since LGN correctly localize at the cell cortex when the NuMA-ΔMT is expressed, we reasoned that lack of interaction with microtubules might prevent NuMA recruitment at the membrane. It has been reported that depolymerization of microtubules with high (10 μM) doses of nocodazole did not affect NuMA recruitment, and that NuMA is present at the cell cortex even when the mitotic spindle is not formed (Seldin *et al.*, 2013). Nocodazole is an antineoplastic agent which disrupts microtubules function by binding of different sites on β-tubulin and inducing microtubules depolymerization. However there are some controversial evidences that increasing concentration of nocodazole causes loss of dynein from the cell cortex (Tame *et al.*, 2014). To investigate the relation between astral MT integrity and NuMA cortical localization, I set out to import protocols to depolymerize astral microtubules. To this end, I decided to use nocodazole on HeLa cells synchronized with a single thymidine block (see Materials and Methods for details). Eight hours after the release, I added increasing concentrations of nocodazole (from 20 to 250 nM) in warm media for one hour, prior to fixation and α-tubulin staining. Cells treated with 20 nM Nocodazole displayed only a partial loss of astral microtubules compared to wild-type HeLa cells, while 100 nM Nocodazole was sufficient to disrupt astral microtubules. An amount of 250 nM nocodazole affects not only astral MTs but also mitotic spindle MTs (Figure 44A).

I then analyzed NuMA cortical localization in nocodazole-treated HeLa cells. None of the nocodazole treatments abolished NuMA cortical recruitment, confirming that NuMA is recruited at the cell cortex independently of microtubules (Figure 44B).

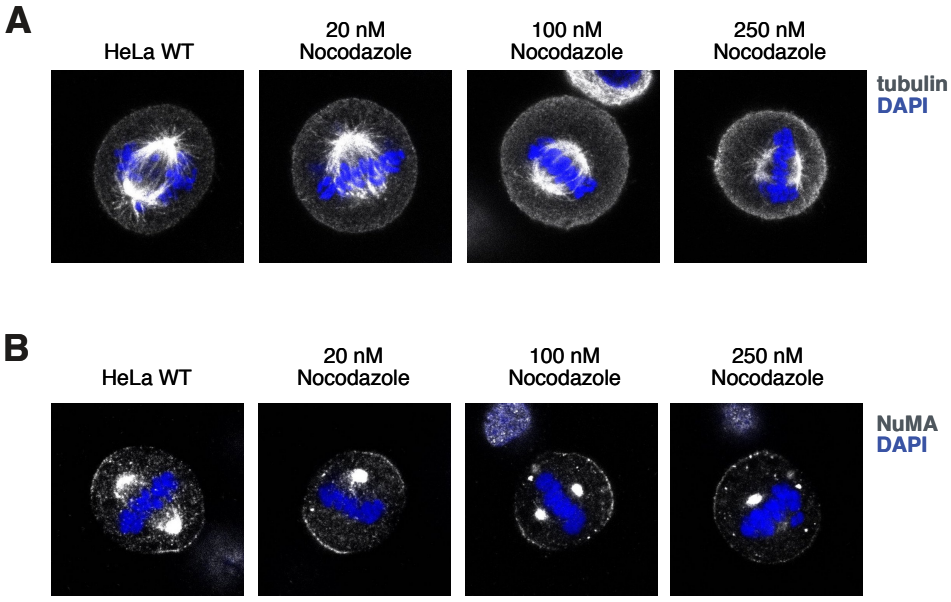

Figure 44 –NuMA cortical recruitment is not affected by nocodazole treatment

(**A**) Representative images of HeLa cells treated with 20, 100 or 250 nM nocodazole. Cells were stained with α-tubulin (white), to visualize astral microtubules and with DAPI (blue). (**B**) Representative images of HeLa cells treated with 20, 100 or 250 nM nocodazole. Cells were stained with NuMA (white) and with DAPI (blue).

3.7.5 NuMA microtubules-binding domain is required to orient the spindle

Since the NuMA-ΔMT mutant displayed an aberrant localization at the poles, and did not localize at the cortex, we reasoned that it could not rescue misorientation phenotype induced by the loss of endogenous NuMA. As expected, spindle orientation analysis analogous to the one conducted in paragraph 3.3.5 confirmed that when NuMA-ΔMT is expressed in HeLa cells lacking NuMA, metaphase cells divide with an average angle of 14˚, while cells transfected with NuMA-WT display a mean angle of division of 7˚ (Figure 45A-B). This result confirmed that the microtubule-binding region of NuMA is required to orient the spindle, although we cannot uncouple the spindle pole defects from the cortical localization defects presented by this mutant.

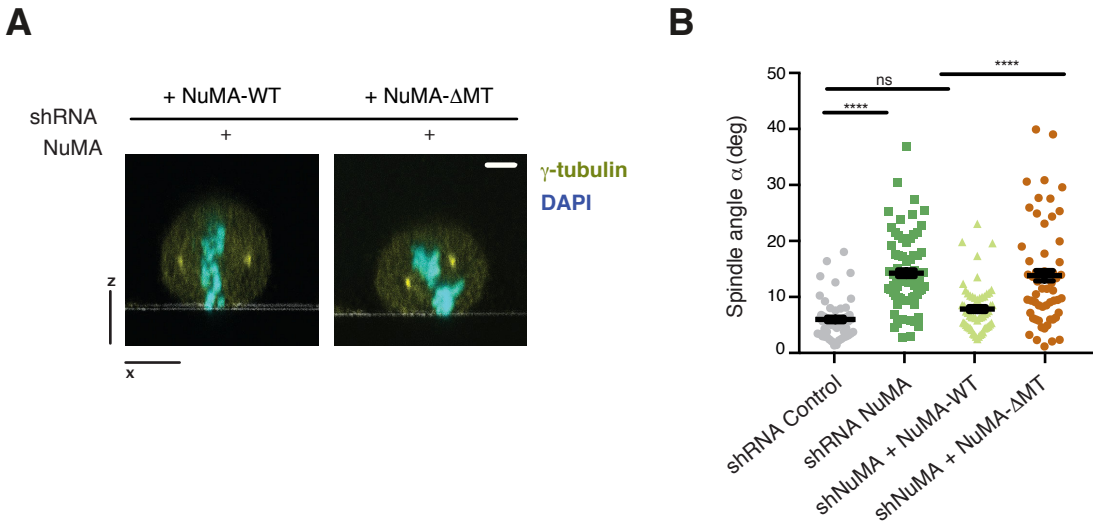

Figure 45 – NuMA-ΔMT does not rescue mitotic spindle orientation

(**A**) Representative images of HeLa cells depleted of depleted of endogenous NuMA and transfected with mCherry-NuMA-WT and mCherry-NuMA-ΔMT. Cells were stained with γ-tubulin (yellow) to visualize the spindle poles and with DAPI (cyan). (**B**) Dot-plot showing the spindle axis angle distribution of HeLa cells imaged in panel A. Mean ± SEM are shown for four independent experiments, with n>55. **** indicates p<0.0001, by the Krustal-Wallis test. Scale bars, 5 μm.

.

4. DISCUSSION

The studies described in the previous Chapter provided evidence that, in metaphase vertebrate cells, the dynein-adaptor NuMA and the scaffold protein LGN form high-order oligomers, and that the formation of the NuMA:LGN oligomer is required to orient the mitotic spindle in both unpolarized and polarized cellular systems. They also showed that the MT-binding domain of NuMA is required for NuMA localization at the cortex during metaphase, and for proper mitotic spindle orientation. These results are presented in the work "Hexameric NuMA:LGN structures promote multivalent interactions required for planar epithelial divisions", published in Nature Communications, in June 2019 (Pirovano *et al.*, 2019).

My studies stemmed from the discovery that NuMA and LGN interact with a 3:3 stoichiometry, forming hetero-hexameric structures with a donut shape. Previous data showed that a 28-residues peptide of NuMA, spanning residues 1899-1926, suffices to bind to the inner groove formed by the TPR repeats of LGN (encompassing residues 15-350), interacting with a 1:1 stoichiometry (Zhu *et al.*, 2011). Our biochemical analyses revealed that longer NuMA and LGN fragments form high-order oligomers. Specifically, we demonstrated that NuMA$^{1861\text{-}1928}$ and LGN$^{7\text{-}367}$ are the minimal constructs interacting with a 3:3 stoichiometry, and any shortening of the C-terminal or the N-terminal ends results in a 1:1 complex. The crystallographic structure of the NuMA:LGN hetero-hexamers revealed that these oligomers arrange in a donut-shaped architecture, in which the α-helices upstream and downstream the TPR repeats of LGN and the region of NuMA spanning residues 1861-1899 are essential for oligomerization. In the donuts, N- and C- terminal helices of the LGN-TPR domain hook on each other in a four-helix bundle to organize the backbone of the donut (Figure 21). In this arrangement, the NuMA fragment 1861-1899 threads in-between two adjacent TPR molecules in the donut before inserting into the inner side of the LGN-TPR domain. The interface between NuMA 1900-1928 (NuMA-peptide) and LGN-TPR observed

in the donut is topologically analogous to the one previously described in the 1:1 complex between LGN 15-350 and the short NuMA stretch 1899-1926. However, in the hetero-hexamers the curvature of LGN-TPR is more pronounced that in the binary 1:1 complex.

The evidence that NuMA and LGN engage in high-order oligomers suggests a new function of NuMA and LGN in promoting clustering of motor proteins at the cortex. In symmetrically dividing cells, spindle orientation relies on Gαi:LGN:NuMA complexes at the cell cortex, which recruit spindle motors and instruct spindle positioning within the cell (Du and Macara, 2004; Morin and Bellaïche, 2011; Kotak, Busso and Gönczy, 2012).

To evaluate the role of NuMA:LGN hexamers in spindle orientation, I performed rescue experiments in both three-dimensional Caco-2 cysts and HeLa cells. Rescue experiments were conducted in HeLa and Caco-2 cells depleted of endogenous LGN and expressing an oligomerization-deficient LGN mutant LGN-ΔOLIGO (lacking residues 1-12 and 350-366). Spindle angle analysis performed in Caco-2 3D cysts confirmed that NuMA:LGN oligomerization is required to orient the spindle during cyst development, and for epithelial architecture. Since, to date, no role in cell polarity have been ascribed to LGN (Zheng *et al.*, 2010), the fact that the oligomerization-deficient mutant LGN-ΔOLIGO could rescue the misorientation induced by the loss of endogenous LGN suggests that the defective cystogenesis can be ascribed to lack of cortical NuMA:LGN assemblies. This hypothesis is supported by actin and tight junctions staining, which showed that epithelial polarity of the cysts was not affected by LGN depletion, and are consistent with data previously reported in literature (Zheng *et al.*, 2010).

Analysis of mitotic spindle orientation in HeLa cells expressing LGN-ΔOLIGO in an LGN-interfered background confirmed that oligomerization is required for proper spindle orientation also in unpolarized systems. However, massive overexpression of LGN-ΔOLIGO in HeLa cells results in spindle rocking, suggesting that the excess of LGN can

target to the cell cortex enough NuMA and dynein/dynactin to bypass the requirement of the oligomerization for spindle orientation.

Spindle orientation rescue experiments performed with an oligomerization-deficient NuMA-mutant (NuMA-ΔOLIGO) showed that expression of NuMA-ΔOLIGO in cells depleted of endogenous NuMA impairs the correct spindle orientation. However, depletion of residues 1862-1899 in the C-terminal part of NuMA also determines a reduced localization of NuMA-ΔOLIGO at the spindle poles (Figure 30). Thus, since proper NuMA localization at the poles is required for spindle organization, our NuMA-ΔOLIGO does not uncouple the spindle assembly and spindle orientation functions of NuMA, therefore we cannot fully ascribe the misorientation phenotype observed in cells expressing NuMA-ΔOLIGO to the impairment in NuMA:LGN oligomer formation (Silk, Holland and Cleveland, 2009; Gallini *et al.*, 2016).

To investigate whether NuMA and LGN organize in hexamers at the cortex in cells, I first expressed two differentially-tagged LGN molecules in HeLa cells and tested their interaction via Proximity Ligation Assay (PLA), which allows to score the interplay between proteins located close proximity within a cell. Unexpectedly, both LGN wild-type and ΔOLIGO produced a PLA signal when transfected in HeLa cells (Figure 31). Although the LGN-ΔOLIGO should not organize oligomeric structures at the cortex, we could not exclude that the high expression levels of transfected constructs induce proteins to be in close proximity triggering the PLA reaction, as we could not foresee how LGN forming 1:1 complexes with NuMA could give rise to PLA signal. Importantly, NuMA is a dimeric protein, and we confirmed its dimerization capability showing that NuMA can oligomerize when overexpressed in HeLa cells. Because of NuMA dimerization, both LGN WT and ΔOLIGO would form at least 2:2 complexes, in which the linker region between NuMA coiled-coil and LGNBD might be too short to prevent the generation of a PLA signal, even in the absence of hexamer formation. Immunoprecipitation experiments with wild-type and oligomerization-deficient LGN constructs confirmed that LGN:NuMA form high-order

oligomers, while LGN-ΔOLIGO:NuMA do not, supporting the notion that hetero-hexamers assemble in cells (Figure 32). As the immunoprecipitation have been performed using the C-terminal part of NuMA that does not include the dimerizing coiled-coil, this experiments also suggests that NuMA:LGN assembly occurs independently on NuMA self-dimerization. To characterize the molecular mechanism driving the misorientation induced by loss of NuMA:LGN oligomerization, I evaluated force generators cortical levels in the HeLa cell lines expressing LGN-ΔOLIGO. To generate the LGN-oligomerization-deficient LGN-ΔOLIGO mutant I depleted the first 13 residues of LGN plus 17 residues after the TPR repeat. In line with the notion that, during metaphase, cortical pool of LGN is recruited at the cortex by binding Gαi thorough its C-terminal GoLoco motif, quantification of LGN-ΔOLIGO amount at the cortex showed that its localization is substantially identical to the wild-type LGN. Also cortical recruitment of NuMA, dynactin-subunit $p150^{Glued}$ and dynein-light intermediate chain-1 (LIC1) was unaffected by the expression of the oligomerization-deficient mutant of LGN-ΔOLIGO (Figure 33-34). These results are consistent with the fact that LGN-ΔOLIGO retains the capability to interact 1:1 with NuMA, and suggest that the cortical localization of spindle orientation proteins *per se* is not sufficient to orient the spindle.

The evidence that in cells expressing the oligomerization-deficient LGN-ΔOLIGO force generators are correctly localized at the cell cortex, but are not able to promote orientation, raised the question of how the lack of NuMA:LGN oligomerization affects spindle positioning. We reasoned that the combination of NuMA dimers and NuMA:LGN hetero-hexamers can result in the formation of a supramolecular organization, in which NuMA:LGN complexes are linked each other, promoting the assembly of a subcortical protein network that clusters dynein/dynactin. *In vitro* experiments showed that the 3:3 stoichiometry of the NuMA:LGN complexes combined with NuMA dimerization capability results in the formation of multivalent assemblies, in which different NuMA:LGN hexamers

are linked by NuMA dimers (Figure 36). These results support the notion that NuMA and LGN form hexamers during mitosis, which can organize multivalent interactions coordinating mitotic spindle orientation. Thus it is not the 3:3 NuMA:LGN stoichiometry nor the 1:1 stoichiometry to be important for pulling forces ensuing, but rather the generation of large NuMA:LGN networks, which in turn organize dynein/dynactin motors by direct binding of dynein to NuMA.

Furthermore, we demonstrated that the ectopic targeting of the oligomerization-deficient NuMA-ΔOLIGO at the cortex via chimeric fusion of the GoLoco domain of LGN is not sufficient to orient the spindle in HeLa cells treated with the Aurora-A inhibitor MLN8237 lacking cortical NuMA, while targeting the wild-type counterpart allows to rescue the orientation (Figure 37). Notably, expression of NuMA-ΔOLIGO-GoLoco in Aurora-A inhibited conditions does not affect astral microtubules organization or dynein recruitment, endorsing the idea that is the lack of a supramolecular organization that impairs mitotic spindle orientation. Collectively, these data fully support the notion that is not the presence, but rather the molecular organization of NuMA in complex with LGN which is required for the production of pulling forces necessary to orient the spindle in metaphase.

A recent work from Okumura and colleagues revealed that dynein/dynactin motors assembly at the cortex is required to generate traction forces on the astral microtubules and to promote spindle positioning (Okumura *et al.*, 2018). Specifically, the authors showed that cortical NuMA generates large pulling forces by clustering dynein-dynactin-NuMA complexes at the cell cortex through a C-terminal highly conserved clustering domain. Interestingly, direct ectopic cortical targeting of NuMA, but not dynein, is sufficient to promote the spindle pulling, suggesting a role of NuMA in organizing spatially dynein and dynactin at the cortex in metaphase cells. The clustering domain identified by the authors (spanning residues 1700-1801) lies in a region of NuMA which is close but different from the oligomerization domain (spanning residues 1861-1928) identified in my studies, and is required for the formation of punctate NuMA signals at the cortex, suggesting that NuMA might assemble cortical clusters

in metaphase. At this regard, it would be of great interest to investigate whether the oligomerization-deficient NuMA-ΔOLIGO mutant would affect cortical puncta formation compared to wild-type NuMA. Although the studies from Okumura and colleagues suggest that production of effective astral-MT traction forces might be independent of LGN and Gαi, these data might be consistent with the idea that cortical NuMA:LGN hetero-hexamers could act as a scaffold to specify the position of dynein/dynactin/NuMA assembly during mitosis, this way promoting spindle orientation and supporting spindle pulling. Whether the dynein/dynactin/NuMA clusters formation synergize with the NuMA:LGN hetero-hexamers to support a robust spindle pulling would need further investigation.

During metaphase, NuMA acts as adaptor for dynein/dynactin and concomitantly interacts with astral microtubules emanating from the spindle poles (Kotak, Busso and Gönczy, 2012). We recently showed that the last 100-residues in the C-terminus of NuMA directly associate with microtubules (Gallini *et al.*, 2016). This evidence identified a NuMA microtubules-binding region, encompassing residues 2002-2115, whose functions are poorly understood. Notably, this newly discovered MTs-binding domain of NuMA is downstream of the LGN binding motif rather than overlapping with it as previously reported (Du *et al.*, 2002; Haren and Merdes, 2002). Accordingly, we found that NuMA can simultaneously associate with LGN and MTs, endorsing the hypothesis of a protein network sustaining spindle orientation. We also showed that $NuMA^{2002\text{-}2115}$ co-sediments with MTs even in the absence of tubulin-tails, suggesting that this domain recognizes MTs lattice. Importantly, a recent study showed that the NuMA MT-binding domain encompassing residues 2002-2115 is important for the generation of pulling forces on the spindle (Okumura *et al.*, 2018). Collectively, these evidence are consistent with a role for NuMA in regulating astral microtubules plus-tips dynamics, while dynein/dynactin/NuMA complexes slides along depolymerizing MTs. Another possibility is that the binding of NuMA to MTs confers processivity to dynein movement towards the minus ends.

With the aim to understand whether the MT-binding functions of NuMA are required for spindle orientation, I performed spindle orientation rescue experiments in NuMA-depleted HeLa cells, and found that NuMA-ΔMT cannot rescue spindle misorientation caused by loss of NuMA (Figure 45). However, as for the NuMA-ΔOLIGO mutant, also NuMA-ΔMT localizes less at the spindle poles (Figure 41), making it impossible to uncouple the polar and cortical function of the protein in mitosis. Surprisingly, we found that NuMA-ΔMT truncated mutant does not enrich at the cortex during metaphase in spite of the fact that it can bind LGN, which is the cortical recruiting factor for NuMA in metaphase. On the other hand, the inability of NuMA-ΔMT to associate with astral MTs cannot explain the evidence that NuMA-ΔMT does not reach the cortex, as we and others (Seldin *et al.*, 2013) showed that astral microtubules are dispensable for NuMA cortical recruitment in mitosis. Depletion of the NuMA region 2002-2115, containing the microtubule-binding domain, implies the elimination of several other known NuMA regulatory motives, including the Cdk1 phosphorylation site on Thr2055 (Kotak, Busso and Gönczy, 2013), and a lipid-binding domain (Figure 12) (Zheng *et al.*, 2013). However, these motives promote cortical accumulation of NuMA during anaphase (Kotak, Busso and Gönczy, 2013; Zheng *et al.*, 2013), thus it is unlikely they are the cause of impaired cortical enrichment of NuMA-ΔMT in metaphase. We recently showed that one of the Aurora-A phosphosites lying on Ser2047 regulates NuMA cortical recruitment during metaphase, and the inhibition of Aurora-A kinase activity abolishes NuMA membrane localization (Gallini *et al.*, 2016). Thus, the impaired NuMA-ΔMT cortical recruitment during metaphase could be due to the depletion of the Aurora-A phosphorylation site on Ser2047. On that note, it would be interesting to analyze cortical recruitment of a NuMA phospho-mutant in which Ser2047 is substituted with an Alanine.

In summary, the experiments I conducted during my PhD uncovered the molecular organization and the working principle of NuMA:LGN complexes at the cell cortex in metaphase, and addressed the function of the MT-binding domain of NuMA. We show that: 1) NuMA and LGN form hetero-hexamers which, combined with the dimeric state of endogenous NuMA, promote the organization of dynein/dynactin networks at the cortex by multivalent interaction; 2) the C-terminal portion of NuMA encompassing residues 2002-2115 and containing the MT-binding domain is essential for the spindle orientation functions of NuMA, though the exact molecular mechanism for this activity still remains elusive. Based on all these findings, and known interactions of LGN and NuMA from previous literature, we propose that the microtubule-binding region of NuMA might work at the cortex stabilizing the Gαi-GDP-loaded hetero-hexameric LGN:NuMA complexes, which can form multimeric proteins networks (Figure 46). These multivalent interactions are essential for spindle orientation and pulling forces generation in HeLa cells and Caco-2 three-dimensional cysts, and might control special organization of dynein/dynactin complexes at the cell cortex. Whether and how the Gαi GTP/GDP cycle and the several NuMA regulation mechanisms affect spatial arrangement of the NuMA:LGN represent an interesting direction for future experiments.

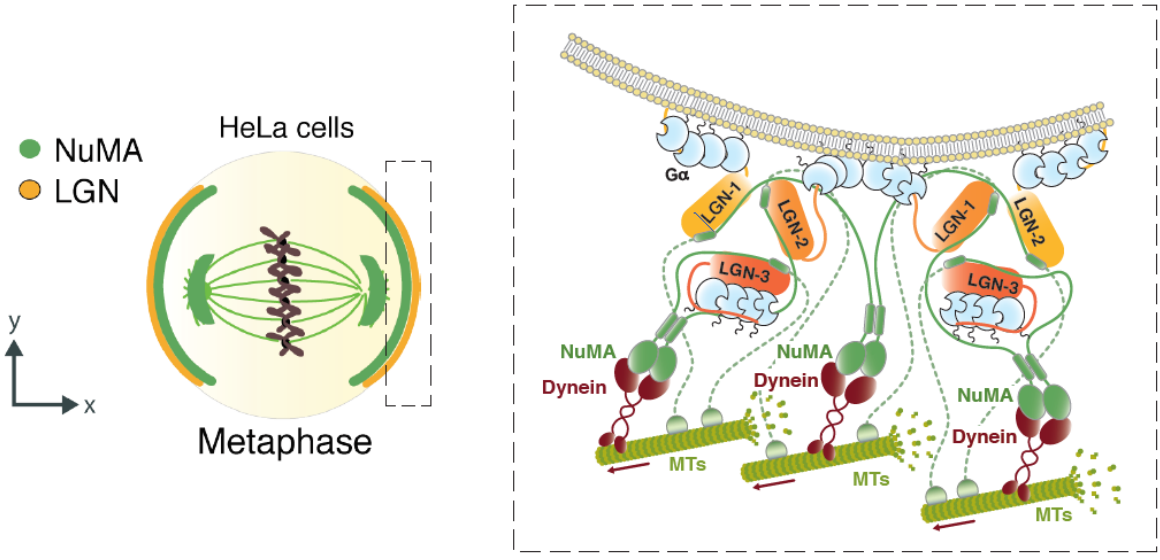

Figure 46 – Schematic representation of the role of NuMA:LGN protein network at the cortex according to our studies

During metaphase, four Gαi-GDP anchored to the lipid bilayer recruit LGN:NuMA complexes by binding the GoLoco motif in the C-terminal region of LGN. Cortical NuMA:LGN complexes can form extended protein network through NuMA self-dimerization. In such arrangement, the N-terminus of NuMA associates with dynein/dynactin and concomitantly with depolymerizing microtubules lattice through its C-terminal microtubules-binding domain, this way promoting spindle orientation and sustaining spindle pulling on the astral microtubules.

5. REFERENCES

Asteriti, I. A. *et al.* (2011) 'Aurora-A inactivation causes mitotic spindle pole fragmentation by unbalancing microtubule-generated forces', *Molecular Cancer*, 10, pp. 1–12. doi: 10.1186/1476-4598-10-131.

Asteriti, I. A. *et al.* (2014) 'The Aurora-A inhibitor MLN8237 affects multiple mitotic processes and induces dose-dependent mitotic abnormalities and aneuploidy', *Oncotarget*, 5(15). doi: 10.18632/oncotarget.2190.

Baker, J. and Garrod, D. (1993) 'Epithelial cells retain junctions during mitosis.', *Journal of cell science*, 104 (Pt 2, pp. 415–25. Available at: http://www.ncbi.nlm.nih.gov/pubmed/7685036.

Bellaiche, Y. and Gotta, M. (2005) 'Heterotrimeric G proteins and regulation of size asymmetry during cell division', *Current Opinion in Cell Biology*, 17(6), pp. 658–663. doi: 10.1016/j.ceb.2005.10.002.

Bergstralh, D. T., Lovegrove, H. E. and St Johnston, D. (2013) 'Discs large links spindle orientation to apical-basal polarity in drosophila epithelia', *Current Biology*. Elsevier, 23(17), pp. 1707–1712. doi: 10.1016/j.cub.2013.07.017.

Betschinger, J. and Knoblich, J. A. (2004) 'Dare to be different: Asymmetric cell division in Drosophila, C. elegans and vertebrates', *Current Biology*, 14(16), pp. 674–685. doi: 10.1016/j.cub.2004.08.017.

Bienz, M. (2014) 'Signalosome assembly by domains undergoing dynamic head-to-tail polymerization', *Trends in Biochemical Sciences*. Elsevier Ltd, 39(10), pp. 487–495. doi: 10.1016/j.tibs.2014.08.006.

Blangy, A. *et al.* (1995) 'Phosphorylation by p34cdc2 Regulates Spindle Association of Human Eg5 , a Kinesin-Related Motor Essential for Bipolar Spindle Formation In Vivo', *Cell*, 63, pp. 1159–1169.

Bosveld, F. *et al.* (2016) 'Epithelial tricellular junctions act as interphase cell shape sensors to orient mitosis', *Nature*. Nature Publishing Group, 530(7591), pp. 495–498. doi: 10.1038/nature16970.

Bowman, S. K. *et al.* (2006) 'The Drosophila NuMA Homolog Mud Regulates Spindle Orientation in Asymmetric Cell Division', *Developmental Cell*, 10(6), pp. 731–742. doi: 10.1016/j.devcel.2006.05.005.

Brüning-Richardson, A. *et al.* (2012) 'NuMA Overexpression in Epithelial Ovarian Cancer', *PLoS ONE*, 7(6), pp. 1–11. doi: 10.1371/journal.pone.0038945.

Cabernard, C. and Doe, C. Q. (2009) 'Apical/Basal Spindle Orientation Is Required for Neuroblast Homeostasis and Neuronal Differentiation in Drosophila', *Developmental Cell*. Elsevier Ltd, 17(1), pp. 134–141. doi: 10.1016/j.devcel.2009.06.009.

Cabernard, C., Prehoda, K. E. and Doe, C. Q. (2010) 'A spindle-independent cleavage furrow positioning pathway', *Nature*. Nature Publishing Group, 467(7311), pp. 91–94. doi: 10.1038/nature09334.

Cai, Y. *et al.* (2003) 'Apical complex genes control mitotic spindle geometry and relative size of daughter cells in Drosophila neuroblast and pI asymmetric divisions', *Cell*, 112(1), pp. 51–62. doi: 10.1016/S0092-8674(02)01170-4.

Carminati, M. *et al.* (2016) 'Concomitant binding of Afadin to LGN and F-actin directs planar spindle orientation', *Nature Structural and Molecular Biology*. Nature Publishing Group, 23(2), pp. 155–163. doi: 10.1038/nsmb.3152.

Chang, C. C. *et al.* (2017) 'Regulation of mitotic spindle assembly factor NuMA by Importin-β', *Journal of Cell Biology*, 216(11), pp. 3453–3462. doi: 10.1083/jcb.201705168.

Ciferri, C. *et al.* (2008) 'Implications for Kinetochore-Microtubule Attachment from the Structure of an Engineered Ndc80 Complex', *Cell*, pp. 427–439. doi: 10.1016/j.cell.2008.03.020.

Clarke, P. R. and Zhang, C. (2008) 'Spatial and temporal coordination of mitosis by Ran

GTPase', *Nature Reviews Molecular Cell Biology*, 9(june). doi: 10.1038/nrm2410.
Clayton, E. *et al.* (2007) 'A single type of progenitor cell maintains normal epidermis', *Nature*, 446(7132), pp. 185–189. doi: 10.1038/nature05574.
Compton, D. A. and Cleveland, D. W. (1993) 'NuMA Is Required for the Proper Completion of Mitosis', *Journal of Cell Biology*, 120(4), pp. 947–957.
Connell, M. *et al.* (2011) 'Asymmetric cortical extension shifts cleavage furrow position in Drosophila neuroblasts', *Molecular Biology of the Cell*, 22(22), pp. 4220–4226. doi: 10.1091/mbc.e11-02-0173.
Cowley, D. O. *et al.* (2009) 'Aurora-A Kinase Is Essential for Bipolar Spindle Formation and Early Development', *Molecular and Cellular Biology*, 29(4), pp. 1059–1071. doi: 10.1128/MCB.01062-08.
Culurgioni, S. *et al.* (2011) 'Inscuteable and NuMA proteins bind competitively to Leu-Gly-Asn repeat-enriched protein (LGN) during asymmetric cell divisions', *Proceedings of the National Academy of Sciences*, 108(52), pp. 20998–21003. doi: 10.1073/pnas.1113077108.
David, N. B. *et al.* (2005) 'Drosophila Ric-8 regulates Gαi cortical localization to promote Gαi-dependent planar orientation of the mitotic spindle during asymmetric cell division', *Nature Cell Biology*, 7(11), pp. 1083–1090. doi: 10.1038/ncb1319.
Desai, A. and Mitchison, T. J. (1997) 'Microtubule polymerization dynamics', *Annual Review of Cell and Developmental Biology*, pp. 83–117.
Dewey, E. B., Sanchez, D. and Johnston, C. A. (2015) 'Warts phosphorylates mud to promote Pins-mediated mitotic spindle orientation in Drosophila, Independent of Yorkie', *Current Biology*. Elsevier Ltd, 25(21), pp. 2751–2762. doi: 10.1016/j.cub.2015.09.025.
Du, Q. *et al.* (2002) 'LGN Blocks the Ability of NuMA to Bind and Stabilize Microtubules: A Mechanism for Mitotic Spindle Assembly Regulation', *Current Biology*, 12(22), pp. 1928–1933. doi: 10.1016/s0960-9822(02)01298-8.
Du, Q. and Macara, I. G. (2004) 'Mammalian Pins Is a Conformational Switch that Links NuMA to Heterotrimeric G Proteins', *Cell*, 119, pp. 503–516.
Du, Q., Stukenberg, P. T. and Macara, I. G. (2001) 'A mammalian Partner of inscuteable binds NuMA and regulates mitotic spindle organization', *Nature Cell Biology*, 3(December).
Dutertre, S., Descamps, S. and Prigent, C. (2002) 'On the role of aurora-A in centrosome function', *Oncogene*, 21(4), pp. 6175–6183. doi: 10.1038/sj.onc.1205775.
den Elzen, N. *et al.* (2009) 'Cadherin Adhesion Receptors Orient the Mitotic Spindle during Symmetric Cell Division in Mammalian Epithelia', *Molecular biology of the cell*, 21(22), pp. 4042–4056. doi: 10.1091/mbc.E09.
Fink, J. *et al.* (2011) 'External forces control mitotic spindle positioning', *Nature Cell Biology*. Nature Publishing Group, 13(7), pp. 771–778. doi: 10.1038/ncb2269.
Fuchs, E. (2016) 'Epithelial Skin Biology. Three Decades of Developmental Biology, a Hundred Questions Answered and a Thousand New Ones to Address', *Current Topics in Developmental Biology*. 1st edn. Elsevier Inc., 116, pp. 357–374. doi: 10.1016/bs.ctdb.2015.11.033.
Fuchs, E. and Chen, T. (2012) 'A matter of life and death: Self-renewal in stem cells', *EMBO Reports*. Nature Publishing Group, 14(1), pp. 39–48. doi: 10.1038/embor.2012.197.
Gadde, S. and Heald, R. (2004) 'Mechanisms and Molecules of the Mitotic Spindle', *Current Biology*, 14, pp. 797–805. doi: 10.1016/j.cub.2004.09.021.
Gallini, S. *et al.* (2016) 'NuMA phosphorylation by aurora-a orchestrates spindle orientation', *Current Biology*. Elsevier Ltd, 26(4), pp. 458–469. doi: 10.1016/j.cub.2015.12.051.
Gillies, T. E. and Cabernard, C. (2011) 'Cell division orientation in animals', *Current Biology*. Elsevier Ltd, 21(15), pp. R599–R609. doi: 10.1016/j.cub.2011.06.055.
Gönczy, P. and Rose, L. S. (2005) 'Asymmetric cell division and axis formation in the embryo', *WormBook*, pp. 1–20. doi: 10.1895/wormbook.1.30.1.
Gotta, M. *et al.* (2003) 'Asymmetrically Distributed C. elegans Homologs of AGS3/PINSControl Spindle Position in theEarly Embryo', *Current Biology*, 10, pp. 53–60.

doi: 10.1016/s.
Götz, M. and Huttner, W. B. (2005) 'The cell biology of neurogenesis', *Nature Reviews Molecular Cell Biology*, 6(10), pp. 777–788. doi: 10.1038/nrm1739.
Gueth-Hallonet, C., Weber, K. and Osborn, M. (1996) 'NuMA: A bipartite nuclear location signal and other functional properties of the tail domain', *Experimental Cell Research*, 225(1), pp. 207–218. doi: 10.1006/excr.1996.0171.
Habib, S. J. *et al.* (2013) 'Asymmetric Stem Cell Division in Vitro', *Science*, 1424(March), pp. 1445–1449.
Hao, Y. *et al.* (2010) 'Par3 controls epithelial spindle orientation by aPKC-mediated phosphorylation of apical pins', *Current Biology*. Elsevier Ltd, 20(20), pp. 1809–1818. doi: 10.1016/j.cub.2010.09.032.
Harborth, J. *et al.* (1999) 'Self assembly of NuMA: multiarm oligomers as structural units of a nuclear lattice', *The EMBO Journal*, 18(6), pp. 1689–1700. doi: 10.1093/emboj/18.6.1689.
Haren, L. *et al.* (2009) 'NuMA is required for proper spindle assembly and chromosome alignment in prometaphase', *BMC Research Notes*, 2, pp. 1–6. doi: 10.1186/1756-0500-2-64.
Haren, L. and Merdes, A. (2002) 'Direct binding of NuMA to tubulin is mediated by a novel sequence motif in the tail domain that bundles and stabilizes microtubules.', *Journal of cell science*, 115(Pt 9), pp. 1815–24. Available at: http://www.ncbi.nlm.nih.gov/pubmed/11956313.
Hepler, J. and Gilman, A. (1992) 'G proteins', *Trends in Biochemical Sciences*, (October), pp. 383–387.
Hertwig, O. (1884) 'Das Problem der Befruchtung und der Isotropie des Eies, eine Theory der Vererbung', *Jenaische Zeitschrift fuer Naturwissenschaf*.
Van Horn, R. D. *et al.* (2010) 'Cdk1 activity is required for mitotic activation of Aurora A during G 2/M transition of human cells', *Journal of Biological Chemistry*, 285(28), pp. 21849–21857. doi: 10.1074/jbc.M110.141010.
Hueschen, C. L. *et al.* (2017) 'NuMA recruits dynein activity to microtubule minus-ends at mitosis', *eLife*, 6, pp. 1–26. doi: 10.7554/elife.29328.
Huttner, W. B. and Kosodo, Y. (2005) 'Symmetric versus asymmetric cell division during neurogenesis in the developing vertebrate central nervous system', *Current Opinion in Cell Biology*, 17(6), pp. 648–657. doi: 10.1016/j.ceb.2005.10.005.
Ito, K. and Hota, Y. (1992) 'Proliferation Pattern of Postembryonic Neuroblasts in the Brain of Drosophila melanogaster', *Developmental Biology*, 149, p. 134148.
Ivanov, A. I. *et al.* (2008) 'Myosin II regulates the shape of three-dimensional intestinal epithelial cysts', *Journal of Cell Science*, 121(11), pp. 1803–1814. doi: 10.1242/jcs.015842.
Izumi, Y. *et al.* (2006) 'Drosophila Pins-binding protein Mud regulates spindle-polarity coupling and centrosome organization', *Nature Cell Biology*, 8(6), pp. 586–593. doi: 10.1038/ncb1409.
Jaffe, A. B. *et al.* (2008) 'Cdc42 controls spindle orientation to position the apical surface during epithelial morphogenesis', *Journal of Cell Biology*, 183(4), pp. 625–633. doi: 10.1083/jcb.200807121.
Jayaraman, S. *et al.* (2017) 'The nuclear mitotic apparatus protein NuMA controls rDNA transcription and mediates the nucleolar stress response in a p53-independent manner', *Nucleic Acids Research*, 45(20), pp. 11725–11742. doi: 10.1093/nar/gkx782.
Johnston, C. A. *et al.* (2009) 'Identification of an Aurora-A / Pins LINKER / Dlg Spindle Orientation Pathway using Induced Cell Polarity in S2 Cells', *Cell*. Elsevier Ltd, 138(6), pp. 1150–1163. doi: 10.1016/j.cell.2009.07.041.
Johnston, C. A. *et al.* (2013) 'Formin-mediated actin polymerization cooperates with Mushroom body defect (Mud)– Dynein during Frizzled – Dishevelled spindle orientation', *Journal of cell science*, pp. 4436–4444. doi: 10.1242/jcs.129544.
Kardon, J. R. and Vale, R. D. (2009) 'Regulators of the cytoplasmic dynein motor', *Nature*

Reviews Molecular Cell Biology. Nature Publishing Group, 10(December). doi: 10.1038/nrm2804.
Khodjakov, A. *et al.* (2003) 'Minus-end capture of preformed kinetochore fibers contributes to spindle morphogenesis', *Journal of Cell Biology*, 160(5), pp. 671–683. doi: 10.1083/jcb.200208143.
Kikuchi, K. *et al.* (2010) 'Dishevelled, a Wnt signalling component, is involved in mitotic progression in cooperation with Plk1', *The EMBO Journal*. Nature Publishing Group, 29(20), pp. 3470–3483. doi: 10.1038/emboj.2010.221.
Kiyomitsu, T. (2015) 'Mechanisms of daughter cell-size control during cell division', *Trends in Cell Biology*. Elsevier Ltd, 25(5), pp. 286–295. doi: 10.1016/j.tcb.2014.12.003.
Kiyomitsu, T. and Cheeseman, I. M. (2012) 'Chromosome-and spindle-pole-derived signals generate an intrinsic code for spindle position and orientation', *Nature Cell Biology*. Nature Publishing Group, 14(3), pp. 311–317. doi: 10.1038/ncb2440.
Kiyomitsu, T. and Cheeseman, I. M. (2013) 'Cortical Dynein and Asymmetric Membrane Elongation Coordinately Position the Spindle in Anaphase', *Cell*. Elsevier Inc., 154(2), pp. 391–402. doi: 10.1016/j.cell.2013.06.010.
Knoblich, J. A. (2008) 'Mechanisms of Asymmetric Stem Cell Division', *Cell*, pp. 583–597. doi: 10.1016/j.cell.2008.02.007.
Knoblich, J. A. (2010) 'Asymmetric cell division: Recent developments and their implications for tumour biology', *Nature Reviews Molecular Cell Biology*. Nature Publishing Group, 11(12), pp. 849–860. doi: 10.1038/nrm3010.
Knoblich, J. A., Jan, L. Y. and Jan, Y. N. (1995) 'Asymmetric segregation of Numb and Prospero during cell division', *Nature*, 3, pp. 77–80.
Konno, D. *et al.* (2007) 'Neuroepithelial progenitors undergo LGN-dependent planar divisions to maintain self-renewability during mammalian neurogenesis', *Nature Cell Biology*, 10(1), pp. 93–101. doi: 10.1038/ncb1673.
Kotak, S., Busso, C. and Gönczy, P. (2012) 'Cortical dynein is critical for proper spindle positioning in human cells', *Journal of Cell Biology*, 199(1), pp. 97–110. doi: 10.1083/jcb.201203166.
Kotak, S., Busso, C. and Gönczy, P. (2013) 'NuMA phosphorylation by CDK1 couples mitotic progression with cortical dynein function', *EMBO Journal*, 32(18), pp. 2517–2529. doi: 10.1038/emboj.2013.172.
Kotak, S., Busso, C. and Gönczy, P. (2014) 'NuMA interacts with phosphoinositides and links the mitotic spindle with the plasma membrane', *EMBO Journal*, 33(16), pp. 1815–1830.
Kotak, S. and Gönczy, P. (2014) 'NuMA phosphorylation dictates dynein-dependent spindle positioning', *Cell Cycle*, 13(2), pp. 177–178. doi: 10.4161/cc.27040.
Kraut, R. *et al.* (1996) 'Role of inscuteable in orienting asymmetric cell division in Drosophila', *Nature*.
Kulukian, A. and Fuchs, E. (2013) 'Spindle orientation and epidermal morphogenesis', *Philosphical Transactions of The Royal Society*, (September).
Kwon, M. *et al.* (2015) 'Direct Microtubule-Binding by Myosin-10 Orients Centrosomes toward Retraction Fibers and Subcortical Actin Clouds', *Developmental Cell*, 118(24), pp. 6072–6078. doi: 10.1002/cncr.27633.Percutaneous.
Lancaster, O. M. and Baum, B. (2014) 'Shaping up to divide: Coordinating actin and microtubule cytoskeletal remodelling during mitosis', *Seminars in Cell and Developmental Biology*. Elsevier Ltd, 34, pp. 109–115. doi: 10.1016/j.semcdb.2014.02.015.
Lázaro-Diéguez, F., Ispolatov, I. and Müsch, A. (2015) 'Cell shape impacts on the positioning of the mitotic spindle with respect to the substratum', *Molecular Biology of the Cell*, 26(7), pp. 1286–1295. doi: 10.1091/mbc.e14-08-1330.
Lechler, T. and Fuchs, E. (2005) 'Asymmetric cell divisions promote stratification and differentiation of mammalian skin', *Nature*, 437(7056), pp. 275–280. doi: 10.1038/nature03922.

Lee, C. Y. *et al.* (2006) 'Drosophila Aurora-A kinase inhibits neuroblast self-renewal by regulating aPKC/Numb cortical polarity and spindle orientation', *Genes and Development*, 20(24), pp. 3464–3474. doi: 10.1101/gad.1489406.
Ludérus, M. E. *et al.* (1994) 'Binding of matrix attachment regions to lamin polymers involves single-stranded regions and the minor groove.', *Molecular and Cellular Biology*, 14(9), pp. 6297–6305. doi: 10.1128/mcb.14.9.6297.
Lydersen, B. K. and Pettijohn, D. E. (1980) 'Human-specific nuclear protein that associates with the polar region of the mitotic apparatus: Distribution in a human/hamster hybrid cell', *Cell*, 22(2), pp. 489–499. doi: 10.1016/0092-8674(80)90359-1.
MacDonald, B. T., Tamai, K. and He, X. (2009) 'Wnt/β-Catenin Signaling: Components, Mechanisms, and Diseases', *Developmental Cell*, 17(1), pp. 9–26. doi: 10.1016/j.devcel.2009.06.016.
Machicoane, M. *et al.* (2014) 'SLK-dependent activation of ERMs controls LGN-NuMA localization and spindle orientation', *Journal of Cell Biology*, 205(6), pp. 791–799. doi: 10.1083/jcb.201401049.
Madrzak, J. *et al.* (2015) 'Ubiquitination of the Dishevelled DIX domain blocks its head-to-tail polymerization', *Nature Communications*. Nature Publishing Group, 6, pp. 1–11. doi: 10.1038/ncomms7718.
Marumoto, T. *et al.* (2003) 'Aurora-A Kinase Maintains the Fidelity of Early and Late Mitotic Events in HeLa Cells', *Journal of Biological Chemistry*, 278(51), pp. 51786–51795. doi: 10.1074/jbc.M306275200.
Matsumura, S. *et al.* (2012) 'ABL1 regulates spindle orientation in adherent cells and mammalian skin', *Nature Communications*. Nature Publishing Group, 3, pp. 610–626. doi: 10.1038/ncomms1634.
Mattagajasingh, S. N., Huang, S. C. and Benz, E. J. (2009) 'Inhibition of Protein 4.1 R and NuMA interaction by mutagenization of their binding-sites abrogates nuclear localization of 4.1 R', *Clinical and Translational Science*, 2(2), pp. 102–111. doi: 10.1111/j.1752-8062.2008.00087.x.
Meraldi, P. and Nigg, E. A. Ã. (2002) 'The centrosome cycle', *FEBS Press*, 521, pp. 9–13.
Merdes, A. *et al.* (1996) 'A Complex of NuMA and Cytoplasmic Dynein Is Essential for Mitotic Spindle Assembly', *Cell*, 87, pp. 447–458.
Merdes, A. *et al.* (2000) 'Formation of Spindle Poles by Dynein / Dynactin-dependent Transport of NuMA', *Journal of Cell Biology*, 149(4), pp. 851–861.
Minc, N., Burgess, D. and Chang, F. (2011) 'Influence of cell geometry on division-plane positioning', *Cell*. Elsevier Inc., 144(3), pp. 414–426. doi: 10.1016/j.cell.2011.01.016.
Morin, X. and Bellaïche, Y. (2011) 'Mitotic Spindle Orientation in Asymmetric and Symmetric Cell Divisions during Animal Development', *Developmental Cell*, 21(1), pp. 102–119. doi: 10.1016/j.devcel.2011.06.012.
Morin, X., Jaouen, F. and Durbec, P. (2007) 'Control of planar divisions by the G-protein regulator LGN maintains progenitors in the chick neuroepithelium', *Nature Neuroscience*, 10(11), pp. 1440–1448. doi: 10.1038/nn1984.
Nachury, M. V. *et al.* (2001) 'Importin β is a mitotic target of the small GTPase ran in spindle assembly', *Cell*, 104(1), pp. 95–106. doi: 10.1016/S0092-8674(01)00194-5.
Nguyen-Ngoc, T., Afshar, K. and Gönczy, P. (2007) 'Coupling of cortical dynein and Gα proteins mediates spindle positioning in Caenorhabditis elegans', *Nature Cell Biology*, 9(11), pp. 1294–1302. doi: 10.1038/ncb1649.
Niessen, M. T. *et al.* (2013) 'Apkc controls epidermal homeostasis and stemcell fate through regulation of division orientation', *Journal of Cell Biology*, 202(6), pp. 887–900. doi: 10.1083/jcb.201307001.
Nikonova, A. S. *et al.* (2013) 'Aurora A kinase (AURKA) in normal and pathological cell division', *Cellular and Molecular Life Sciences*, 70(4), pp. 661–687. doi: 10.1007/s00018-012-1073-7.
O'Connell, C. B. and Wang, Y. -l. (2000) 'Mammalian Spindle Orientation and Position

Respond to Changes in Cell Shape in a Dynein-dependent Fashion', *Molecular Biology of the Cell*, 11(5), pp. 1765–1774. doi: 10.1091/mbc.11.5.1765.
O Morgan, D. (2007) 'Cell Cycle: Principles of Control', *The Yale Journal of Biology and Medicine*, pp. 141–142.
Okumura, M. *et al.* (2018) 'Dynein – Dynactin – NuMA clusters generate cortical spindle-pulling forces as a multi- arm ensemble', *eLife*, pp. 1–24.
Ou, G. *et al.* (2010) 'Polarized Myosin Produces Unequal-Size Daughters During Asymmetric Cell Division', *Science*, 18(11), pp. 1492–1501. doi: 10.1016/j.str.2010.08.012.Structure.
Park, D. H. and Rose, L. S. (2008) 'Dynamic localization of LIN-5 and GPR-1/2 to cortical force generation domains during spindle positioning', *Developmental Biology*. Elsevier Inc., 315(1), pp. 42–54. doi: 10.1016/j.ydbio.2007.11.037.
Peyre, E. *et al.* (2011a) 'A lateral belt of cortical LGN and NuMA guides mitotic spindle movements and planar division in neuroepithelial cells', 193(1), pp. 141–154. doi: 10.1083/jcb.201101039.
Peyre, E. *et al.* (2011b) 'A lateral belt of cortical LGN and NuMA guides mitotic spindle movements and planar division in neuroepithelial cells', *Journal of Cell Biology*, 193(1), pp. 141–154. doi: 10.1083/jcb.201101039.
Peyre, E. and Morin, X. (2012) 'An oblique view on the role of spindle orientation in vertebrate neurogenesis', *Development Growth and Differentiation*, 54(3), pp. 287–305. doi: 10.1111/j.1440-169X.2012.01350.x.
Pietro, F., Echard, A. and Morin, X. (2016) 'Regulation of mitotic spindle orientation : an integrated view', *EMBO Reports*, 17(8), pp. 1106–1130.
Pirovano, L. *et al.* (2019) 'Hexameric NuMA : LGN structures promote multivalent interactions required for planar epithelial divisions', *Nature Communications*. doi: 10.1038/s41467-019-09999-w.
Poulson, N. D. and Lechler, T. (2010a) 'Robust control of mitotic spindle orientation in the developing epidermis', *Journal of Cell Biology*, 191(5), pp. 915–922. doi: 10.1083/jcb.201008001.
Poulson, N. D. and Lechler, T. (2010b) 'Robust control of mitotic spindle orientation in the developing epidermis', *Journal of Cell Biology*, 191(5), pp. 915–922. doi: 10.1083/jcb.201008001.
Ragkousi, K. and Gibson, M. C. (2014) 'Cell division and the maintenance of epithelial order', *Journal of Cell Biology*, 207(2), pp. 181–188. doi: 10.1083/jcb.201408044.
Reboutier, D. *et al.* (2013) 'Aurora a is involved in central spindle assembly through phosphorylation of ser 19 in P150Glued', *Journal of Cell Biology*, 201(1), pp. 65–79. doi: 10.1083/jcb.201210060.
Reinsch, S. and Karsenti, E. (1994) 'Orientation of spindle axis and distribution of plasma membrane proteins during cell division in polarized MDCKII cells', *The Journal of Cell Biology*, 126(6), pp. 1509–1526. doi: 10.1083/jcb.126.6.1509.
Roghi, C. *et al.* (1998) 'The Xenopus protein kinase pEg2 associates with the centrosome in a cell cycle-dependent manner, binds to the spindle microtubules and is involved in bipolar mitotic spindle assembly', *Journal of cell science*, 111 (Pt 5, pp. 557–72. Available at: http://www.ncbi.nlm.nih.gov/pubmed/9454730.
Romé, P. *et al.* (2010) 'Aurora A contributes to p150glued phosphorylation and function during mitosis', *Journal of Cell Biology*, 189(4), pp. 651–659. doi: 10.1083/jcb.201001144.
Saadaoui, M. *et al.* (2014) 'Dlg1 controls planar spindle orientation in the neuroepithelium through direct interaction with LGN', *Journal of Cell Biology*, 206(6), pp. 707–717. doi: 10.1083/jcb.201405060.
Sana, S. *et al.* (2018) 'Plk1 regulates spindle orientation by phosphorylating NuMA in human cells', *Life Science Alliance*, 1(6), pp. 1–14. doi: 10.26508/lsa.201800223.
Schober, M., Schaefer, M. and Knoblich, J. A. (1999) 'Bazooka recruits Inscuteable to orient asymmetric cell divisions in Drosophila neuroblasts', *Nature*, 402(December).

Ségalen, M. *et al.* (2010) 'The Fz-Dsh planar cell polarity pathway induces oriented cell division via Mud / NuMA in Drosophila and zebrafish', *Developmental Cell*, 19(5), pp. 740–752.
Segalen, M. and Bellaïche, Y. (2009) 'Cell division orientation and planar cell polarity pathways', *Seminars in Cell and Developmental Biology*, 20(8), pp. 972–977. doi: 10.1016/j.semcdb.2009.03.018.
Seldin, L. *et al.* (2013) 'NuMA localization , stability , and function in spindle orientation involve 4 . 1 and Cdk1 interactions', *Molecular Biology of the Cell*, 24. doi: 10.1091/mbc.E13-05-0277.
Seldin, L., Muroyama, A. and Lechler, T. (2016) 'NuMA-microtubule interactions are critical for spindle orientation and the morphogenesis of diverse epidermal structures', *eLife*, pp. 1–18. doi: 10.7554/eLife.12504.
Silk, A. D., Holland, A. J. and Cleveland, D. W. (2009) 'Requirements for NuMA in maintenance and establishment of mammalian spindle poles', *Journal of Cell Biology*, 184(5), pp. 677–690. doi: 10.1083/jcb.200810091.
Siller, K. H., Cabernard, C. and Doe, C. Q. (2006) 'The NuMA-related Mud protein binds Pins and regulates spindle orientation in Drosophila neuroblasts', *Nature Cell Biology*, 8(6), pp. 594–600. doi: 10.1038/ncb1412.
Siller, K. H. and Doe, C. Q. (2009) 'Spindle orientation during asymmetric cell division', *Nature Cell Biology*, 11(4), pp. 365–374. doi: 10.1038/ncb0409-365.
Solinet, S. *et al.* (2013) 'The actin-binding ERM protein Moesin binds to and stabilizes microtubules at the cell cortex', *Journal of Cell Biology*, 202(2), pp. 251–260. doi: 10.1083/jcb.201304052.
Srinivasan, D. G. *et al.* (2003) 'A complex of LIN-5 and GPR proteins regulates G protein signaling and spindle function in C. elegans', *Genes and Development*, 17(10), pp. 1225–1239. doi: 10.1101/gad.1081203.
Tall, G. G. and Gilman, A. G. (2005) 'Resistance to inhibitors of cholinesterase 8A catalyzes release of G i-GTP and nuclear mitotic apparatus protein (NuMA) from NuMA/LGN/G i-GDP complexes', *Proceedings of the National Academy of Sciences*, 102(46), pp. 16584–16589. doi: 10.1073/pnas.0508306102.
Tame, M. A. *et al.* (2014) 'Astral microtubules control redistribution of dynein at the cell cortex to facilitate spindle positioning', *Cell Cycle*, 13(7), pp. 1162–1170.
Théry, M. *et al.* (2005) 'The extracellular matrix guides the orientation of the cell division axis', *Nature Cell Biology*, 7(10), pp. 947–953. doi: 10.1038/ncb1307.
Toyoshima, F. and Nishida, E. (2007a) 'Integrin-mediated adhesion orients the spindle parallel to the substratum in an EB1- and myosin X-dependent manner', *EMBO Journal*, 26(6), pp. 1487–1498. doi: 10.1038/sj.emboj.7601599.
Toyoshima, F. and Nishida, E. (2007b) 'Integrin-mediated adhesion orients the spindle parallel to the substratum in an EB1- and myosin X-dependent manner', 26(6), pp. 1487–1498. doi: 10.1038/sj.emboj.7601599.
Tuncay, H. *et al.* (2015) 'JAM-A regulates cortical dynein localization through Cdc42 to control planar spindle orientation during mitosis', *Nature Communications*, 6(May). doi: 10.1038/ncomms9128.
Uzbekov, R. *et al.* (1999) 'The Xenopus laevis Aurora-related Protein Kinase pEg2 Associates with and Phosphorylates the Kinesin-related Protein XlEg5 *', *Journal of Biological Chemistry*, 274(21), pp. 15005–15013.
Vader, G. and Lens, S. M. A. (2008) 'The Aurora kinase family in cell division and cancer', *Biochimica et Biophysica Acta - Reviews on Cancer*, 1786(1), pp. 60–72. doi: 10.1016/j.bbcan.2008.07.003.
Vidi, P.-A. *et al.* (2012) 'Interconnected contribution of tissue morphogenesis and the nuclear protein NuMA to the DNA damage response', *Journal of Cell Science*, 125(2), pp. 350–361. doi: 10.1242/jcs.089177.
Vidi, P. A. *et al.* (2014) 'NuMA promotes homologous recombination repair by regulating

the accumulation of the ISWI ATPase SNF2h at DNA breaks', *Nucleic Acids Research*, 42(10), pp. 6365–6379. doi: 10.1093/nar/gku296.
Wang, G., Jiang, Q. and Zhang, C. (2014) 'The role of mitotic kinases in coupling the centrosome cycle with the assembly of the mitotic spindle', *Journal of Cell Science*, pp. 4111–4122. doi: 10.1242/jcs.151753.
Wang, H. *et al.* (2006) 'Aurora-A acts as a tumor suppressor and regulates self-renewal of Drosophila neuroblasts', *Genes and Development*, 20(24), pp. 3453–3463. doi: 10.1101/gad.1487506.
Wei, C. *et al.* (2012) 'The LKB1 tumor suppressor controls spindle orientation and localization of activated AMPK in mitotic epithelial cells', *PLoS ONE*, 7(7). doi: 10.1371/journal.pone.0041118.
Williams, S. E. *et al.* (2011) 'Asymmetric cell divisions promote Notch-dependent epidermal differentiation', *Nature*. Nature Publishing Group, 470(7334), pp. 353–358. doi: 10.1038/nature09793.
Williams, S. E. *et al.* (2014) 'Par3–mInsc and Gαi3 cooperate to promote oriented epidermal cell divisions through LGN', *Nature Cell Biology*, 16(8), pp. 758–769. doi: 10.1038/ncb3001.Par3.
Wodarz, A. *et al.* (1999) 'Bazooka provides an apical cue for Inscuteable localization in Drosophila neuroblasts', *Nature*, 402(December), pp. 2–5.
Woodard, G. E. *et al.* (2010) 'Ric-8A and Gia Recruit LGN , NuMA , and Dynein to the Cell Cortex To Help Orient the Mitotic Spindle', *Molecular and Cellular Biology*, 30(14), pp. 3519–3530. doi: 10.1128/MCB.00394-10.
Xia, J. *et al.* (2015) 'Semaphorin-Plexin Signaling Controls Mitotic Spindle Orientation during Epithelial Morphogenesis and Repair', *Developmental Cell*, 33(3), pp. 299–313. doi: 10.1016/j.devcel.2015.02.001.
Yamashita, Y. M., Jones, D. L. and Fuller, M. T. (2003) 'Orientation of asymmetric stem cell division by the APC tumor suppressor and centrosome', *Science*, 301(5639), pp. 1547–1550. doi: 10.1126/science.1087795.
Yang, Y. *et al.* (2014) 'CYLD regulates spindle orientation by stabilizing astral microtubules and promoting dishevelled-NuMA-dynein / dynactin complex formation', *Proceedings of the National Academy of Sciences*. doi: 10.1073/pnas.1319341111.
Yuzawa, S. *et al.* (2011) 'Structural basis for interaction between the conserved cell polarity proteins Inscuteable and Leu-Gly-Asn repeat-enriched protein (LGN)', *Proceedings of the National Academy of Sciences*, 108(48), pp. 19210–19215. doi: 10.1073/pnas.1110951108.
Zheng, Z. *et al.* (2010) 'LGN regulates mitotic spindle orientation during epithelial morphogenesis', *Journal of Cell Biology*, 189(2), pp. 275–288. doi: 10.1083/jcb.200910021.
Zheng, Z. *et al.* (2013) 'Cell cycle – regulated membrane binding of NuMA contributes to efficient anaphase chromosome separation', *Molecular Biology of the Cell*. doi: 10.1091/mbc.E13-08-0474.
Zhu, J. *et al.* (2011) 'LGN/mInsc and LGN/NuMA Complex Structures Suggest Distinct Functions in Asymmetric Cell Division for the Par3/mInsc/LGN and Gαi/LGN/NuMA Pathways', *Molecular Cell*. Elsevier Inc., 43(3), pp. 418–431. doi: 10.1016/j.molcel.2011.07.011.
Zhu, M. *et al.* (2013) 'MISP is a novel Plk1 substrate required for proper spindle orientation and mitotic progression', *Journal of Cell Biology*, 200(6), pp. 773–787. doi: 10.1083/jcb.201207050.
Zorba, A. *et al.* (2014) 'Molecular mechanism of Aurora A kinase autophosphorylation and its allosteric activation by TPX2', *eLife*, 3, pp. 1–24. doi: 10.7554/elife.02667.